

Ørsted Lecture at DTU, 1 November 2013 at 14:00

# ***Mechanics on our planet: Ice sheets, Earthquakes, Hydraulic fractures***

James R. Rice (*Harvard*)

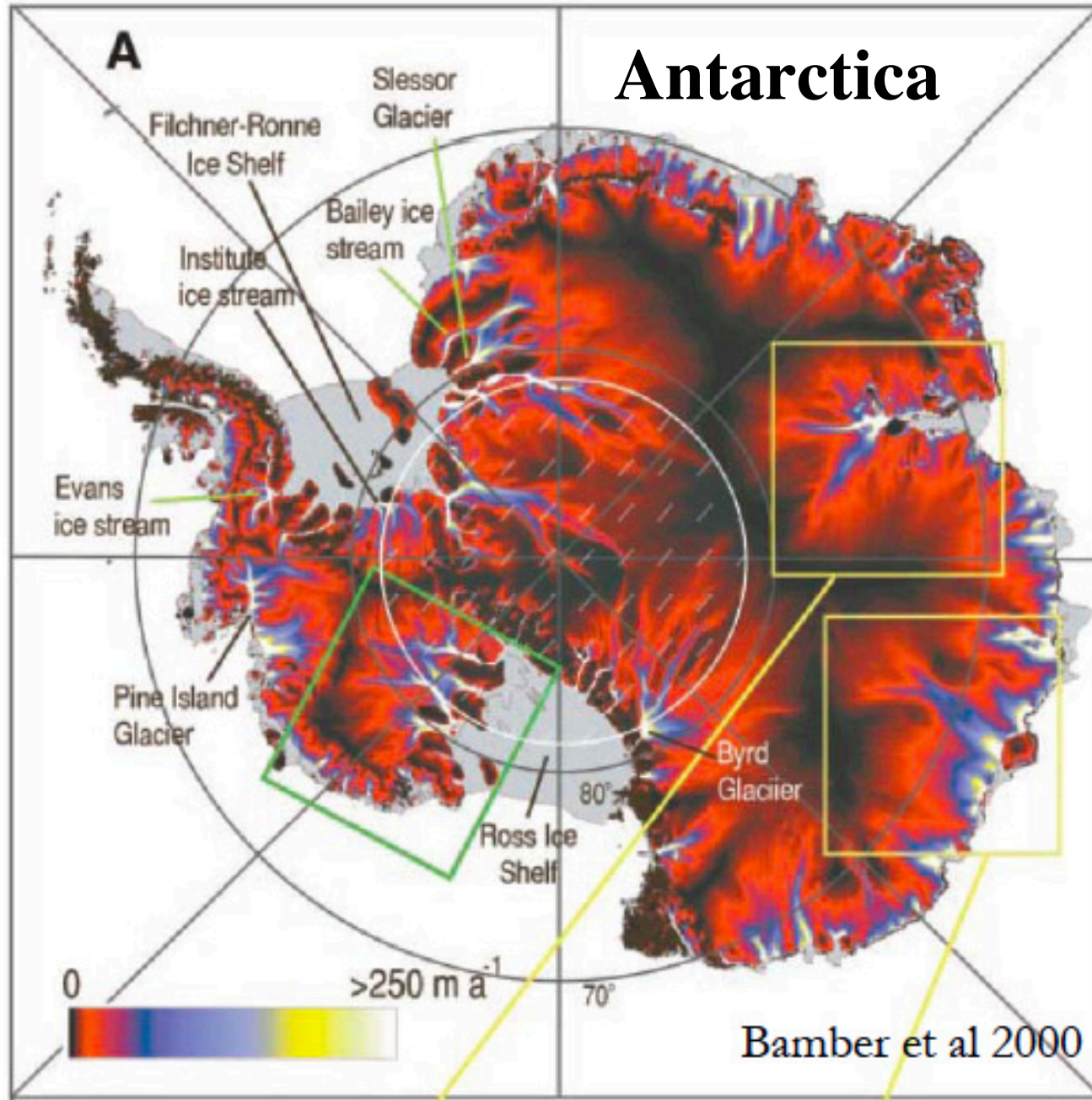
## ***Ice sheet collaborators:***

Thibaut Perol (*Harvard*), John D. Platt (*Harvard*),  
Jenny Suckale (*Harvard*), Victor C. Tsai (*Caltech*)

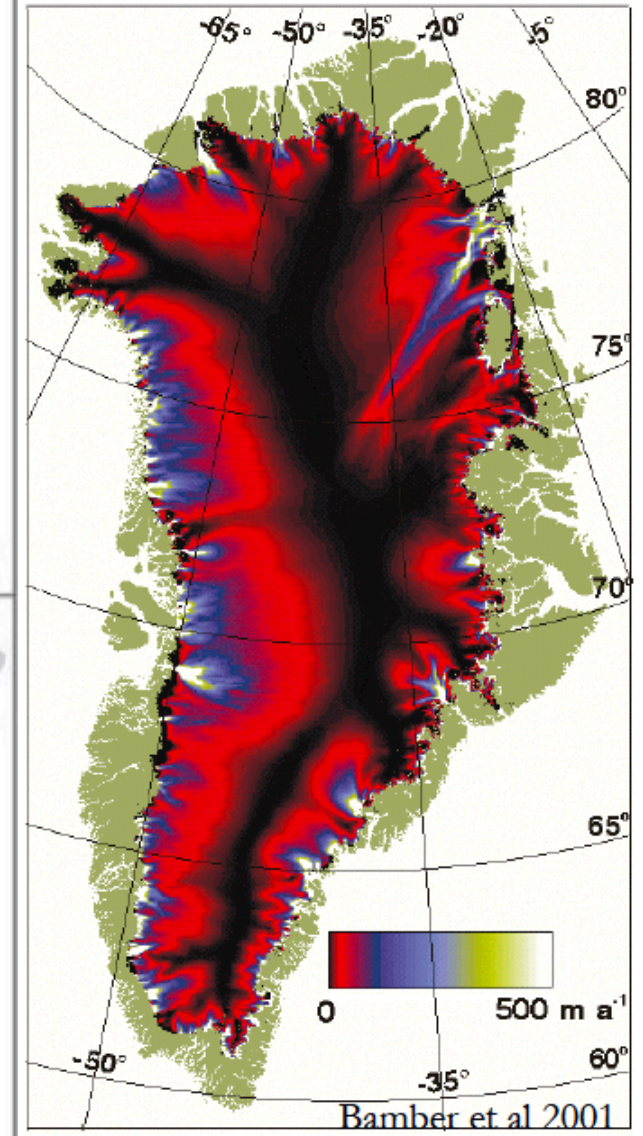
## ***Fault mechanics collaborators:***

Nicolas Brantut (*Univ.Col.London*), John D. Platt (*Harvard*),  
John W. Rudnicki (*Northwestern*)

# The major ice sheets - *not to scale*



## Greenland



From USGS Fact Sheet fs002-00: Sea Level and Climate  
(R. Z. Poore, R. S. Williams, Jr., and C. Tracey)

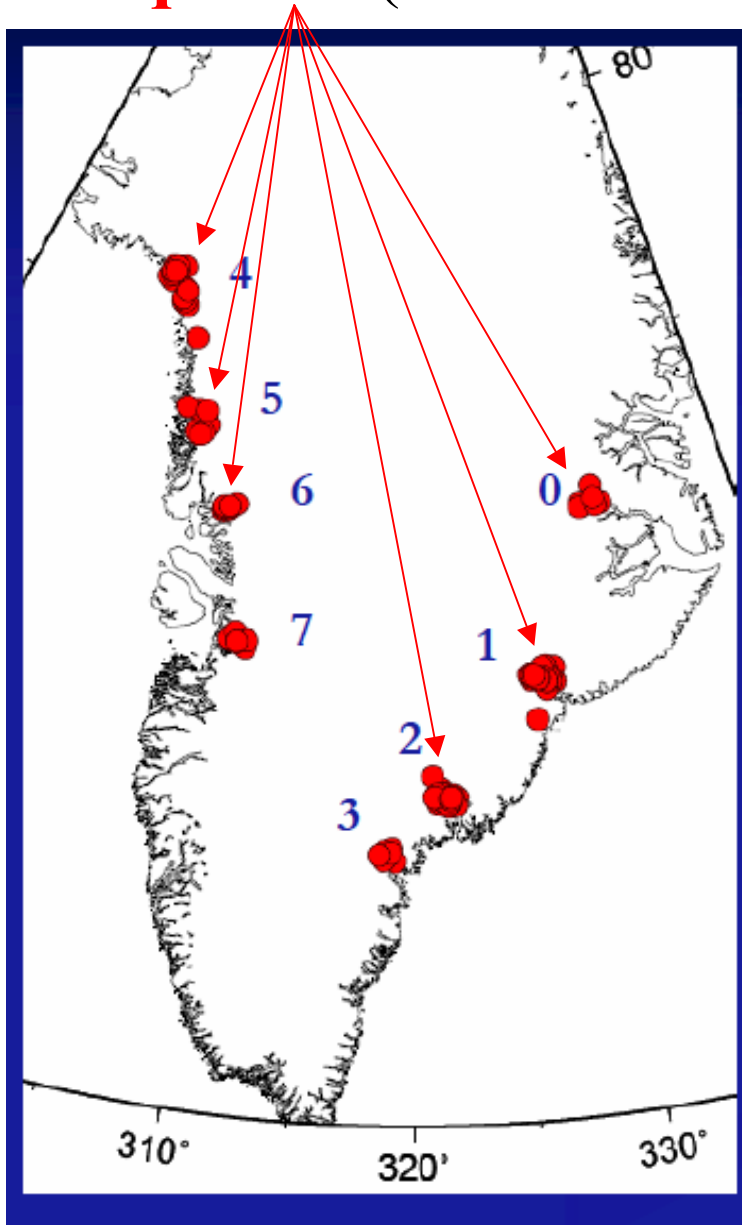
*Average sea level rises due to melting:*

*Greenland Ice Sheet: ~ 6.5 m*

*West Antarctic Ice Sheet: ~ 8 m*

“The West Antarctic ice sheet is especially vulnerable, because much of it is grounded below sea level. Small changes in global sea level or a rise in ocean temperatures could cause a breakup of the two buttressing ice shelves (Ronne/Filchner and Ross).”

Source locations of **glacial earthquakes** (G. Ekström)

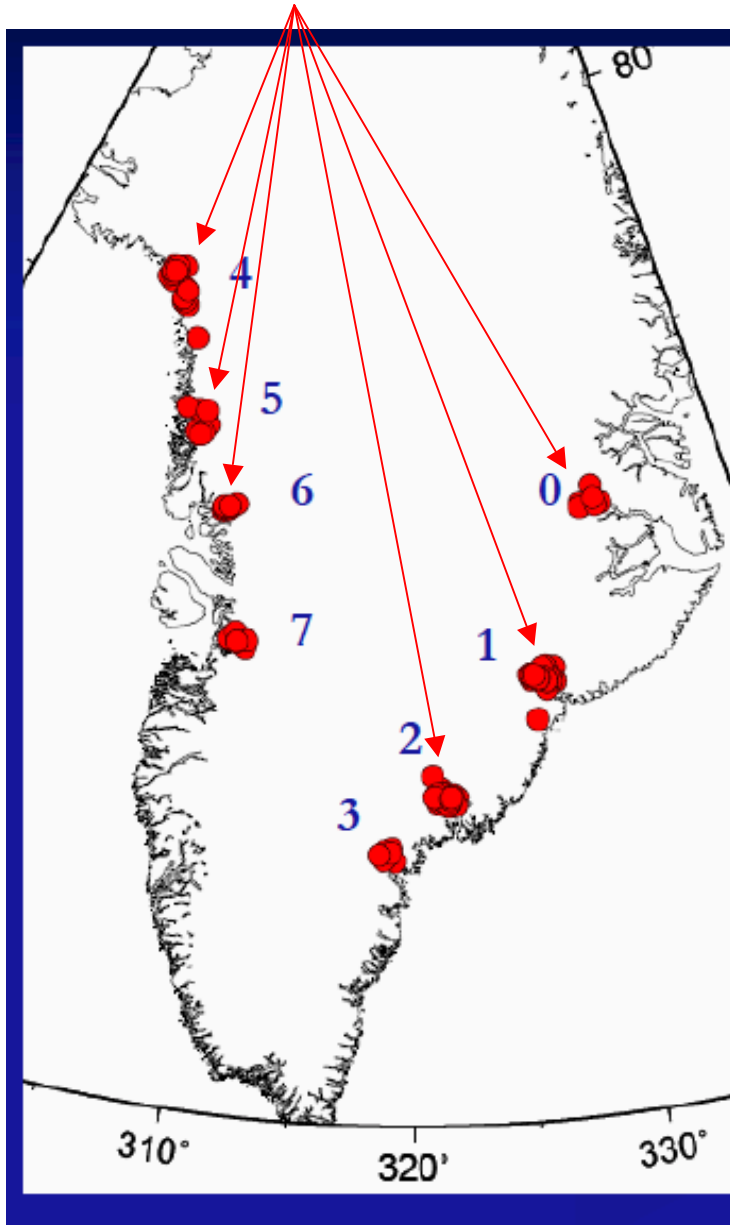


*Unusual earthquakes:*

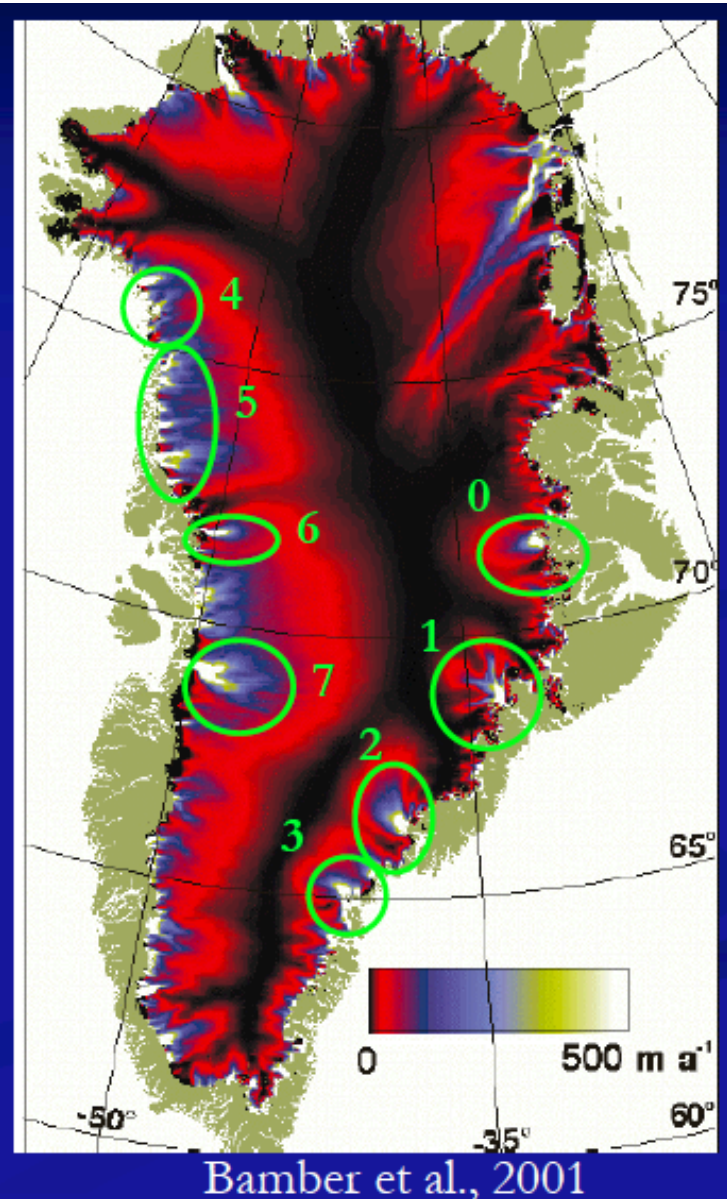
- Magnitude  $M_{sw} \sim 4.6$  to 5.1, measured at 35-150 sec periods; significant energy in periods between 20 and 100 sec (much longer than for standard earthquakes of similar  $M_s$ ).
- Distant seismic wave patterns consistent with applying a horizontal point impulse +  $I$  followed, after  $\sim$ tens of seconds to minute, by  $-I$  at shallow source location.



Source locations of **glacial earthquakes** (G. Ekstrom)

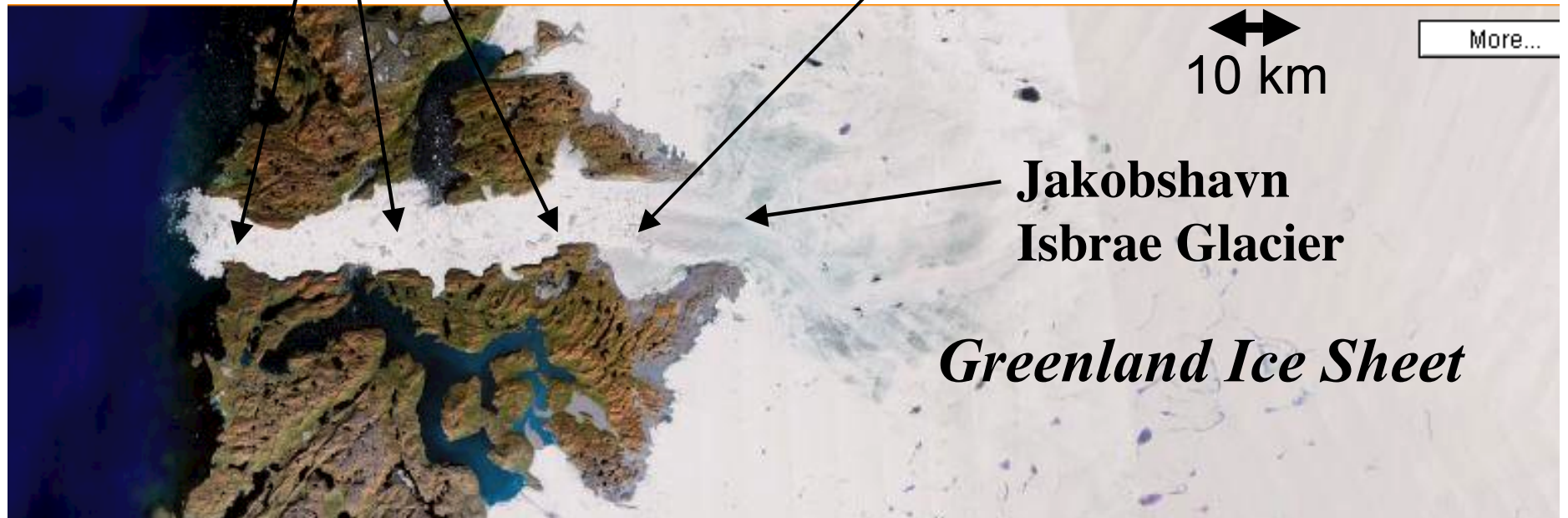


Correlation with areas of high ice flow rates -- at major fjords



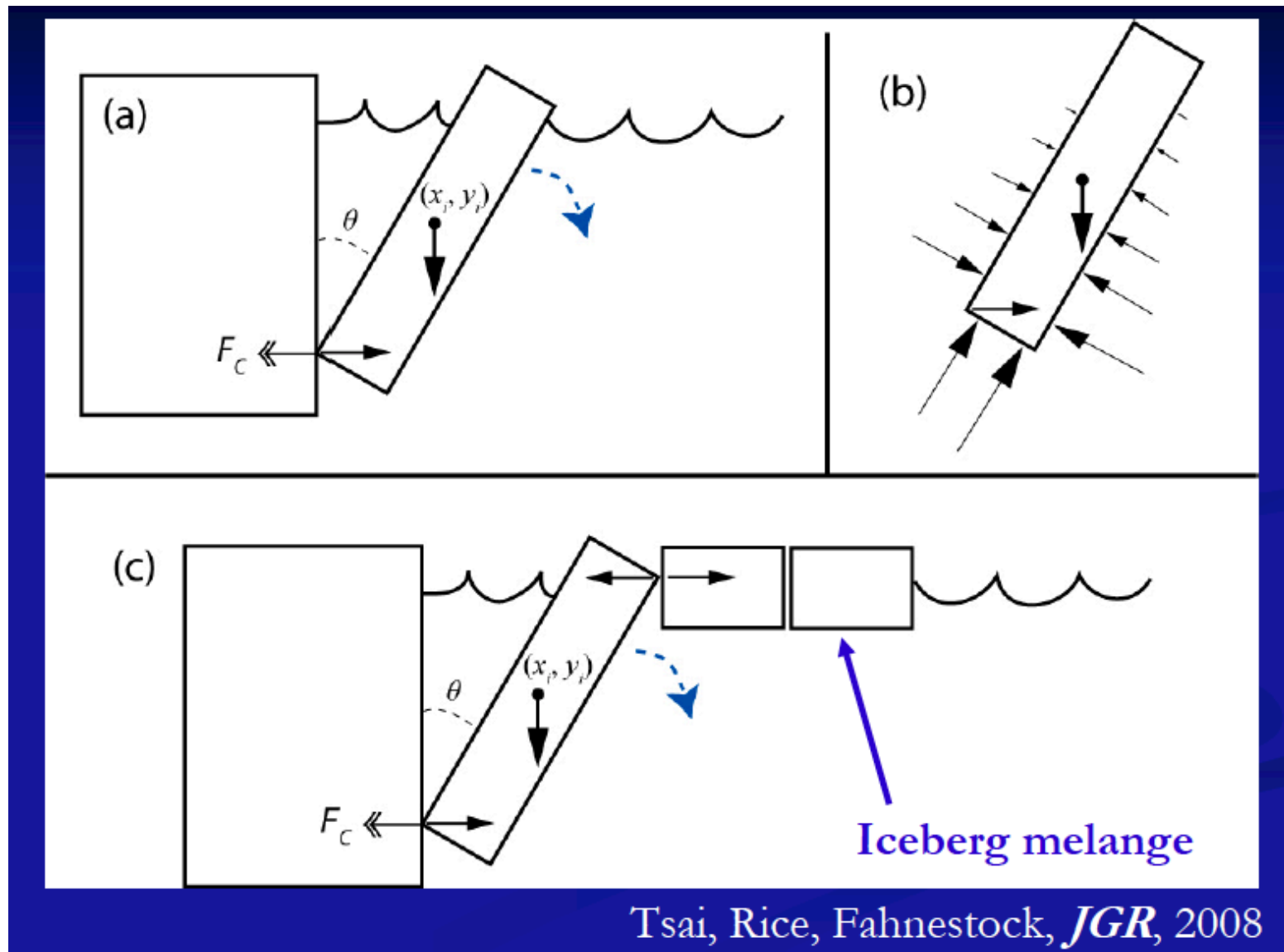
**Melange of calved icebergs**

**Iceberg calving front, glacier terminus**



## What causes glacial EQs?

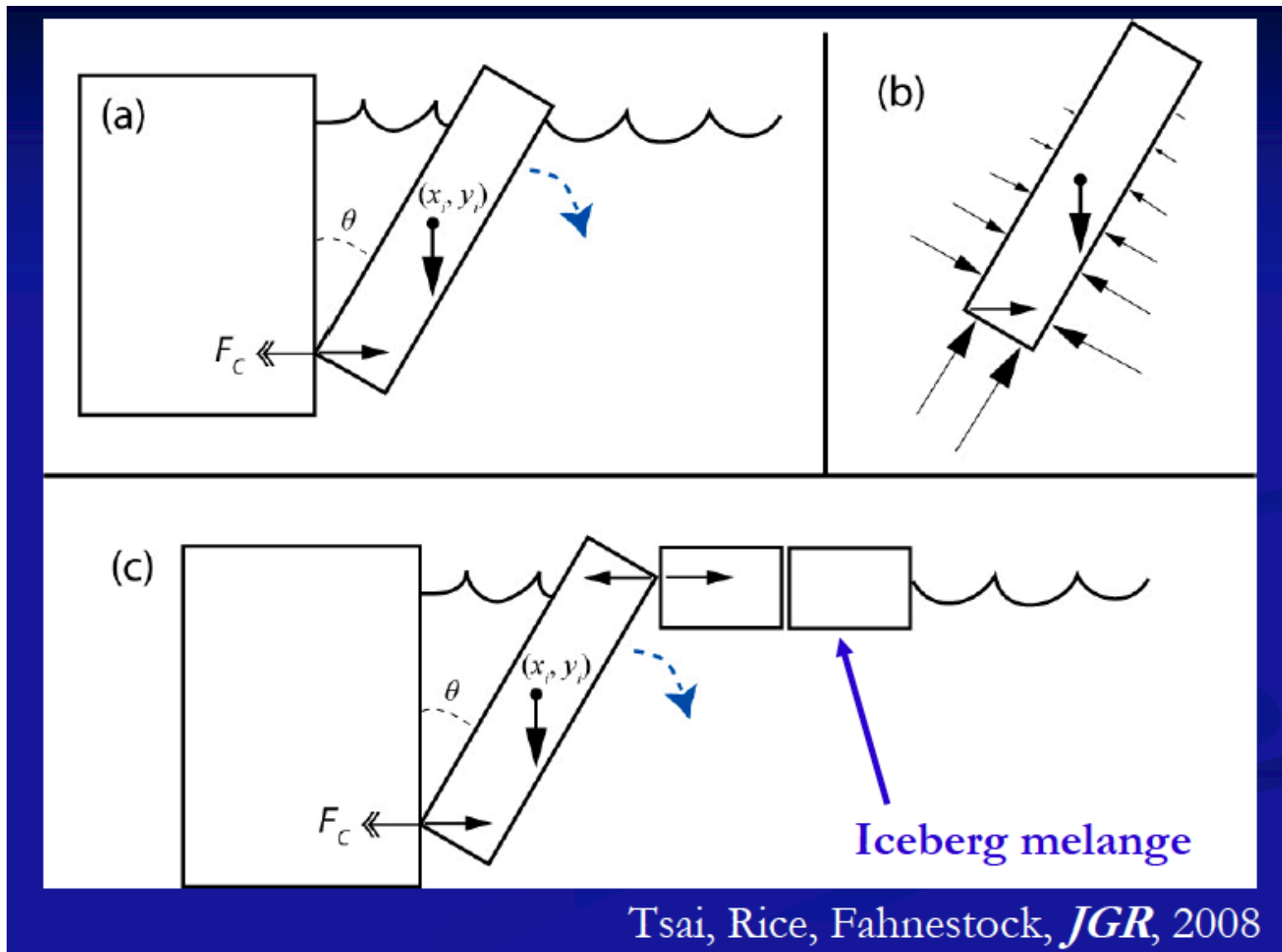
- Fast sliding at bed of ice sheet? -- analogous to normal EQs.
- Simple iceberg calving models work best! -- timescale.





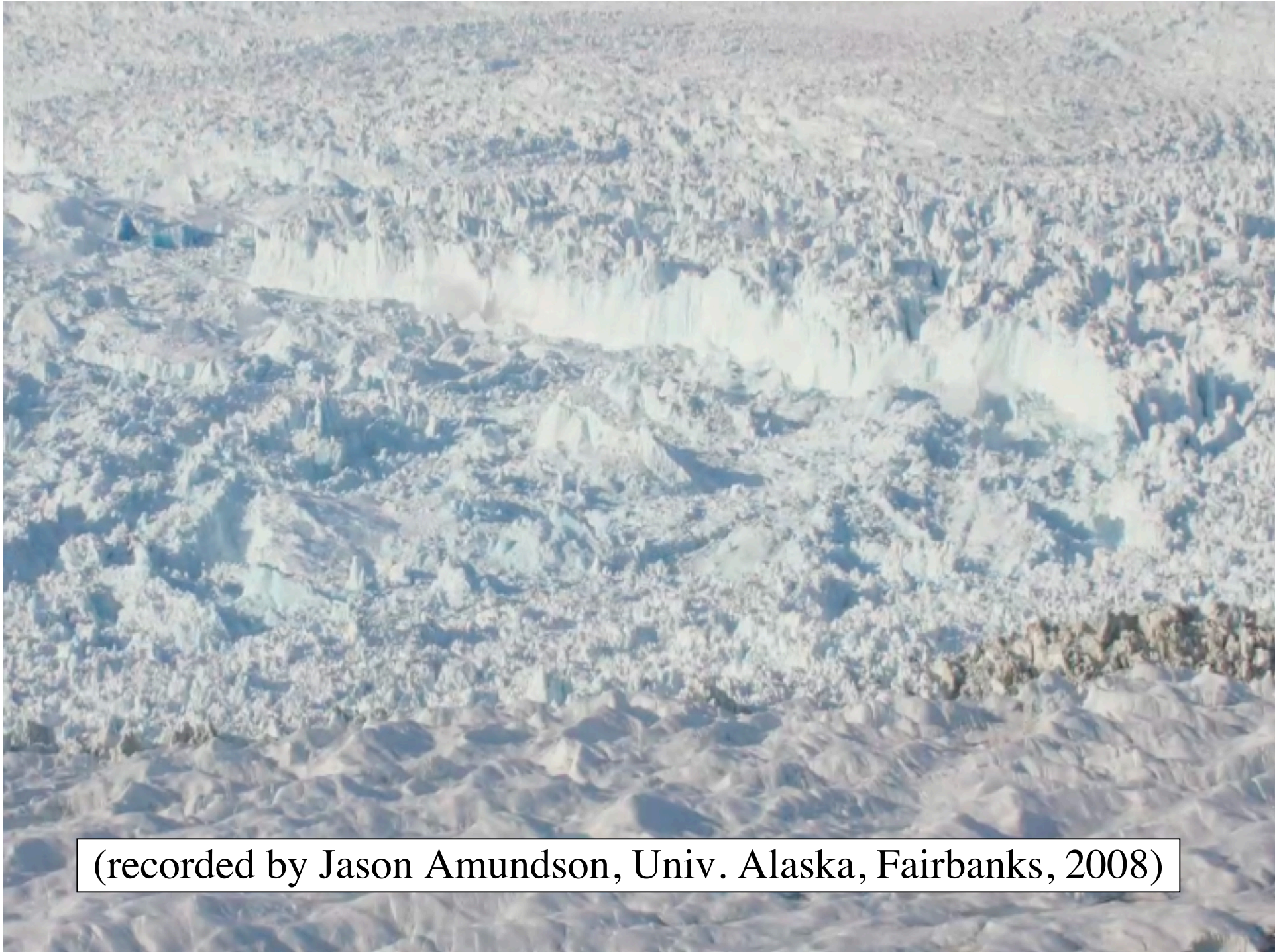
Long period of calved block turnover, because:

1. Long pendulum period (size scale large);
2. Small gravity drive,  $\rho_{\text{water}} \approx \rho_{\text{ice}}$ ;
3. Mélange adds effective mass.



Tsai, Rice, Fahnestock, *JGR*, 2008





(recorded by Jason Amundson, Univ. Alaska, Fairbanks, 2008)





(recorded by Jason Amundson, Univ. Alaska, Fairbanks, 2008)





(recorded by Jason Amundson, Univ. Alaska, Fairbanks, 2008)





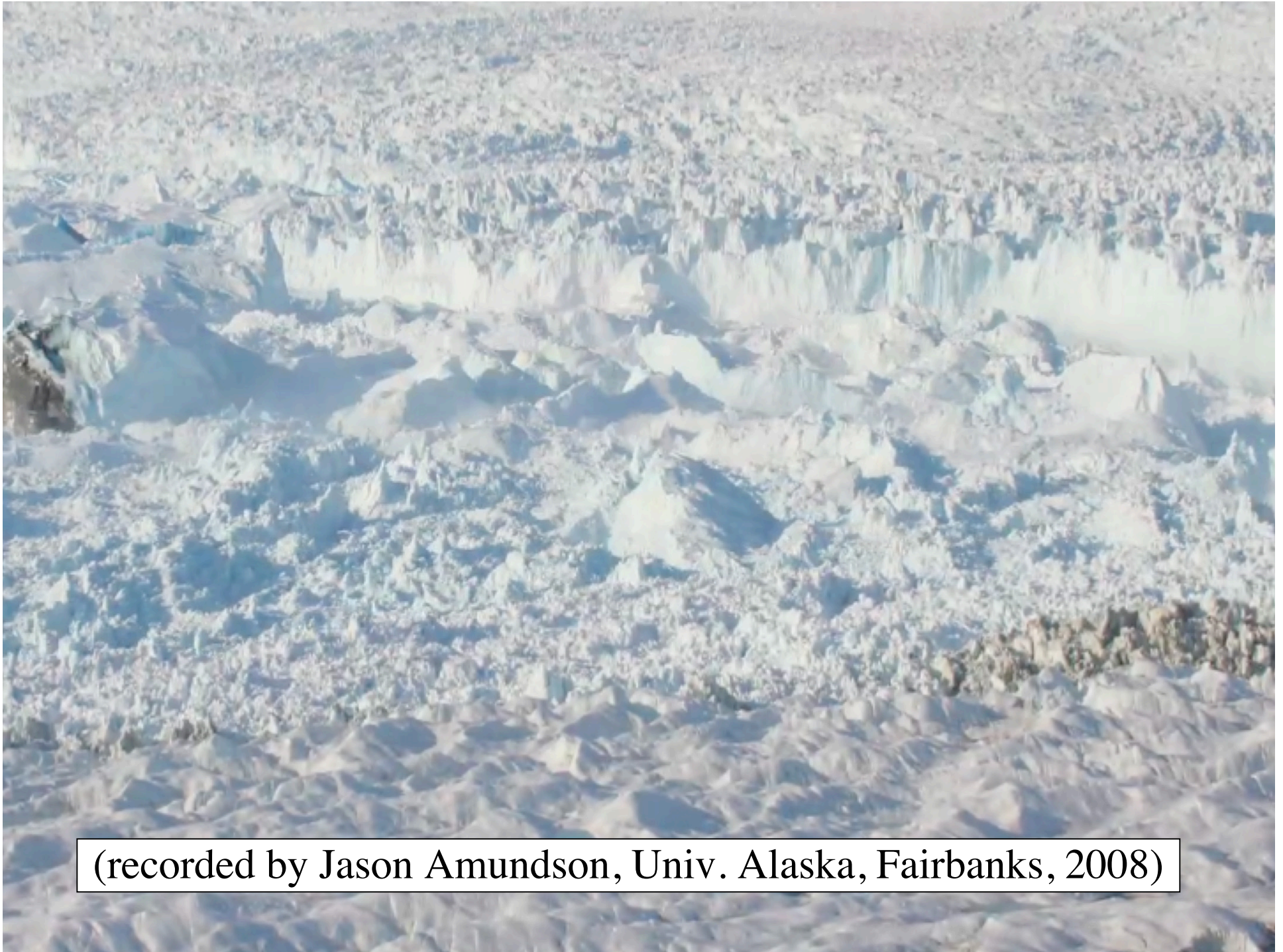
(recorded by Jason Amundson, Univ. Alaska, Fairbanks, 2008)





(recorded by Jason Amundson, Univ. Alaska, Fairbanks, 2008)



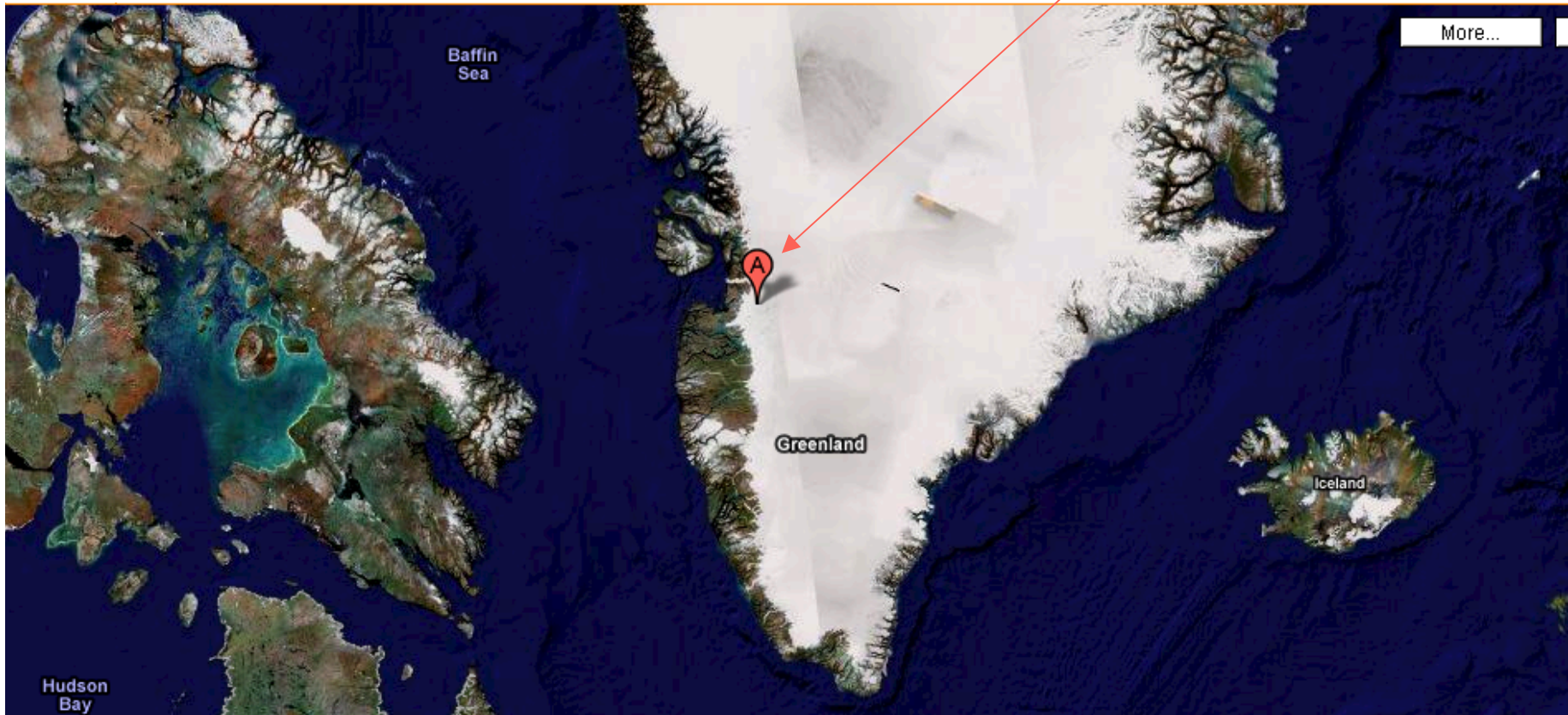


(recorded by Jason Amundson, Univ. Alaska, Fairbanks, 2008)



**A natural hydraulic fracture of interest for evaluating scenarios of accelerated deglaciation**

**Where are we?  
A below**



Study motivated by the paper *Fracture Propagation to the Base of the Greenland Ice Sheet During Supraglacial Lake Drainage*, by Das, Joughin, Behn, Howat, King, Lizarralde & Bhatia, *Science*, May 2008.

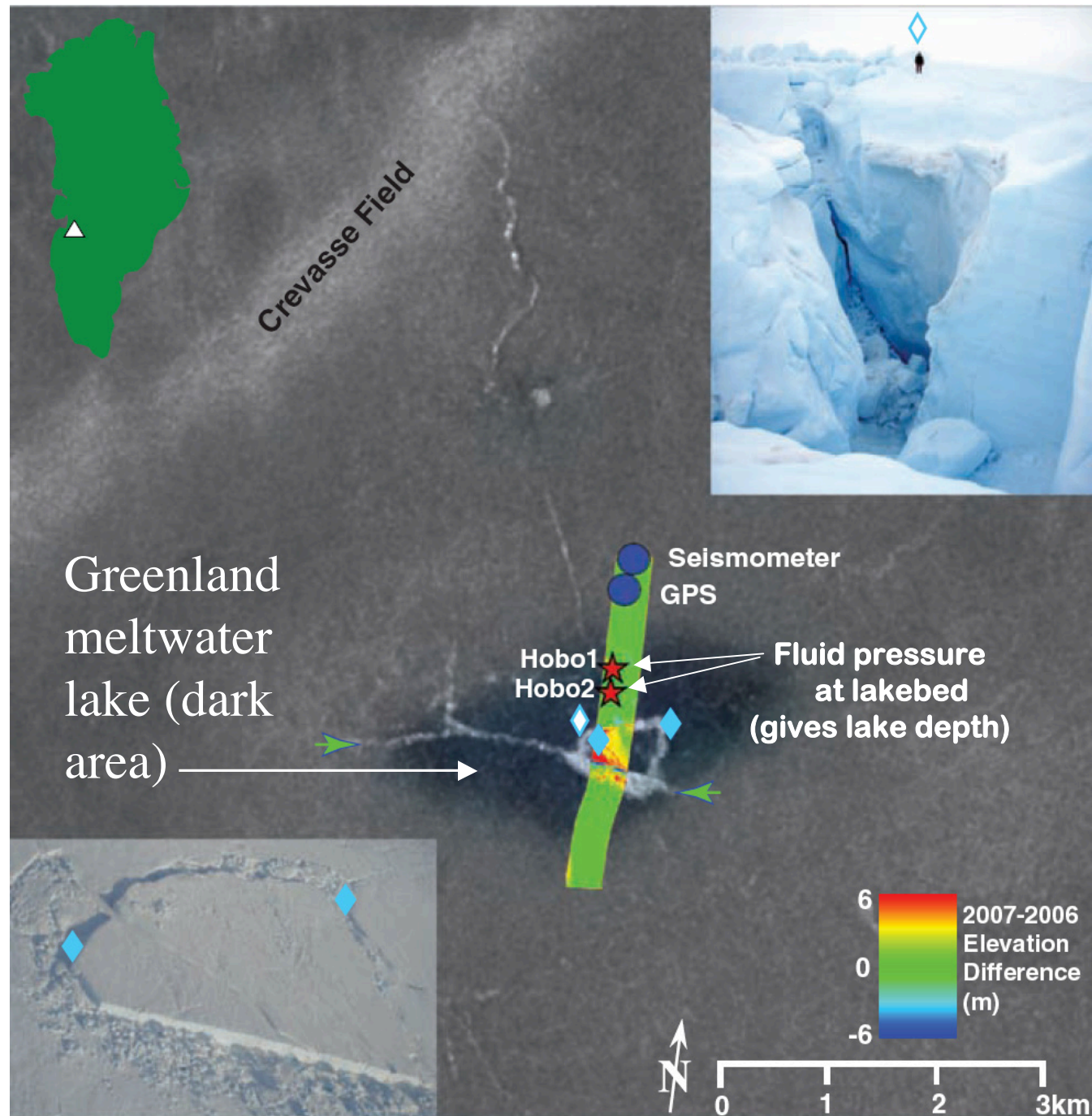


Study motivated by the paper *Fracture Propagation to the Base of the Greenland Ice Sheet During Supraglacial Lake Drainage*, by Das, Joughin, Behn, Howat, King, Lizarralde & Bhatia, *Science*, May 2008.



(Das et al.,  
*Sci.*, 2008)

Early October 2006  
SAR image (gray-  
scale background)  
overlaid with a  
semi-transparent  
image recorded by  
NASA's Moderate  
Resolution Imaging  
Spectroradiometer  
(MODIS) showing  
the lake extent  
(blue) on 29 July  
2006.

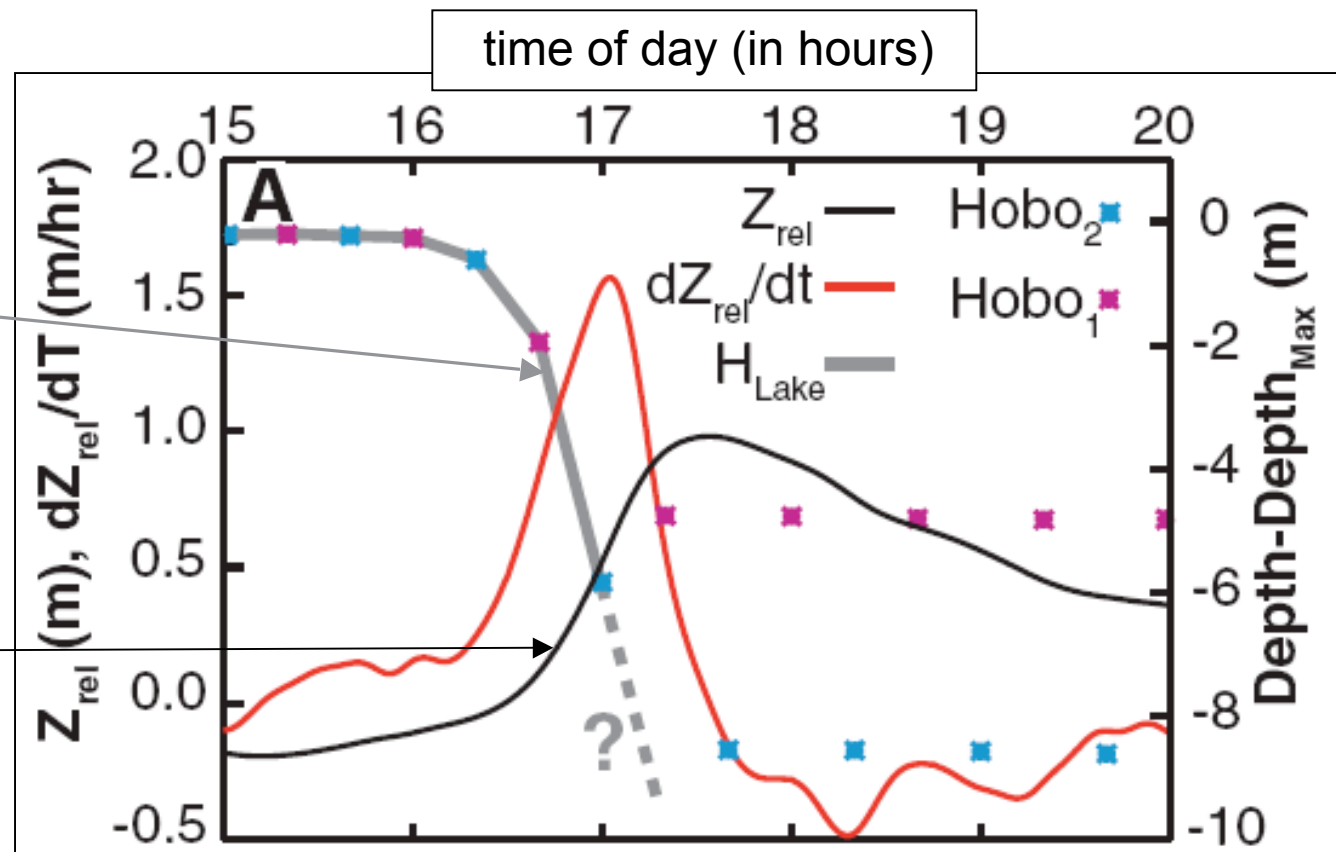


- *Supraglacial meltwater lake* began filling July 2006
- Maximum  $\sim 0:00$  29 July 2006,  $44 \times 10^6 \text{ m}^3$ ,  $5.6 \text{ km}^2$
- Level slowly/steadily falls,  $15 \text{ mm/hr}$
- Rapid from 16:00-17:30, max  $12 \text{ m/hr}$  ( $Q > 10,000 \text{ m}^3/\text{s}$ ),  
avg  $Q \sim 8,700 \text{ m}^3/\text{s}$  [Compare, Niagra Falls  $Q \sim 6,000 \text{ m}^3/\text{s}$ ]

(Das et al.,  
*Sci.*, 2008)

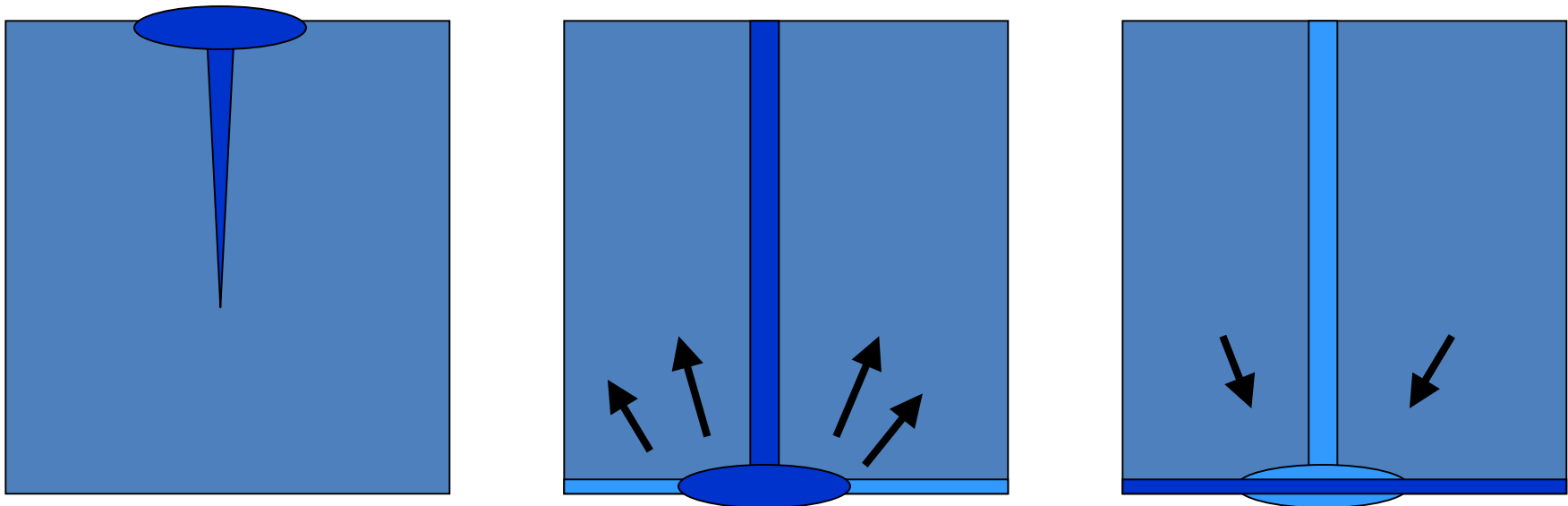
Falling  
lake level  
[m]  
(right scale)

Ice surface  
uplift [m]  
(left scale)



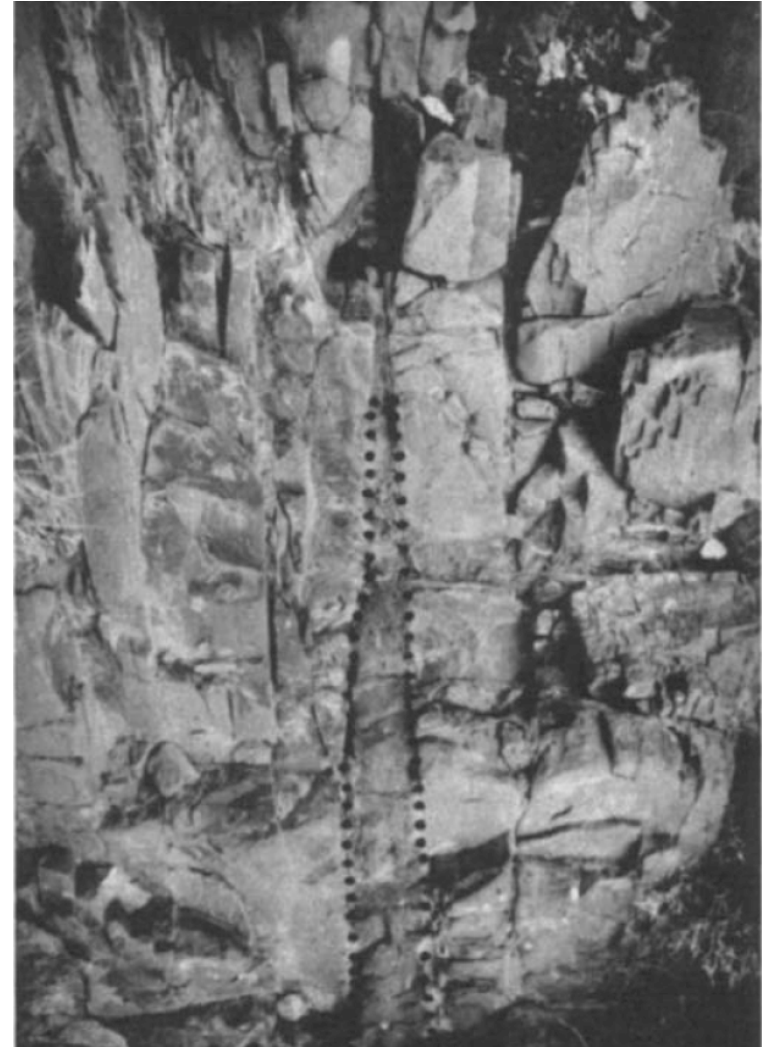
## *Interpretation*

- Initially: Crack/moulin system gradually propagates to bed by *Weertman* gravitational instability,  $\rho_{water} > \rho_{ice}$  .
- Middle Stage: Hydraulic cracking and flooding along bed by over-pressure,  $p > \sigma_o$  ( $\sigma_o$ = ice overburden pressure).
- End: Fracture closes, subglacial water layer drains.



Rubin, ***Propagation of magma-filled cracks*** [Annu. Rev. Earth Planet. Sci., 1995]

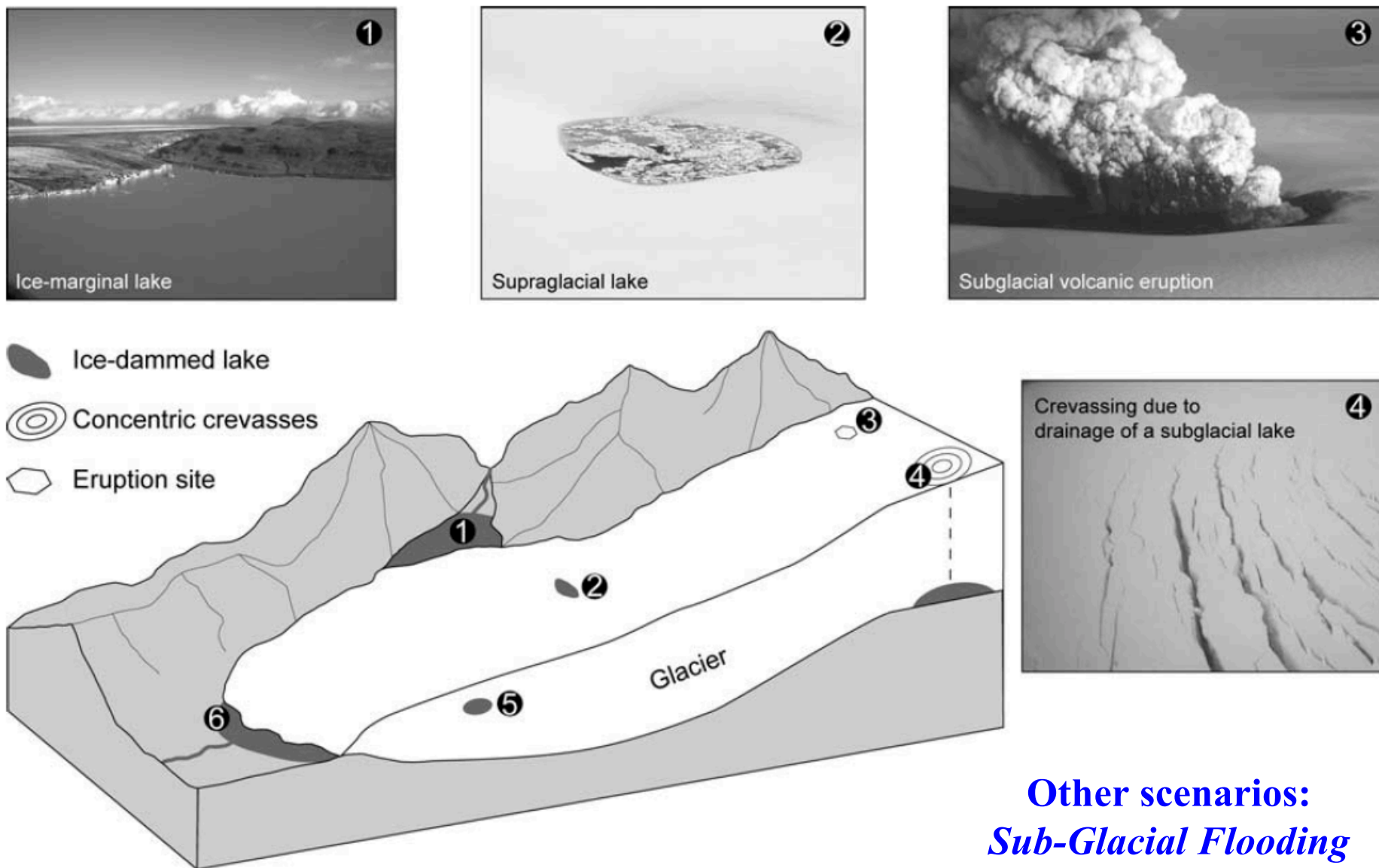
$$\rho_{\text{magma}} < \rho_{\text{rock}}$$



Basaltic dike at tip of Reykjanes Peninsula, southwest Iceland, exposed by glacial erosion (did not make it to surface). Thickness = 40 cm.

Dike (boundaries dotted) terminating in shear zone on Colorado Plateau.





**Other scenarios:  
Sub-Glacial Flooding  
(Jökulhlaup)**

**Figure 1.** Reservoir sites and meltwater sources for jökulhlaups.

from: Roberts, M. J. (2005), Jökulhlaups: A reassessment of floodwater flow through glaciers, *Rev. Geophys.*, 43, RG1002.

## Alaska Looks for Answers in Glacier's Summer Flood Surges

**New York Times  
July 22, 2013**

**First observed  
in July 2011,  
also in July  
2012 & 2013.**

**“... in July  
2011, ... an  
estimated ten  
billion gallons  
gushed out in  
three days ...  
two smaller  
bursts this  
year ...”**



Mathew Ryan Williams for The New York Times

**Visitors leaving caves under the Mendenhall Glacier, near Juneau,  
Alaska. Unpredictable flood surges have elevated concerns.**

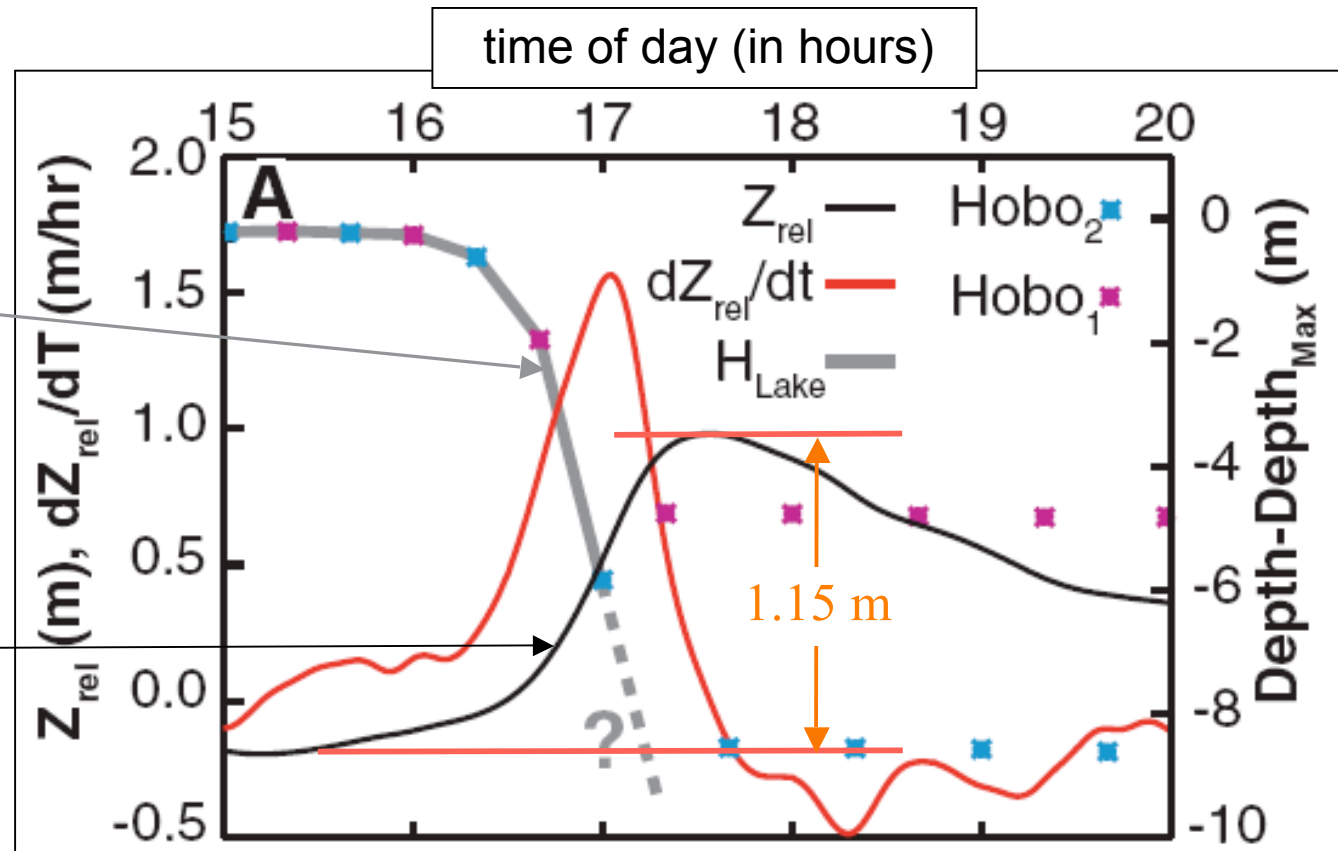
By [KIRK JOHNSON](#)

**JUNEAU, Alaska -- .... unpredictable flood surges at the [Mendenhall Glacier](#),  
about 14 miles from downtown Juneau, Alaska's capital ....**

(Das et al.,  
*Sci.*, 2008)

Falling  
lake level  
[m]  
(right scale)

Ice surface  
uplift [m]  
(left scale)



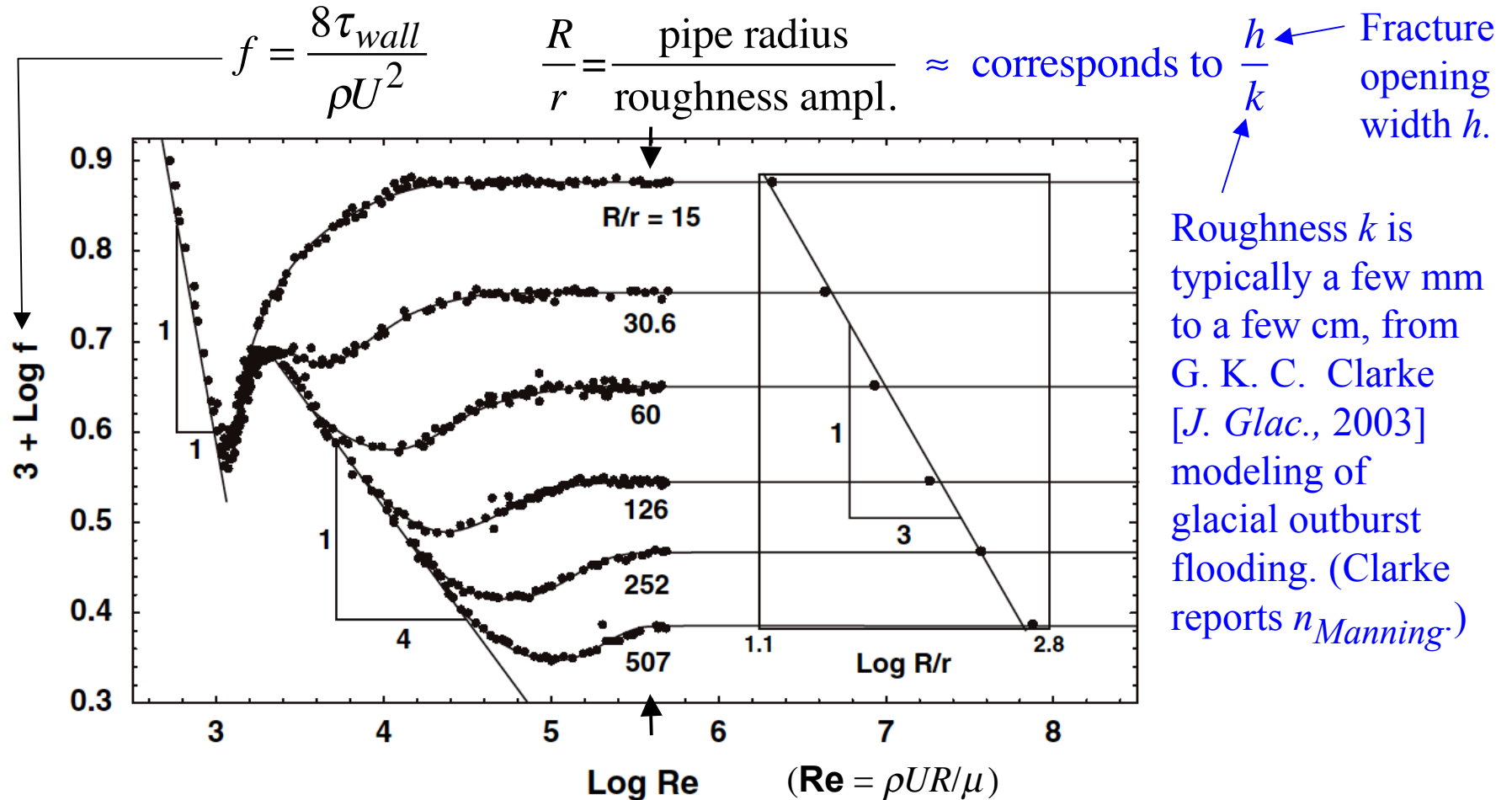
**Approximate radius  $R$  of sub - glacial fracture at full lake discharge :**

$$\pi R^2 \times \text{Uplift of } 1.15 \text{ m} = \text{Lake volume of } 44 \times 10^6 \text{ m}^3 \Rightarrow R \approx 3.5 \text{ km}$$

$$\Rightarrow \text{Average growth speed} \approx R / 1.2 \text{ hr} \approx 3 \text{ km / hr}$$

$$\Rightarrow \text{Reynolds number } \mathbf{Re} \text{ for flow in fracture} \approx \frac{3 \text{ km / hr} \times 0.5 \text{ m}}{10^{-6} \text{ m}^2/\text{s}} \approx 4 \times 10^5$$

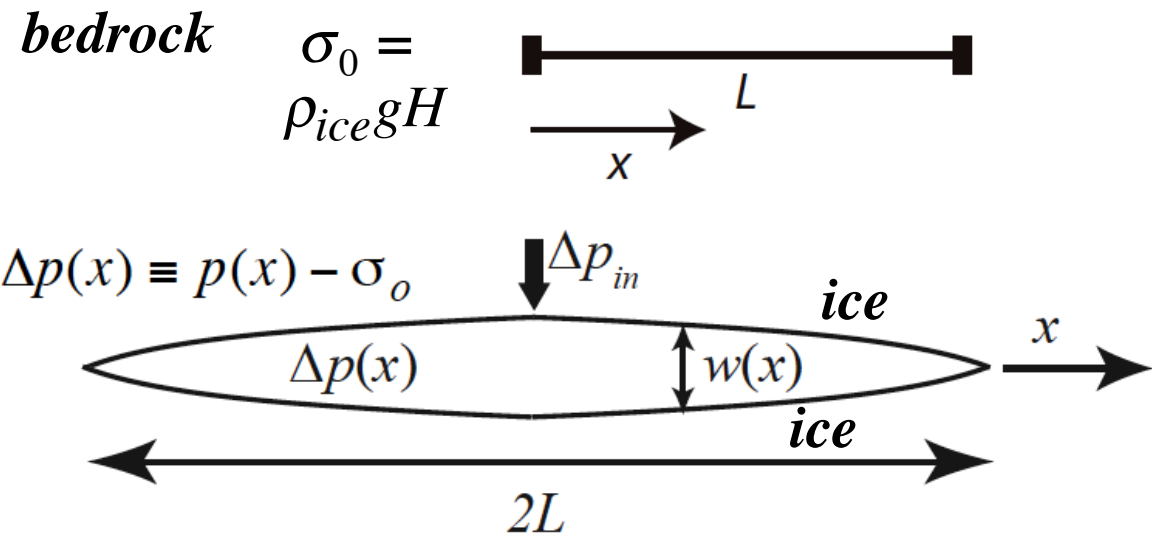
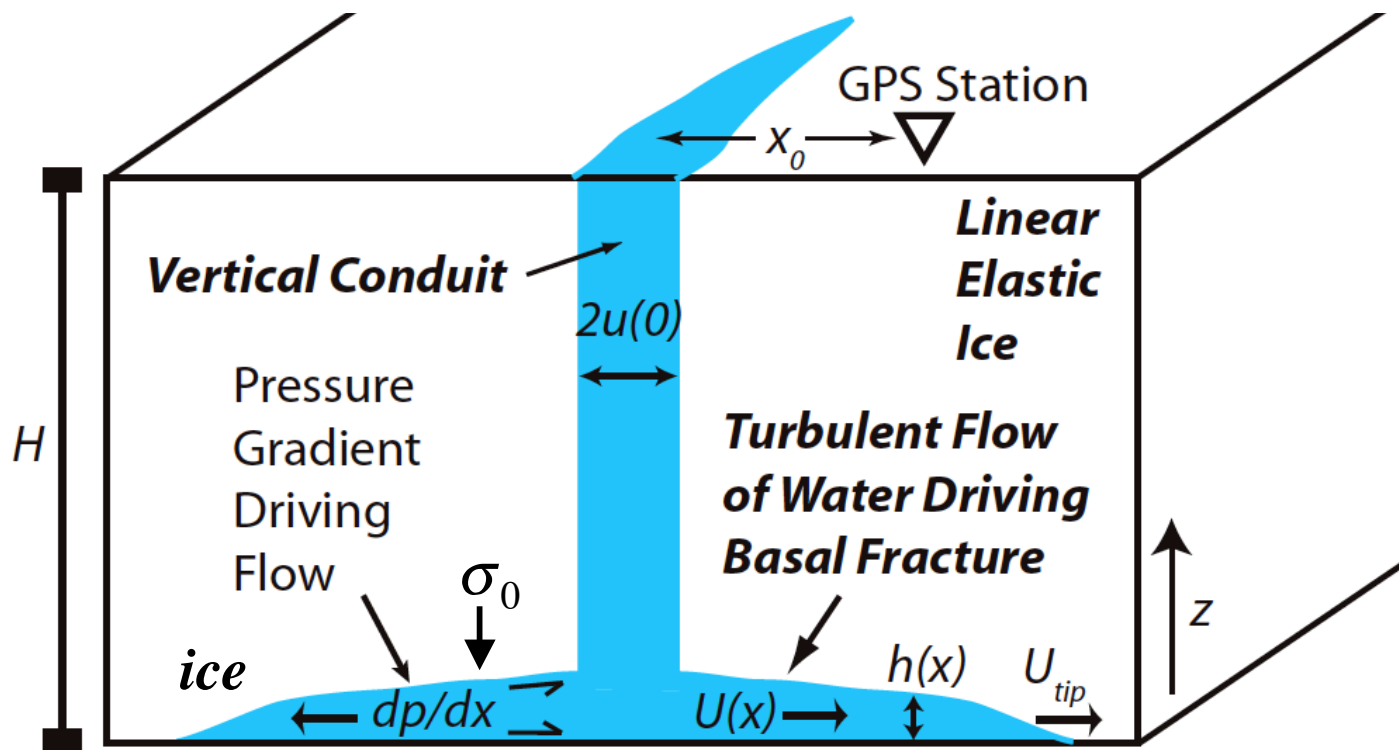
Gioia & Chakraborty [*PRL*, 2006] replot, Nikuradse [1933] rough-wall pipe-flow data



Nikuradse's data, Darcy-Weisbach  $f$  versus Reynolds number  $\text{Re}$ , pipe flow with rough walls. At large  $\text{Re}$ ,  $f$  becomes independent of  $\text{Re}$ .

Inset: Manning-Strickler scaling,  $f \approx 0.143(r/R)^{1/3}$ . Means  $f \approx 0.143(k/h)^{1/3}$ .





$$h(x,t) \approx \xi w(x,t), \quad \xi \approx 0.55$$

# Governing Equations, valid for range $L \ll H = \text{ice thickness} \approx 1 \text{ km}$

[ Tsai & Rice, *JGR*, 2010 ]

$p(x,t) - \sigma_0$ ,  $h(x,t) = \xi w(x,t)$ , and  $U(x,t)$  related by

- Linear elasticity for cracks:  
 ( $w = \text{opening in homog. ice}$ ;  
 $h = \text{opening in ice/rock}$ )

$$p(x,t) - \sigma_0 = \frac{E'}{2\pi\xi} \int_{-L}^L \frac{\partial h(x',t)}{\partial x'} \frac{dx'}{x-x'}$$
- Fracture mechanics, ice-rock interface:  
 (toughness  $K_{Ic} \approx 0.1 \text{ MPa m}^{1/2}$  ;  
 negligible, for  $L > \sim 10 \text{ m}$ )

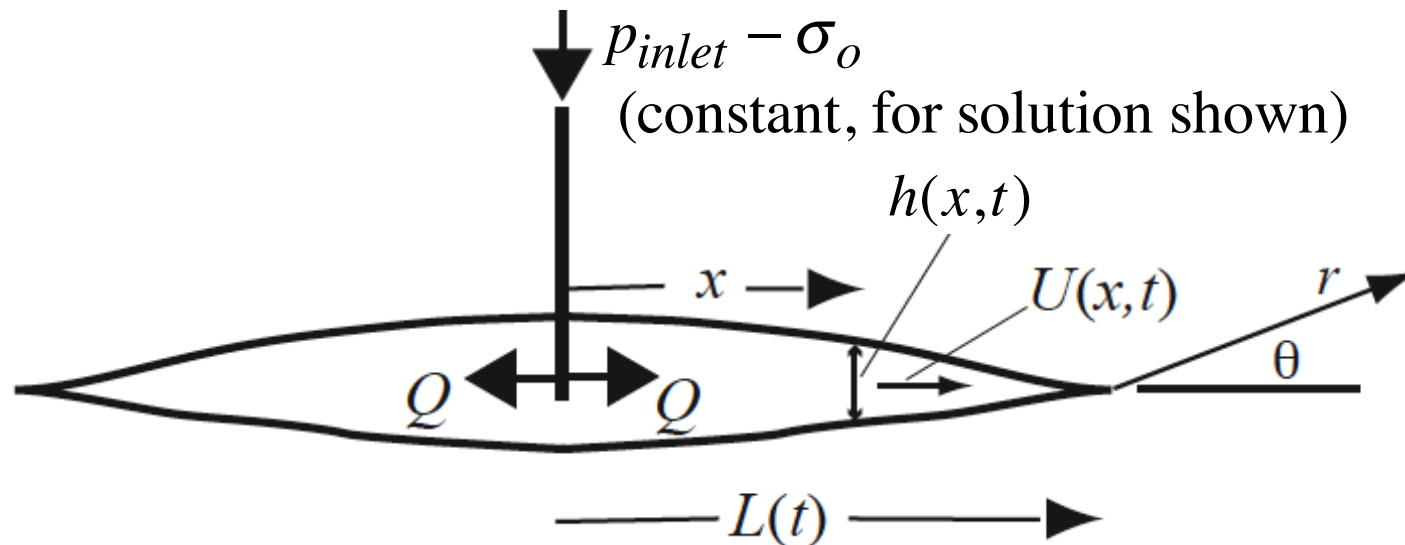
$$K_{Ic} = 0 \Rightarrow r^{1/2} \sigma_{ij} \rightarrow 0 \text{ as } r \rightarrow 0$$
- Conserv. of fluid mass (fluid volume):

$$\frac{\partial(hU)}{\partial x} + \frac{\partial h}{\partial t} = 0$$
- Manning-Strickler turbulent flow:  
 ( $k = \text{Nikuradse}$   
 roughness scale)

$$-h \frac{\partial p}{\partial x} = \underbrace{0.0357}_{2\tau_{wall}} \rho U^2 \frac{k^{1/3}}{h^{1/3}}$$

**Self-Similar Solution** (2D plane-strain,  $L \ll H$  [Tsai & Rice, *JGR*, 2010])

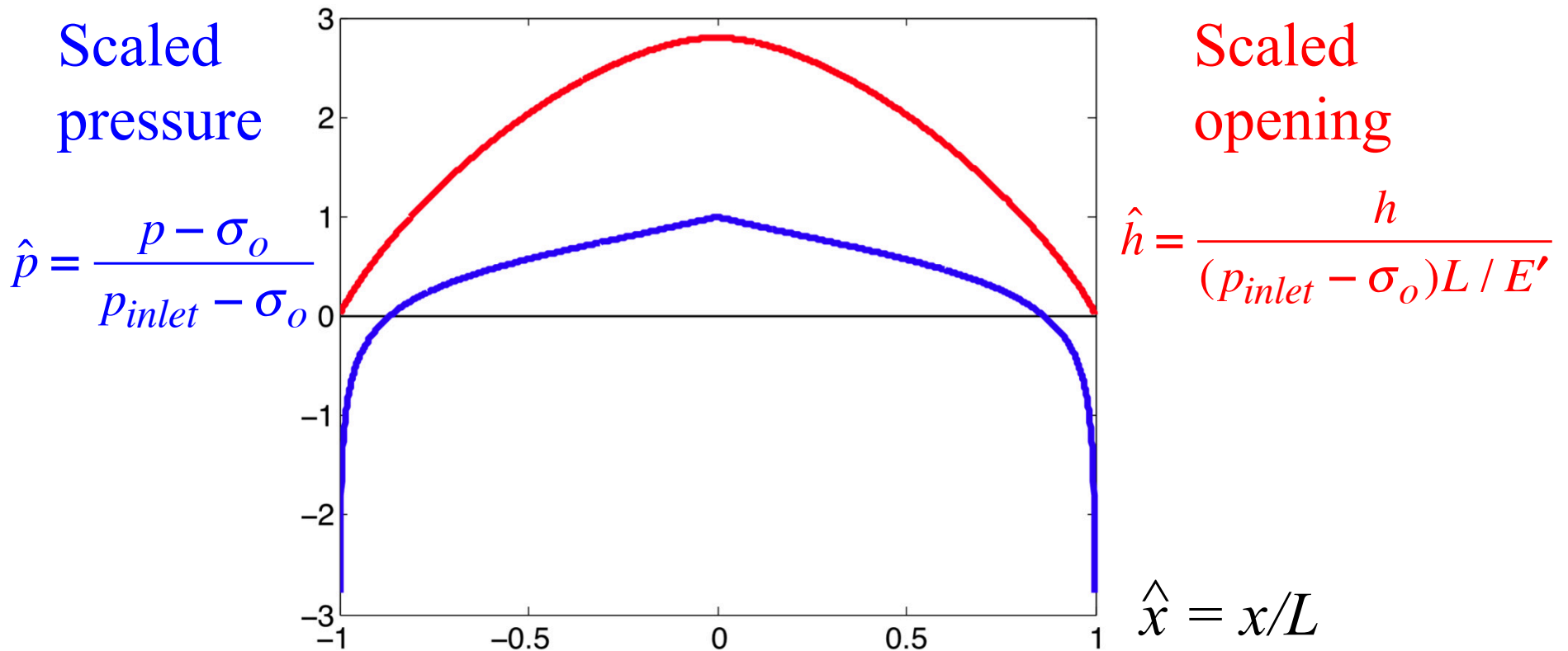
(Approach similar to Adachi and Detournay [*Int. J. Numer. Anal. Meth. Geomech.*, 2002], who solved the same problem for a power-law viscous fluid in locally laminar flow.)



**Our case** (turbulent, high **Re**):  $\tau_{wall} = \frac{f}{8} \rho U^2 = -\frac{1}{2} h \frac{\partial p}{\partial x}$ ,  $f = 0.143 \left( \frac{k}{h} \right)^{1/3}$

$$L(t) = C t^{6/5}, \quad h(x,t) \sim C t^{6/5} F(x / L(t)),$$

$$p(x,t) - p_o = G(x / L(t)), \quad U(x,t) = C t^{1/5} H(x / L(t)).$$



- Crack growth rate:

$$\frac{dL(t)}{dt} = 5.17 \sqrt{\frac{p_{inlet} - \sigma_o}{\rho}} \left( \frac{p_{inlet} - \sigma_o}{E'} \right)^{2/3} \left( \frac{L(t)}{k} \right)^{1/6}$$



***Making contact with the observations [Das et al., '08] of surface-lake drainage driving hydraulic fracture near a margin of the Greenland Ice Sheet, and using analytical results for self-similar plane strain fracture:***

For  $p_{hydrostatic} - \sigma_o = 0.87 \text{ MPa}$  ,  $k = 1 \text{ cm}$  ,  $L = 1 \text{ km}$ :

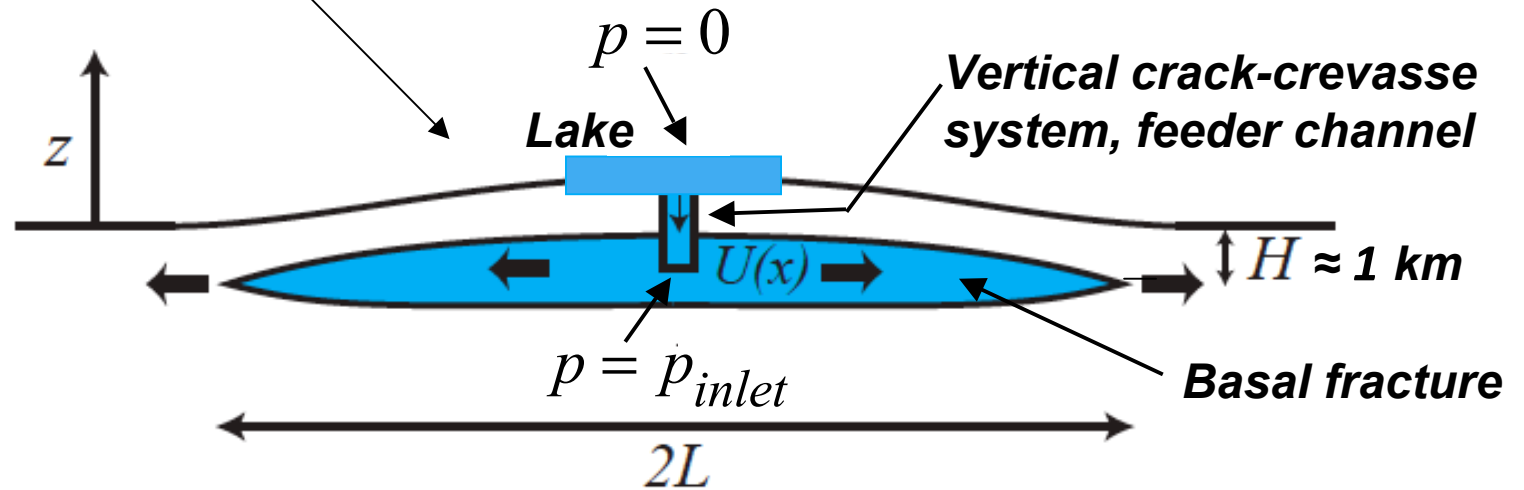
- If  $p_{inlet} - \sigma_o = p_{hydrostatic} - \sigma_o$  ,  $U_{tip} = 9.4 \text{ km/hr}$  ,  $h_{avg} = 0.13 \text{ m}$ .
  - If  $p_{inlet} - \sigma_o = 0.5 (p_{hydrostatic} - \sigma_o)$  ,  $U_{tip} = 4.3 \text{ km/hr}$  ,  $h_{avg} = 0.07 \text{ m}$ .
  - If also  $k$  decreased by factor of 5, to  $k = 2 \text{ mm}$  ,  $U_{tip} = 5.6 \text{ km/hr}$  ,  $h_{avg} = 0.07 \text{ m}$ .
- 

- Young's modulus  $E = 6.2 \text{ GPa}$  at  $-5^\circ\text{C}$  [Jellinek et al., '55] and Poisson's ratio  $\nu = 0.3$  [Vaughan, '95], gives  $E' = 6.8 \text{ GPa}$ .
- Liquid density  $\rho = 1000 \text{ kg/m}^3$ , ice density  $\rho_{ice} = 910 \text{ kg/m}^3$ .
- Ice thickness  $H = 980 \text{ m}$  [Das et al., '08], so  $p_{hydrostatic} - \sigma_o = 0.87 \text{ MPa}$ .
- Dependence of  $U$  on channel wall roughness  $k$  is weak (power law exponent = 1/6); estimate  $k = 1 \text{ cm}$ , which is consistent with  $n_{\text{Manning}} \sim 0.018 \text{ s m}^{-1/3}$ .

[Tsai & Rice, *J. Appl. Mech.*, 2012]

Finite  $L / H$

*Features not to scale!*



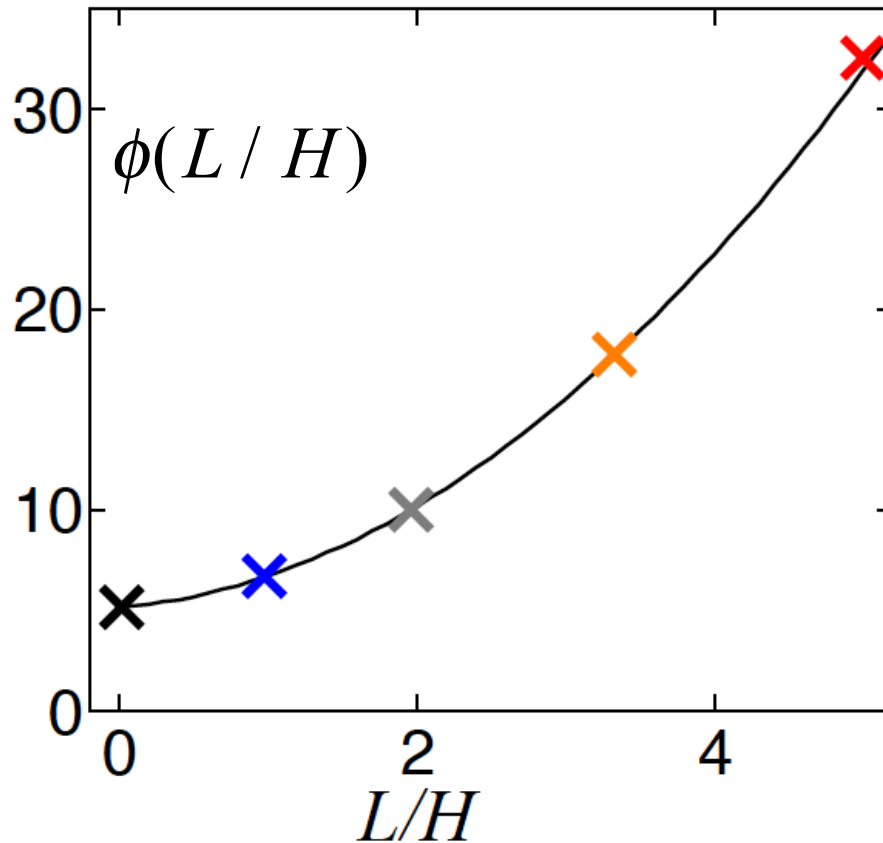
$$p_{hydrostatic} \equiv \rho_{water} g H \geq p_{inlet} \geq \rho_{ice} g H \equiv \sigma_o$$

**Schematic for turbulent hydraulic fracture**

(Analysis simplified by treating ice and bed as a *homogeneous* medium.)

### Crack growth rate =

$$\frac{dL}{dt} \equiv U_{tip} = \left( \frac{p_{inlet} - \sigma_o}{\rho} \right)^{1/2} \left( \frac{p_{inlet} - \sigma_o}{E'} \right)^{2/3} \left( \frac{L}{k} \right)^{1/6} \phi(L/H)$$

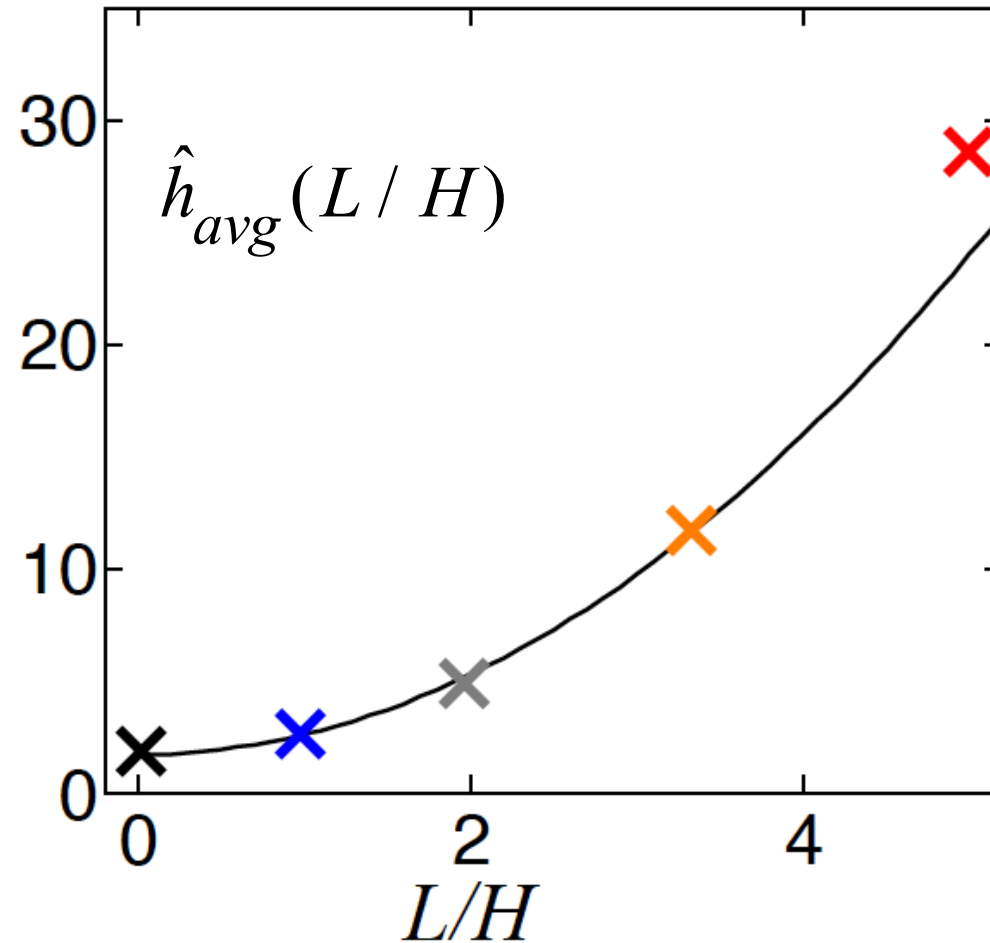


For a given  $L/H$ ,  
 $dL/dt \propto (p_{inlet} - \sigma_o)^{7/6}$

—  $\phi(L/H) \approx 5.13[1 + 0.125(L/H) + 0.183(L/H)^2]$



**Average opening of fracture**  $\equiv h_{avg} = \frac{(p_{inlet} - \sigma_o)L}{E'} \hat{h}_{avg}(L/H)$



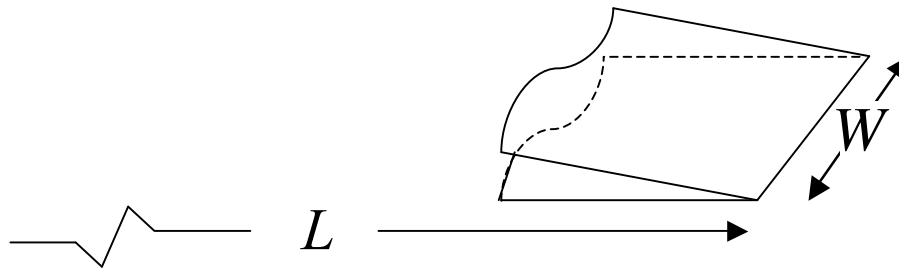
—  $\hat{h}_{avg}(L/H) \approx 1.72 [1 + 0.517 (L/H)^2]$

***Volumetric inflow rate to glacier bed***

***( $W \sim 2 - 3$  km is effective length perpendicular to plane for use of our 2D plane - strain solution - - 3D is needed!) :***

$$Q_{basal} = \frac{d(2LWh_{avg})}{dt} = \frac{2(p_{inlet} - \sigma_o)W}{E'} \frac{\partial[L^2 \hat{h}_{avg}(L/H)]}{\partial L} \frac{dL}{dt}$$

***( here,  $\partial[L^2 \hat{h}_{avg}(L/H)] / \partial L \approx 3.44L[1 + 1.035(L/H)^2]$  )***



***Note :*** For a given  $L/H$ ,  $dL/dt \propto (p_{inlet} - \sigma_o)^{7/6}$ ,  
 so  $Q_{basal} \propto (p_{inlet} - \sigma_o)^{13/6}$

[Rice & Platt, 2012-2013, in progress]

$$p_{hydrostat} \equiv \rho_{water}gH \geq p_{inlet} \geq \rho_{ice}gH \equiv \sigma_o$$

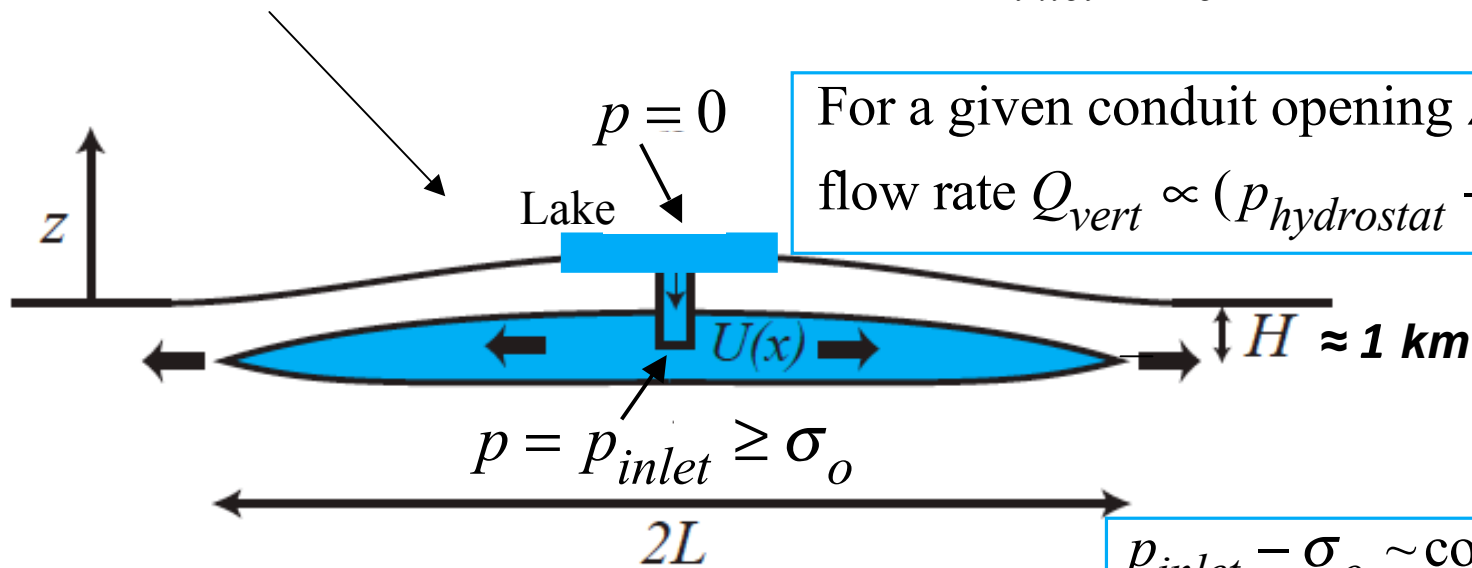
Finite  $L / H$

Average vertical conduit opening:  
 $\Delta\bar{u} = \Delta\bar{u}^{el} + \Delta\bar{u}^{cr}$  (elastic + prior creep)

$$\Delta\bar{u}^{el} \propto p_{inlet} - \sigma_o$$

*Features not to scale!*

For a given conduit opening  $\Delta\bar{u}$ , vertical flow rate  $Q_{vert} \propto (p_{hydrostat} - p_{inlet})^{1/2}$



$p_{inlet} - \sigma_o \sim$  controls flow rate  $Q_{basal}$  into basal fracture

**Schematic for turbulent hydraulic fracture**

(Analysis simplified by treating ice and bed as a *homogeneous* medium, thus  $h = w =$  opening.)

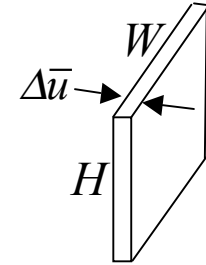
$p_{inlet}$  ultimately determined by setting  $Q_{basal} = Q_{vert}$



***To evaluate the vertical crack - crevasse system as a feeder channel :***

For evaluating **flow resistance**: Vertical crack-crevasse system treated as a vertical slit of depth  $H$ , uniform width  $W$ , and uniform (but time-dependent) opening gap  $\Delta\bar{u}$ :

$$\Rightarrow Q_{vert} \approx 1.97 \left( \frac{\rho g H - p_{inlet}}{\rho g H - \sigma_o} \right)^{1/2} g^{1/2} W \Delta\bar{u}^{3/2} \left( \frac{\Delta\bar{u}}{k} \right)^{1/6}$$



$\Delta\bar{u}$  = short-time **elastic** ( $\Delta\bar{u}^{el}$ ) + longer term **creep** ( $\Delta\bar{u}^{cr}$ )

**Elastic** opening gap  $\Delta\bar{u}^{el}$  calculated by 2D plane strain elasticity,  $\Delta\bar{u}^{el} = \frac{\pi(p_{inlet} - \sigma_o)}{2E'} W$

**Creep** opening gap  $\Delta\bar{u}^{cr}$  will be constant during the short timescale of rapid drainage.

Will depend on how long the vertical crack-crevasses system has been hydrostatically pressurized before nucleation of basal fracture.

**Power - law creep**,  $\dot{\gamma} / 2 = A(T)\tau^n$ , where  $n = 3$  (Glen's law) is typical for glacial flow.

$$\frac{d\Delta\bar{u}^{cr}}{dt} \approx \frac{\pi}{4} A(T) \left( \frac{(\rho - \rho_{ice})gH}{2n} \right)^3 W \text{ during hydrostatic pressure loading of walls}$$

**Define**  $C \equiv \frac{\Delta\bar{u}^{cr}}{(\Delta\bar{u}^{el})_{p_{inlet}=p_{hydrostat}}}$ , so that  $\Delta\bar{u} \approx C \frac{\pi(\rho g H - \sigma_o)}{2E'} W + \frac{\pi(p_{inlet} - \sigma_o)}{2E'} W$

**At  $-5^\circ\text{C}$ ,  $C = 1$ , is reached in  $\approx 13$  hours -- so we expect  $C > 1$  ( $> 16$  hr of slow leakage)**

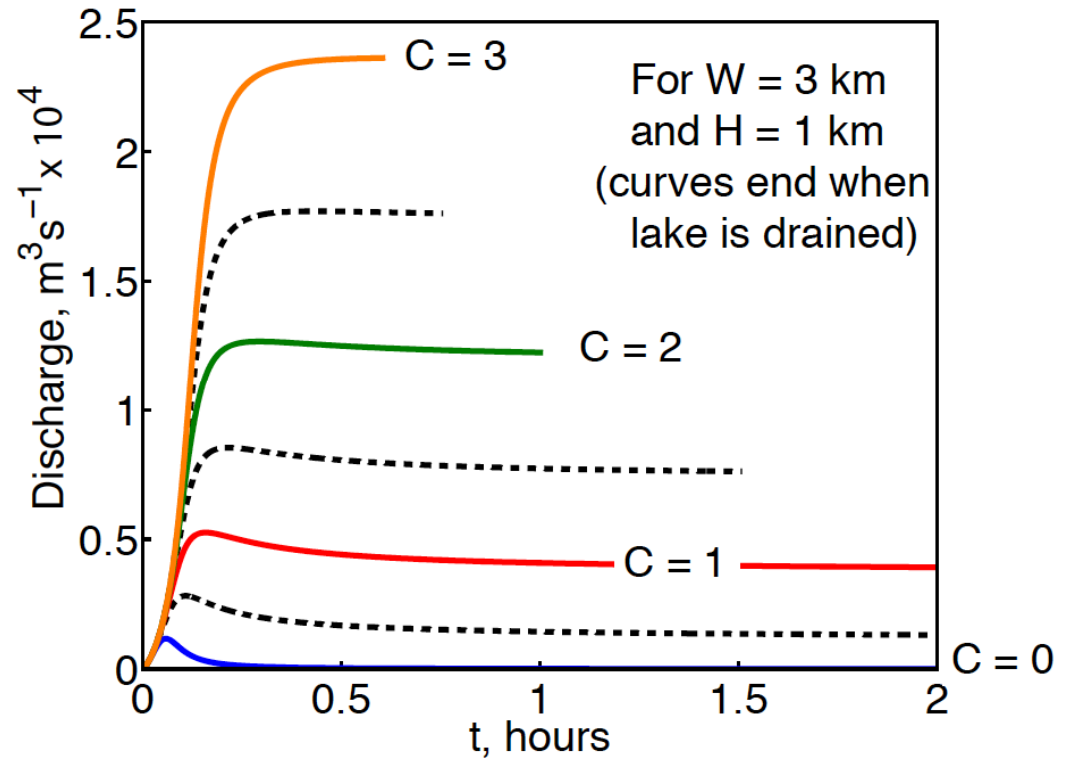
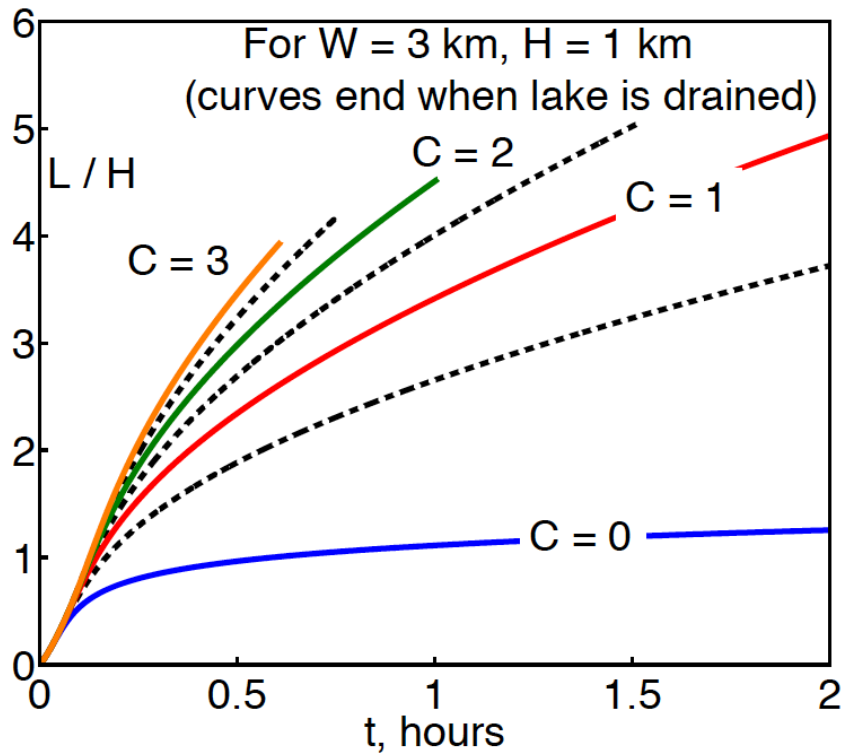
(based on  $H = 1$  km,  $E' = 6.8$  GPa,  $n = 3$ , and  $A = 9 \times 10^{-25} \text{s}^{-1} \text{Pa}^{-3}$ ).

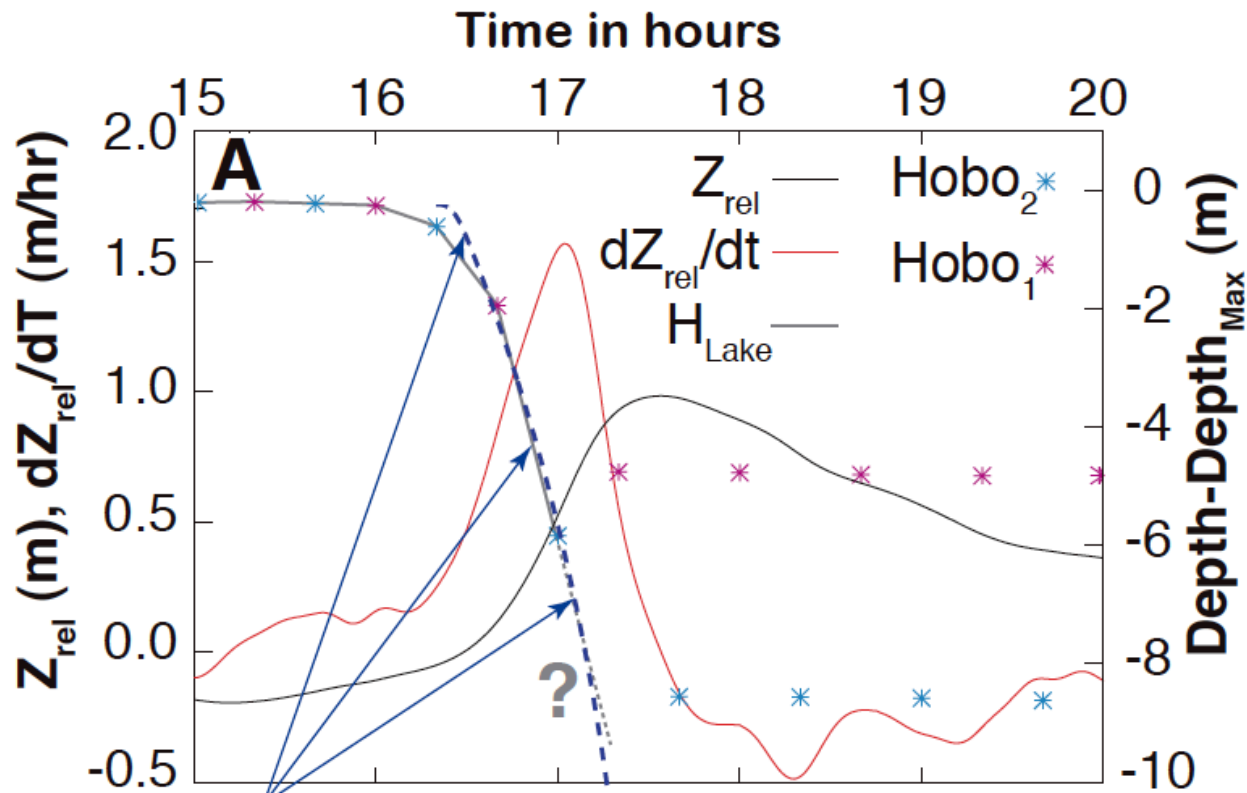
$$C = \frac{\text{prior creep opening of vertical crevasse channel}}{\text{elastic opening under hydrostatic pressurization}} = \frac{\Delta \bar{u}^{cr}}{(\Delta \bar{u}^{el})_{p=\text{hydrostatic}}}$$

$C = 1$  is achieved in  $\sim 13$  hours of hydrostatic pressurization

Slow prior drainage suggests at least  $\sim 16$  hours of prior high pressurization  $\Rightarrow C > 1$

Plots by John D. Platt:





Results of model including creep opening of vertical crack-crevasse system, with  $C = 1.75$  (creep opening = 1.75 X initial elastic opening),  $H = 1$  km, and  $W = 3$  km.

$C = 1.75 \Rightarrow$  Time for Drainage = 1.21 hr;

$\frac{\text{Lake Volume}}{\text{Crack Area } 2WL \text{ at Drainage}} = 1.54 \text{ m; compare, } 1.15 \text{ m GPS uplift } (Z_{rel}).$



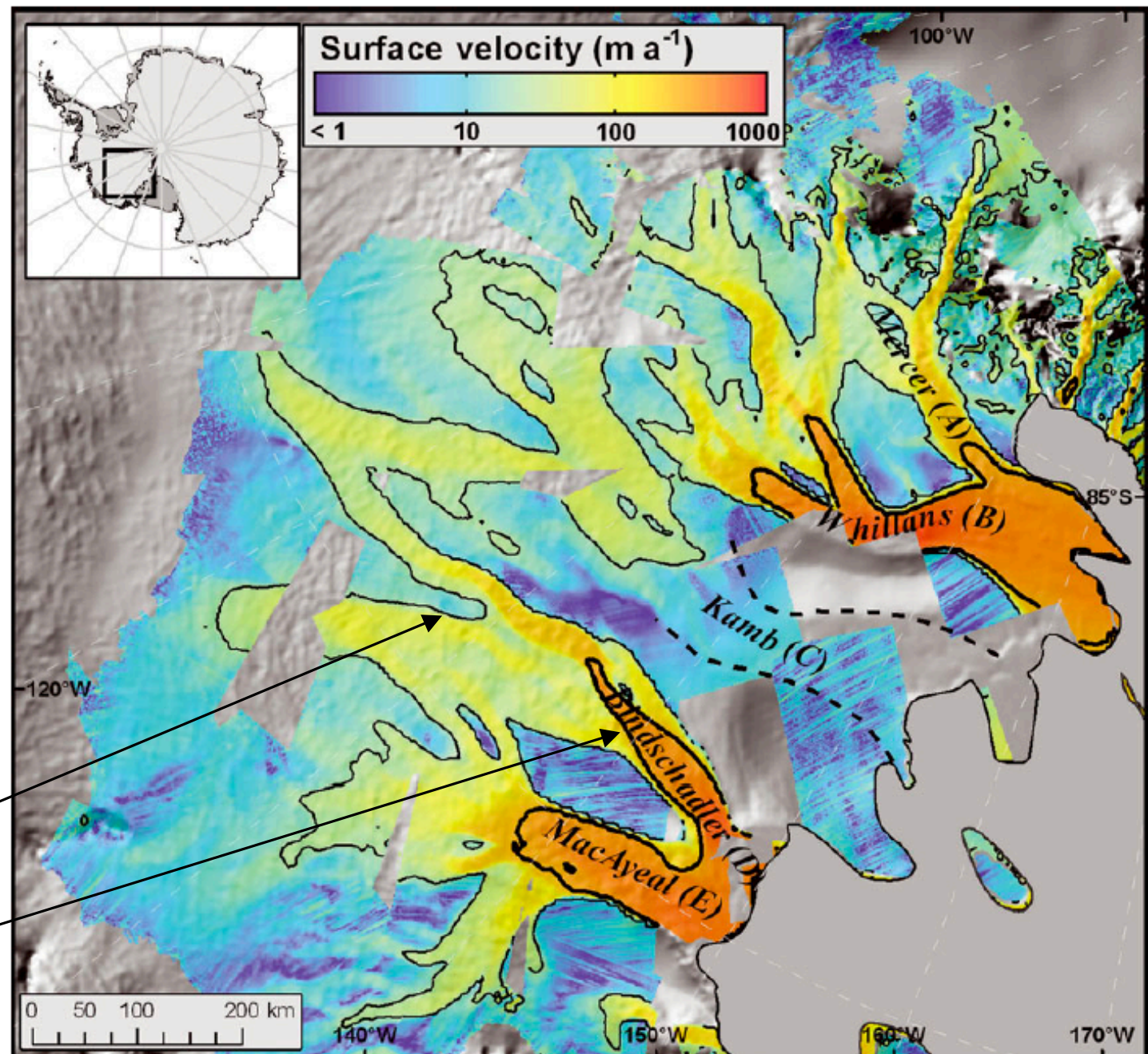


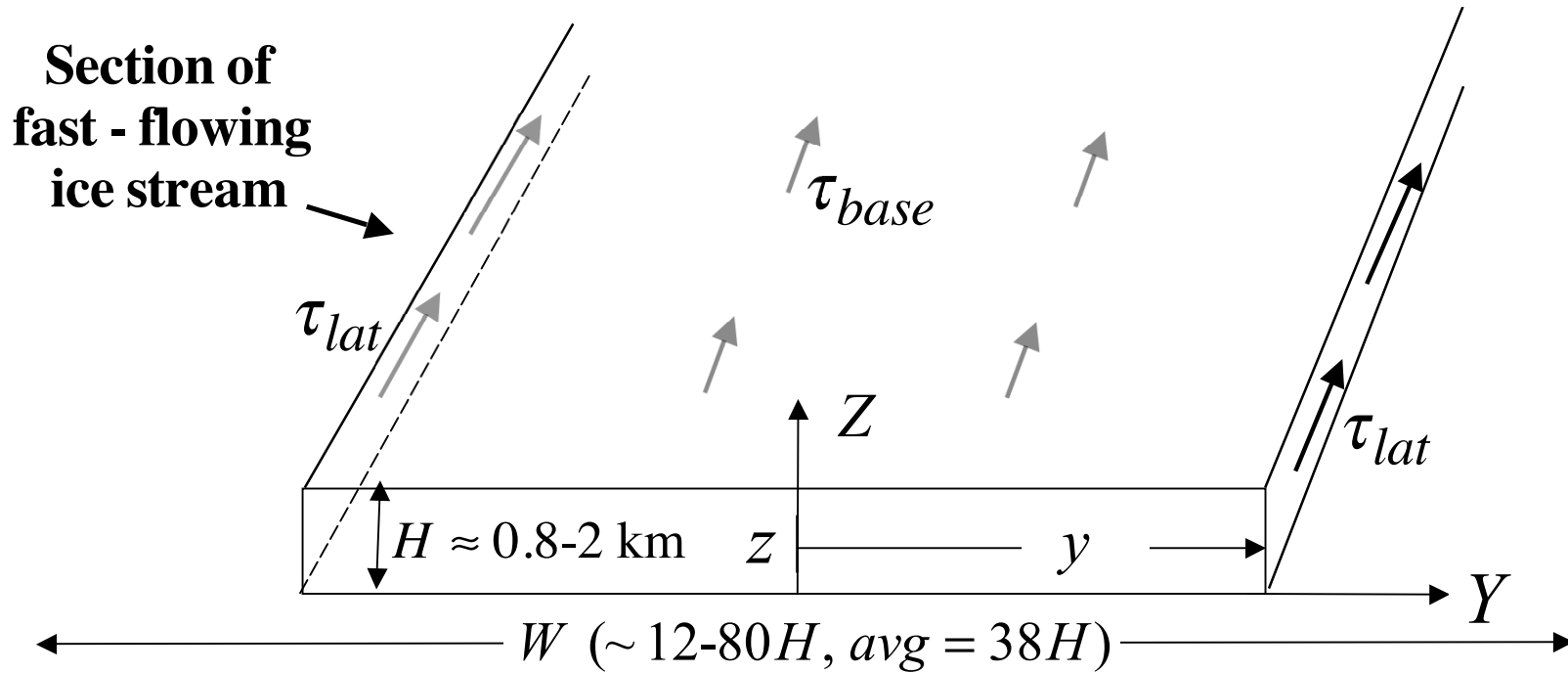
[from Le Brocq, Payne, Siegert & Alley, *J. Glac.*, 2009]

- **Western Antarctica, Siple Coast, Ice Streams,** flowing to the Ross Sea ice shelf.

- InSAR velocity (from Joughin et al., *J. Geophys. Res.*, 2002) overlaid on a digital elevation model (Bamber et al., 2009).

- Velocity contours shown are 25 m/yr (thin line) and 250 m/yr (thick line).





$$\tau_{grav} = \rho g H S \quad (S = \text{slope})$$

= downslope gravity force per unit base area

Equilibrium\*:  $\bar{\tau}_{lat} H = (\tau_{grav} - \tau_{base})_{avg} y$

$\bar{\tau}_{lat} \rightarrow (\tau_{grav} - \tau_{base})_{avg} \quad W / 2H$  at margins

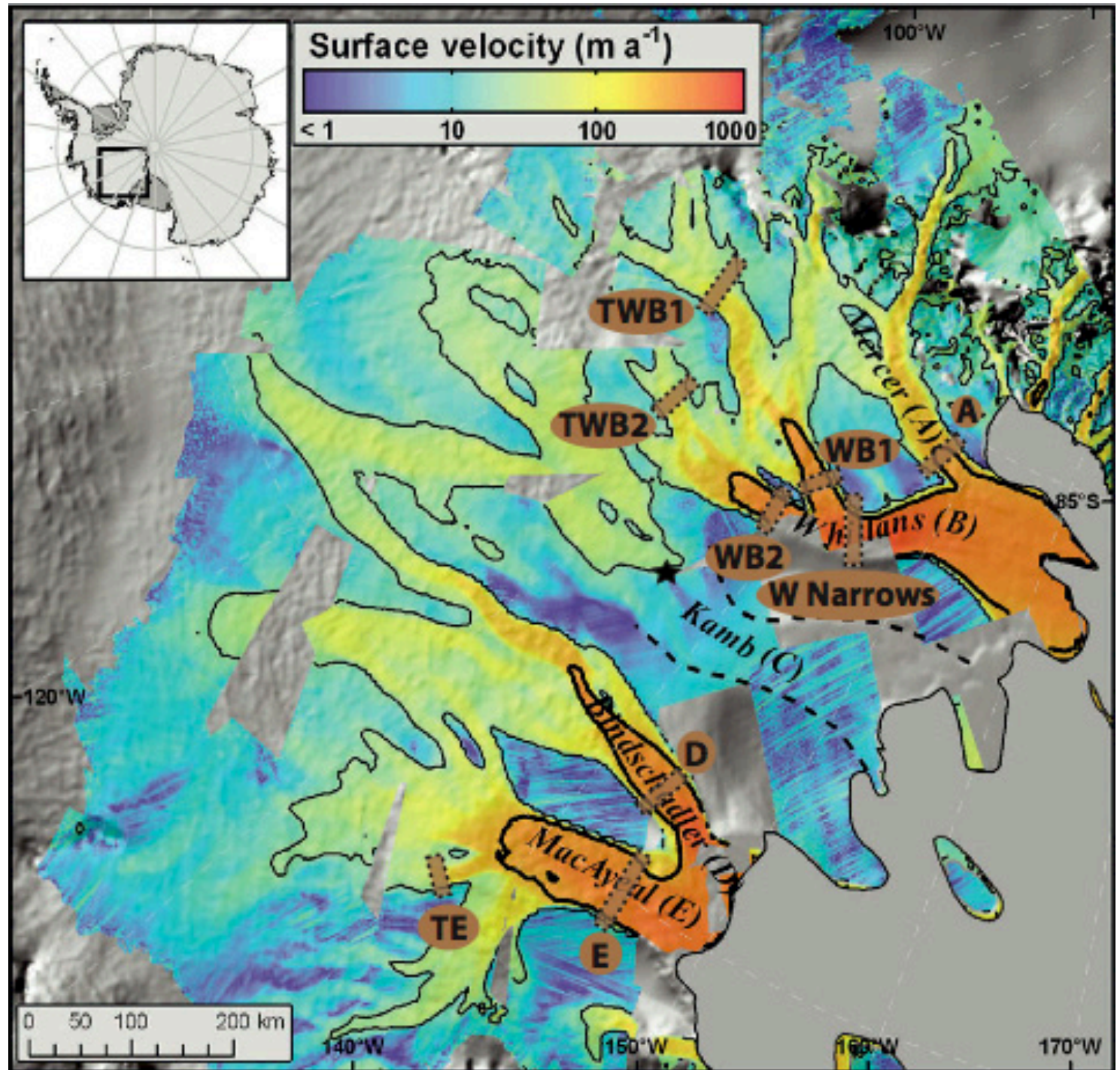
\*neglecting any variation in net axial force in sheet, roughly justified [Whillans and van der Veen, *J. Glac.*, 1993]

Increases with stream width  $W$  (~6-40 at current margins)

⇒ increasing strain rate,  
 $\dot{\gamma}_{lat} \sim \bar{\tau}_{lat}^3 \sim (W / H)^3$ ,  
 ⇒ increasing shear heating,  $\sim (W / H)^4$ ,  
 ⇒ onset of melting ?



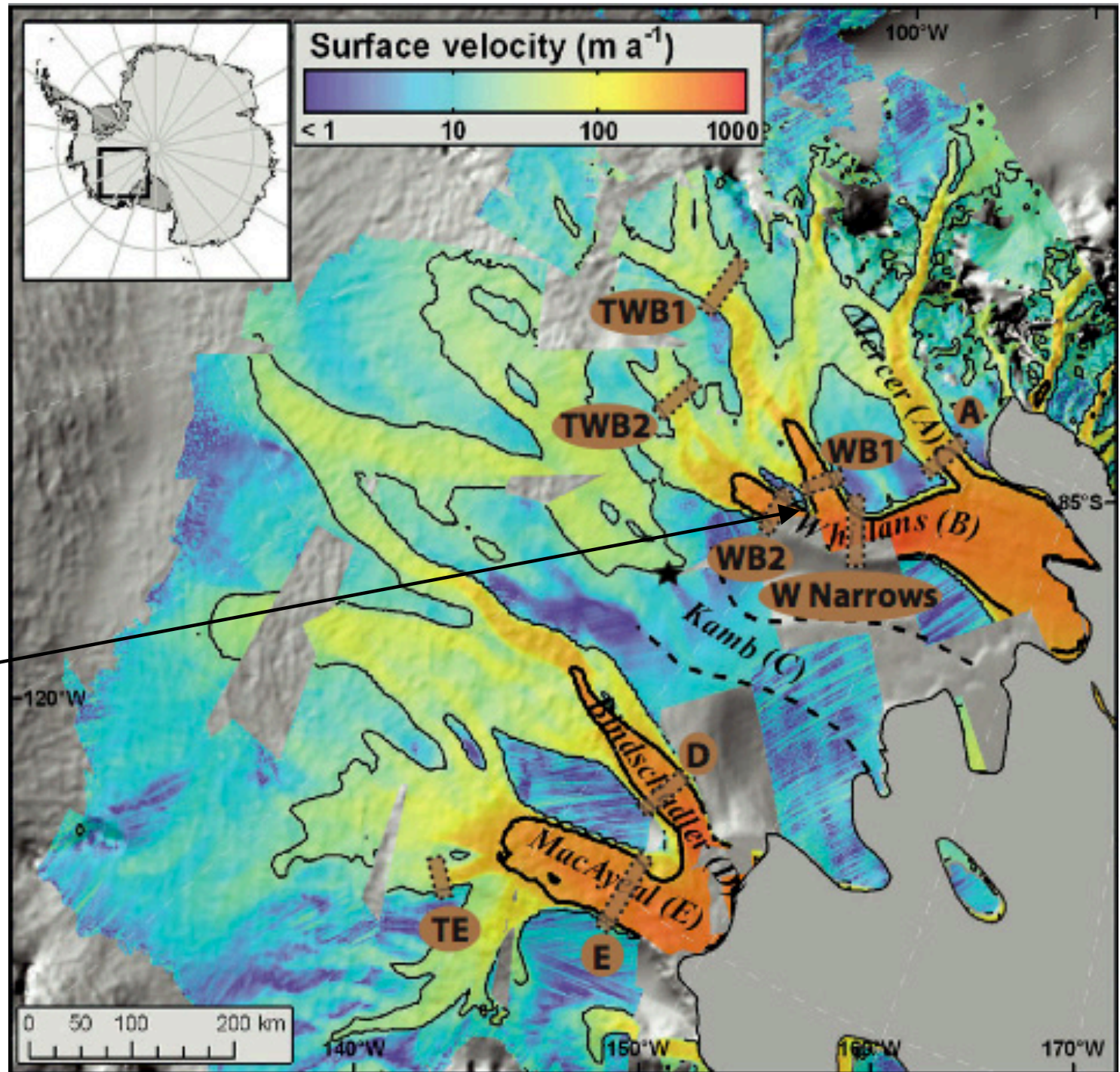
Nine ice stream traverses (dotted-lines) for velocity profiles measured by Joughin et al. (*J. Geophys. Res.*, 2002)

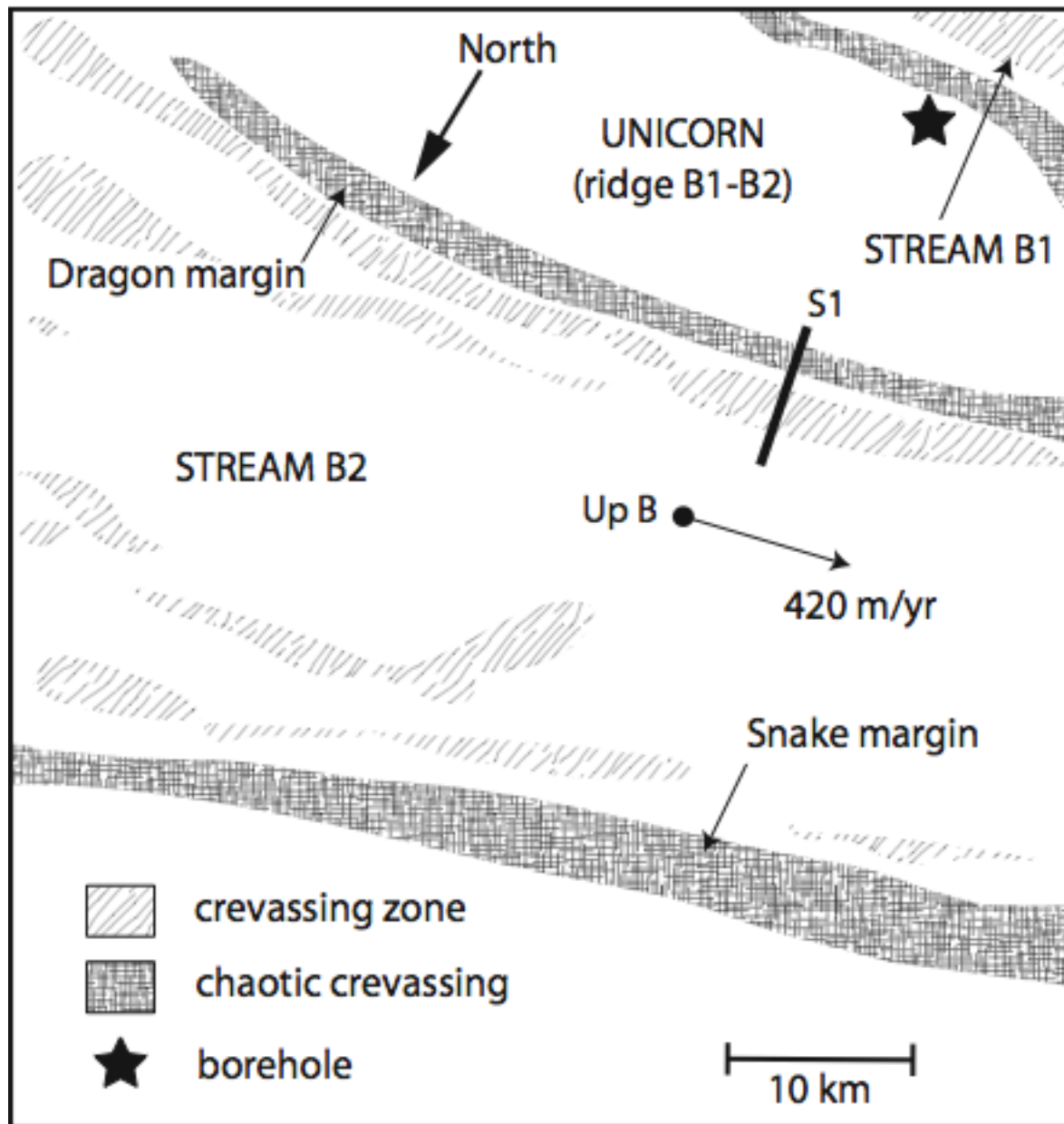




Nine ice stream traverses (dotted-lines) for velocity profiles measured by Joughin et al. (*J. Geophys. Res.*, 2002)

Dragon Margin (near to, but not the same as, the WB2 profile)

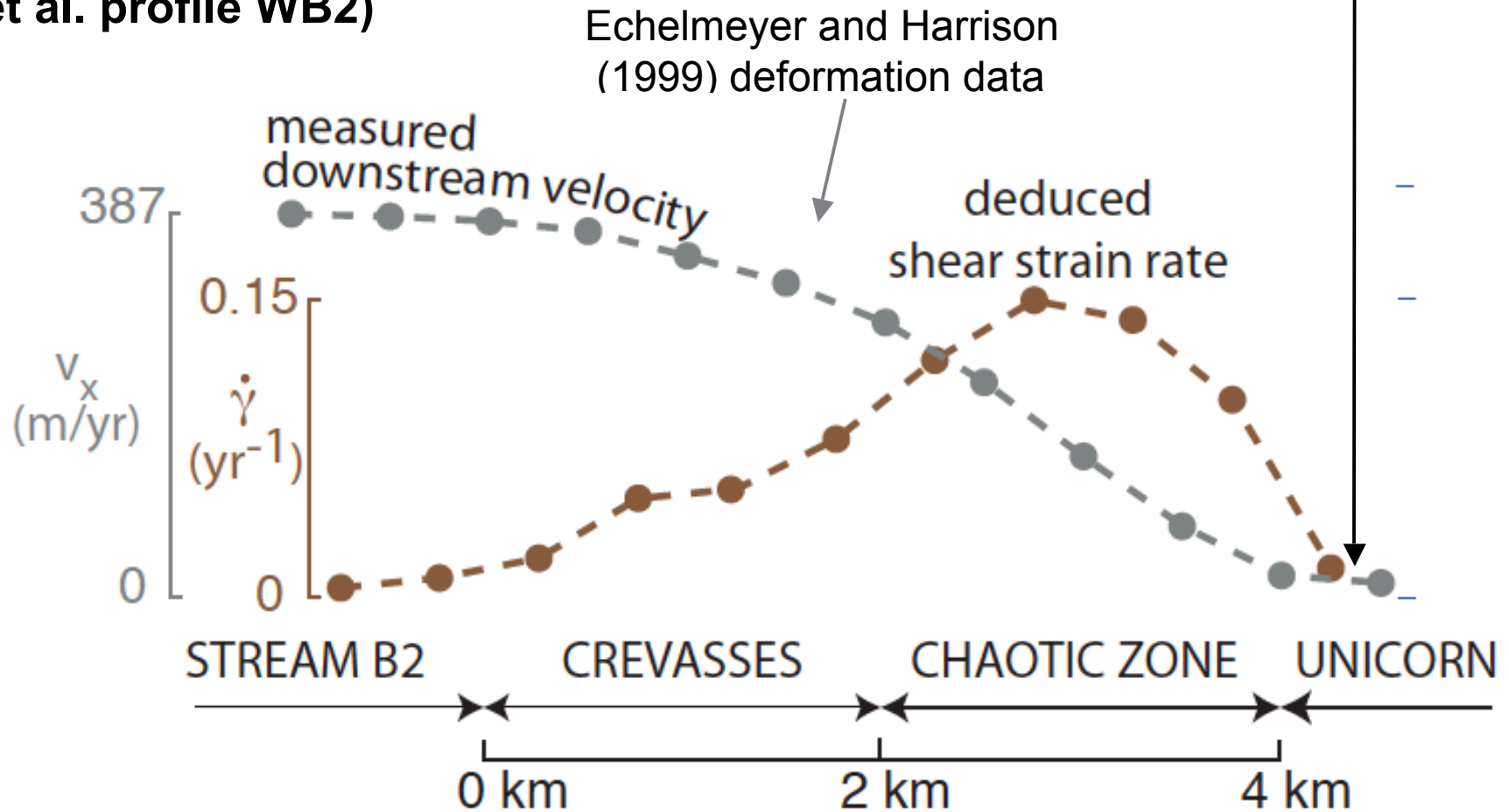




Echelmeyer and Harrison (1999)



**Dragon Margin, along  
Whillans upstream  
branch B2, profile S1  
(located near Joughin  
et al. profile WB2)**



Ice Stream (Joughin et al. group)	Profile	$H^a$ (m)	$W^b$ (km)	$T_{melt}^c$ (° C)	$\dot{\gamma}_{lat}^d$ ( $10^{-2} \cdot \text{yr}^{-1}$ )
Dragon Margin		985	34		15
Mercer	A	1242	39	-0.8	4.2
Whillans	WB1	1205	35	-0.8	7.0
	WB2	985	34	-0.6	9.5
	W Narrows	846	48	-0.6	13.5
	TWB1	2188	25	-1.5	3.8
	TWB2	1538	25	-0.9	4.0
Bindschadler	D	888	55	-0.6	5.8
MacAyeal	E	916	78	-0.6	8.1
	TE	1177	19	-0.8	5.5



*Tributaries*



From Joughin et al. [2002]:

a. Ice sheet thickness  $H$ ; b. Ice stream width  $W$ ; d. Maximum shear strain rate at margin,  $\dot{\gamma}_{lat}$ .

c. Melting temperature at bed. When allowing for a temperate zone in modeling, we set this temperature to be the uniform melting temperature over the zone.

## ***Temperature distribution implied at West Antarctic Ice Stream margins.***

**1-D Model:** Neglecting horizontal (but not vertical) advective ice motions, and horizontal  $T$  gradients at the margins, and considering only  $\dot{\gamma}_{lat}$ , the temperature distribution through the column of ice at *steady state* ( $\partial T(z,t) / \partial t = 0$ ;  $T = T(z)$ ) satisfies:

$$\frac{d}{dz} \left( K(T) \frac{dT}{dz} \right) + \tau_{lat}(\dot{\gamma}_{lat}, T) \dot{\gamma}_{lat} = \rho C_i(T) w \frac{dT}{dz}$$

- We take  $\dot{\gamma}_{lat}$  to be ***uniform*** in depth, with ***Glen's law*** giving

$\tau_{lat}(\dot{\gamma}_{lat}, T) = \left(1 / A(T)\right)^{1/3} (\dot{\gamma}_{lat} / 2)^{1/3}$ , and write *vertical velocity*  $w$  as  $w = -az / H$  (Zotikov form, where  $a \approx$  surface accumulation rate).

- Thus, ***with solutions constrained by***  $T \leq T_{melt}$ ,  $T(z)$  is given by

$$\frac{d}{dz} \left( K(T) \frac{dT}{dz} \right) + 2 \left(1 / A(T)\right)^{1/3} (\dot{\gamma}_{lat} / 2)^{4/3} = -\rho C_i(T) \left( \frac{az}{H} \right) \frac{dT}{dz}$$



# Thermo - mechanical properties of ice

**Glen's flow law for ice (dislocation creep) :**

$$\dot{\gamma} / 2 = A(T)\tau^3,$$

$$\tau = B(T)(\dot{\gamma} / 2)^{1/3}$$

$$\left( B(T) = [1 / A(T)]^{1/3} \right)$$

With diffusion creep too,

$$\dot{\gamma} / 2 = C(T, d_g)\tau + A(T)\tau^3$$

Ice is still strong at  $T_{melt}$ :

For a given  $\dot{\gamma}$ :

$$\tau_{T=0^\circ\text{C}} \approx 0.5 \times \tau_{T=-13^\circ\text{C}}$$

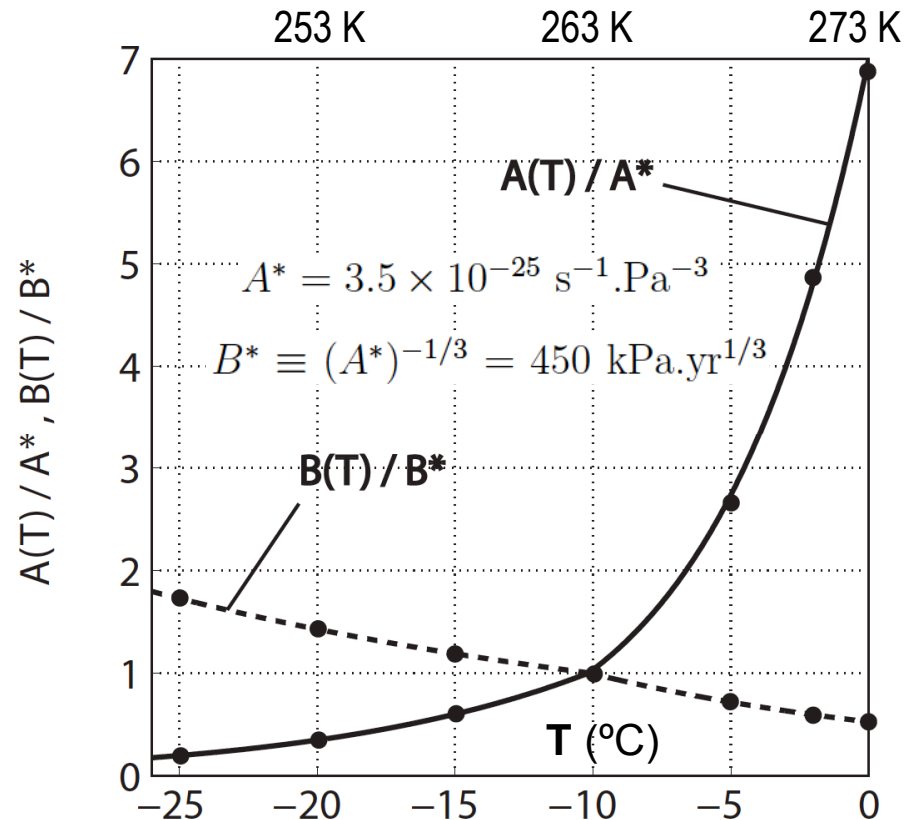
**Thermal conductivity :**

$$K(T) = 9.828 \frac{\text{J}}{\text{m s K}} \exp\left(-5.7 \times 10^{-3} \frac{T}{\text{K}}\right)$$

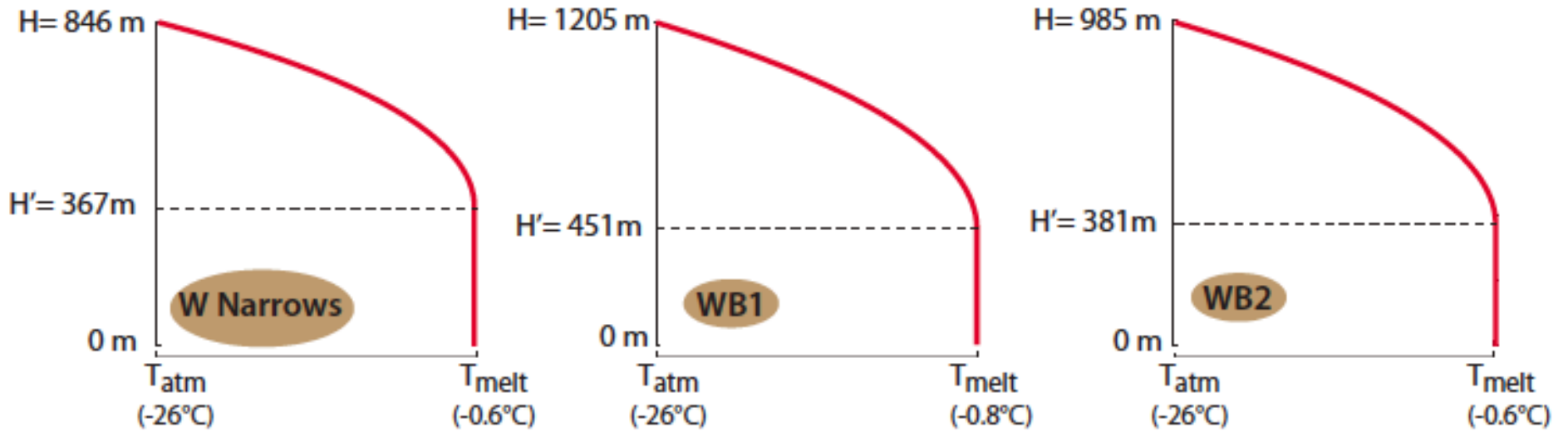
**Specific heat :**

$$C_i(T) = \left(152.5 + 7.122 \frac{T}{\text{K}}\right) \frac{\text{J}}{\text{kg K}}$$

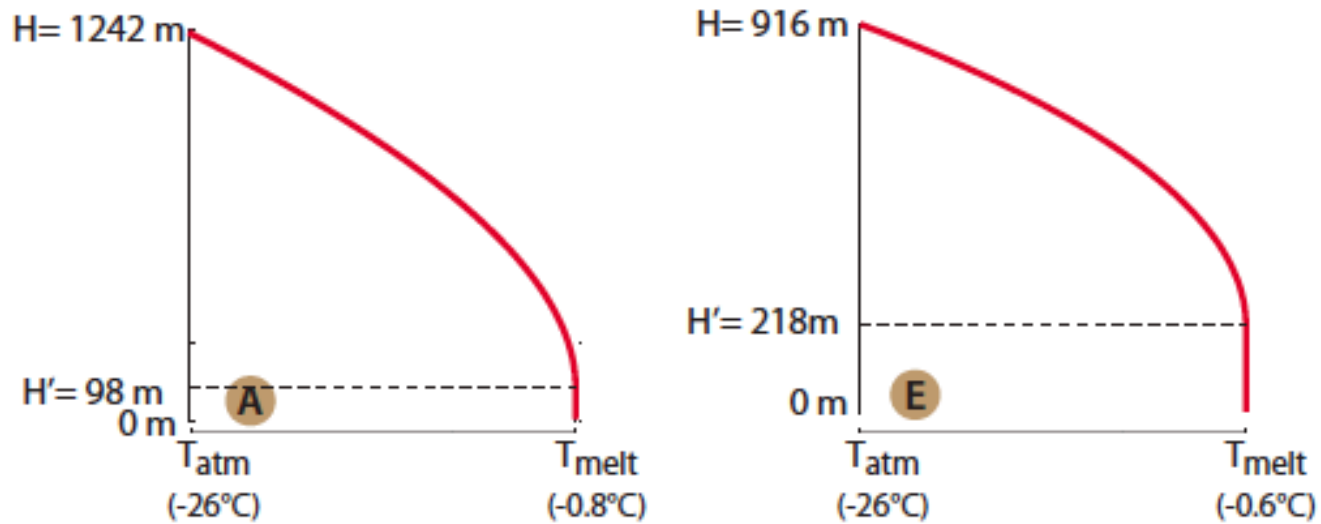
**Data fits as suggested by Cuffy & Paterson [2010]**



$$\frac{d}{dz} \left( K(T) \frac{dT}{dz} \right) + \left( \frac{1}{2A(T)} \right)^{1/3} (\dot{\gamma}_{lat})^{4/3} + \rho C_i(T) (az / H) \frac{dT}{dz} = 0 \quad \& \quad T \leq T_{melt} \Rightarrow$$



(For all cases,  
 $a = 0.1$  m/yr)



Results of calculations of  $T = T(z)$  at margins for the *major ice streams*:

% of margin that is temperate, &  $\bar{\tau}_{lat} = \frac{1}{H} \int_0^H \tau_{lat}(z) dz$  with  $\tau_{lat}(z) = \left( \frac{\dot{\gamma}_{lat}}{2A(T(z))} \right)^{1/3}$

Ice Stream	Profile	$\tau_{grav}^a$ (kPa)	$H'/H^b$ (%)	$\bar{\tau}_{lat}$ (kPa)	$\tau_{base}$ (kPa)	$\tau_{base}/\tau_{grav}$ (%)
Dragon Margin		11.0	56	132.0	3.2	29
Mercer	A	14.9	8	119.0	7.7	52
Whillans	WB1	12.5	37	115.6	4.5	36
	WB2	10.8	39	127.0	3.4	32
	W Narrows	7.6	43	138.5	2.7	36
Bindschadler	D	10.0	0 <sup>c</sup>	131.7	5.7	58
MacAyeal	E	15.3	24	128.9	12.3	80

<sup>a</sup> Inferred by *Joughin et al. [2002]*,  $\tau_{grav} = \rho_{ice} g H S$  where  $S$  is the downstream slope.

<sup>b</sup> Predicted temperate height fraction of the ice sheet at margin.

<sup>c</sup> The ratio increases to  $\sim 53\%$  when evaluated 30 km downstream (see text).

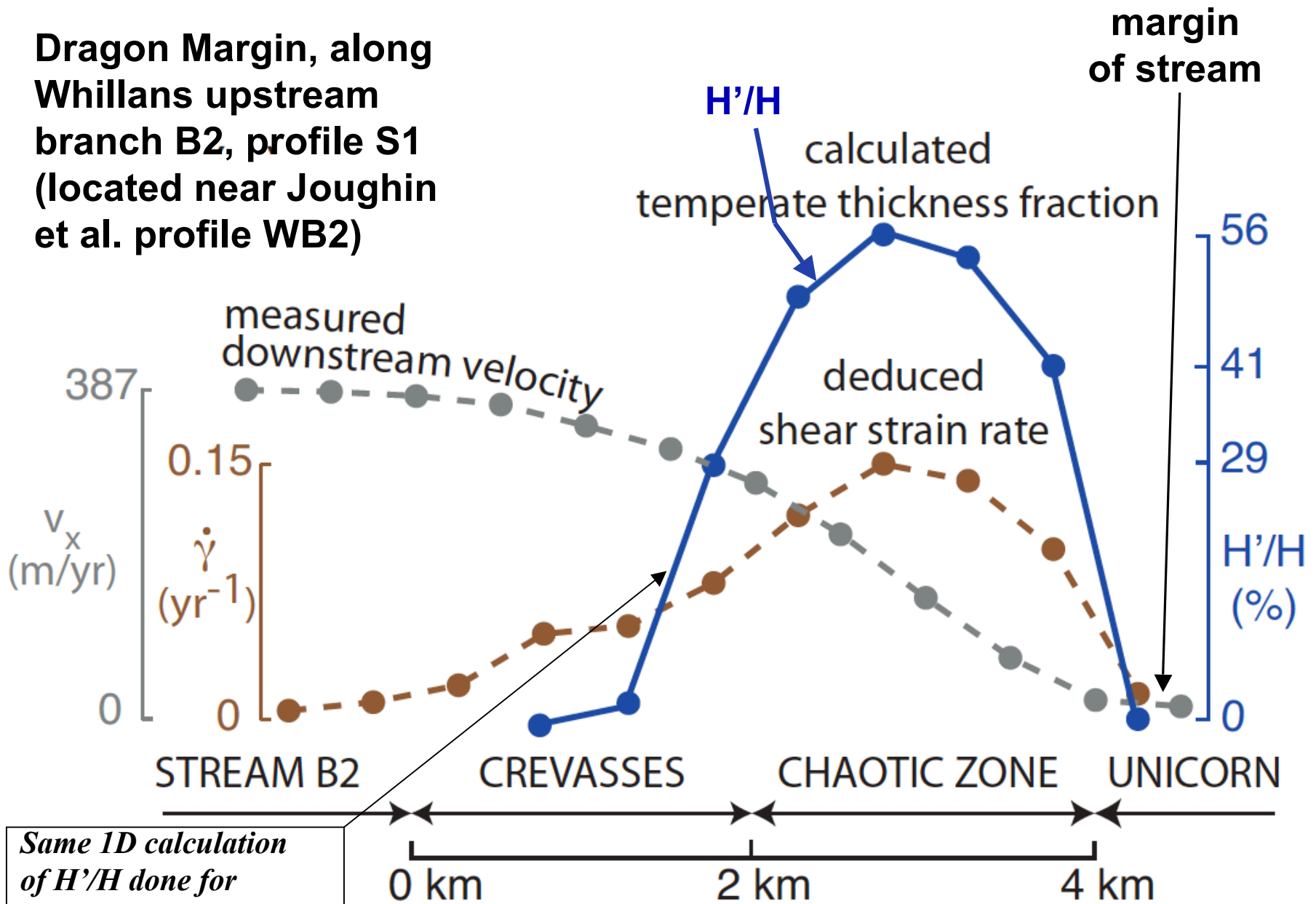


Results of calculations of  $T = T(z)$  at margins for the *upstream tributaries*:

% of margin that is temperate, &  $\bar{\tau}_{lat} = \frac{1}{H} \int_0^H \tau_{lat}(z) dz$  with  $\tau_{lat}(z) = \left( \frac{\dot{\gamma}_{lat}}{2A(T(z))} \right)^{1/3}$

Ice Stream	Profile	$\tau_{grav}^a$ (kPa)	$H'/H^b$ (%)	$\bar{\tau}_{lat}$ (kPa)	$\tau_{base}$ (kPa)	$\tau_{base}/\tau_{grav}$ (%)
<b>Dragon Margin</b>		<b>11.0</b>	<b>56</b>	<b>132.0</b>	<b>3.2</b>	<b>29</b>
Whillans	TWB1	47.5	50	90.8	31.6	67
	TWB2	40.9	26	101.9	28.4	69
MacAyeal	TE	44.9	23	113.6	30.8	69

**Dragon Margin, along Whillans upstream branch B2, profile S1 (located near Joughin et al. profile WB2)**



*Same 1D calculation of  $H'/H$  done for various locations, with  $\dot{\gamma}_{lat}$  taken as the local  $\dot{\gamma}$*

Echelmeyer and Harrison (1999) deformation data

## Mass rate of melt production per unit volume in temperate zone:

$$\dot{m} = \frac{\tau_{lat} \dot{\gamma}_{lat}}{L}, \quad \tau_{lat} = \left( \frac{\dot{\gamma}_{lat}}{2A_{melt}} \right)^{1/3} F(n) \quad (\text{where } F(n) \leq 1), \quad \dot{m} = \frac{\dot{\gamma}_{lat}^{4/3} F(n)}{(2A_{melt})^{1/3} L}$$

Latent heat per unit mass
Porosity
Strength reduction due to porosity

## Darcy seepage flux of melt water:

$$\vec{\nabla} \cdot (\rho_w \vec{q}) = \dot{m} \quad \Rightarrow \quad \frac{dq_z}{dz} = \frac{\dot{m}}{\rho_w} = \frac{\dot{\gamma}_{lat}^{4/3} F(n)}{(2A_{melt})^{1/3} L \rho_w} \quad [\text{assumes } \vec{q} = (0, 0, q_z)]$$

$$\Rightarrow \quad (q_z)_{z=0} = - \left[ \frac{1}{H'} \int_0^{H'} F(n) dz \right] \frac{\dot{\gamma}_{lat}^{4/3} H'}{(2A_{melt})^{1/3} L \rho_w}$$

(we assume this is  $\sim 1$  -- see next page)

$$\text{Also, for } F(n) \approx 1, \quad q_z = - \frac{\dot{\gamma}_{lat}^{4/3} (H' - z)}{(2A_{melt})^{1/3} L \rho_w}$$



# Water permeation through the partially melted ice:

J. F. Nye and F. C. Frank,  
 [J. Glac., 1973], building on  
 Frank's [Nat., 1968]  
 analysis of melt convection  
 in Earth's mantle:

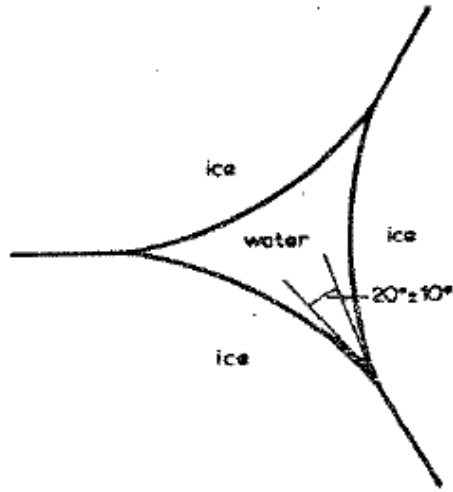


Fig. 2. Cross-section of a vein of liquid situated at a grain edge, where three grain boundaries meet. The figure is drawn for a dihedral angle  $\varphi$  equal to  $20^\circ$ , as measured for ice—water by Ketcham and Hobbs (1969).

Permeability  
 $k = \alpha n^2 d_g^2$   
 $n =$  porosity,  
 $d_g =$  grain size (1-10 mm),  
 $\alpha \approx 1/2000$  to  $1/1500$

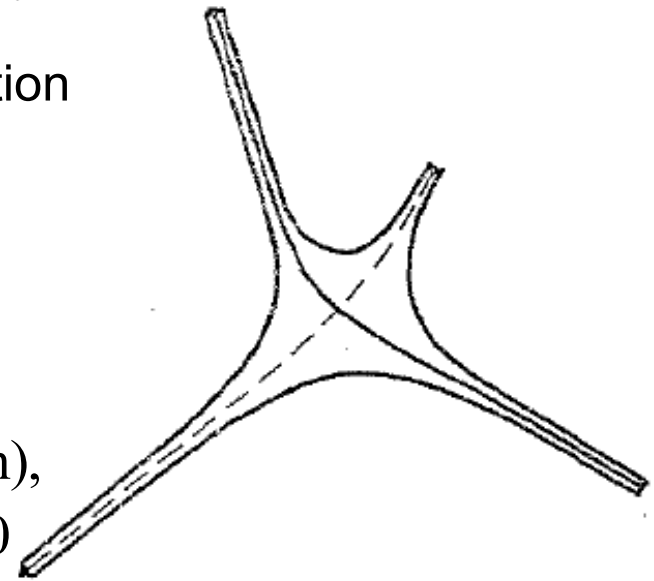


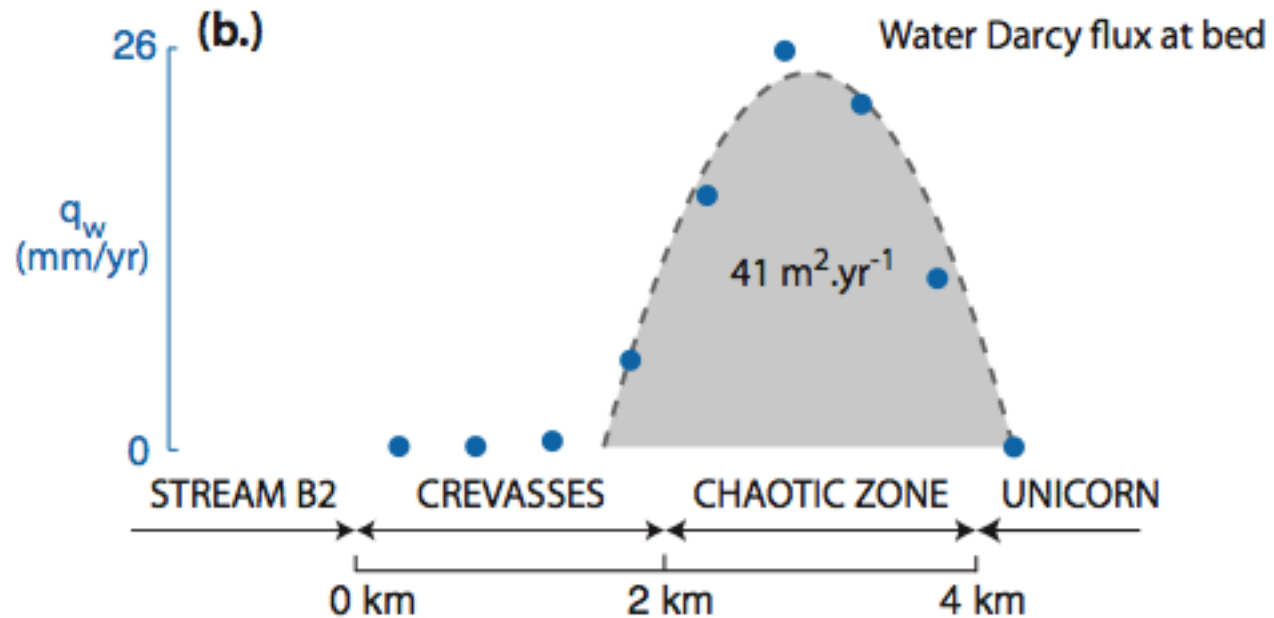
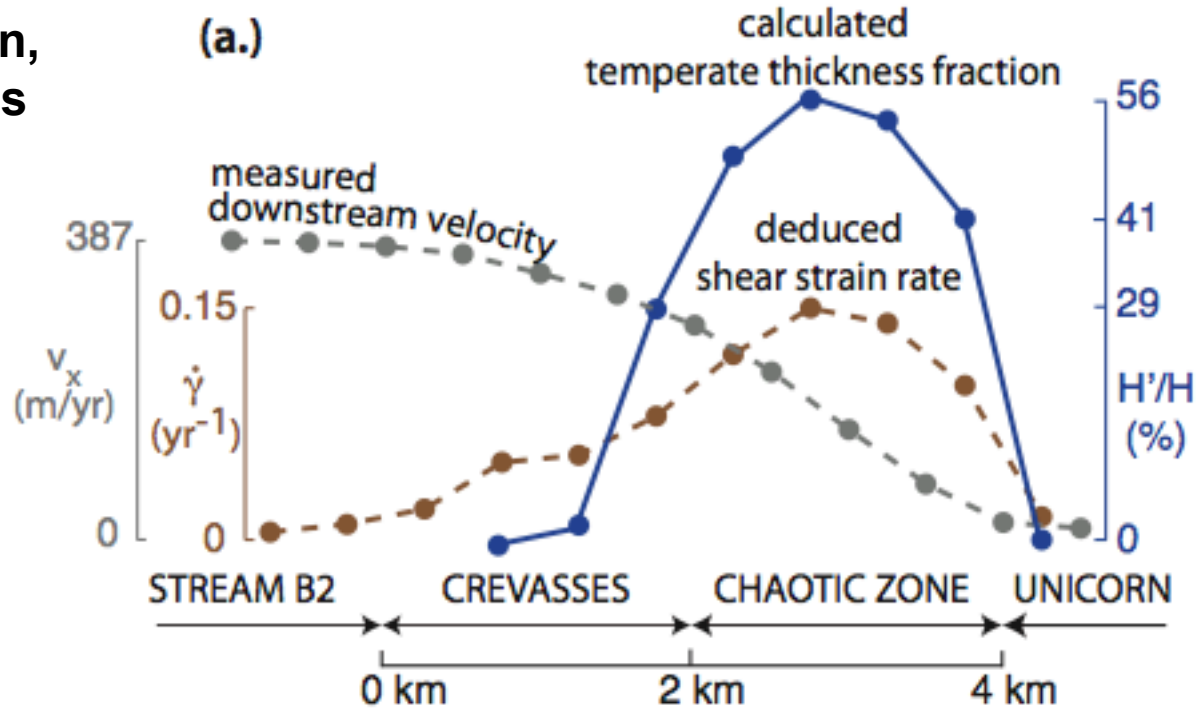
Fig. 3. A junction between four water veins in polycrystalline ice. The figure is a tetrahedron with non-spherical faces and with open corners.

$$q_z = - \frac{\dot{\gamma}_{lat}^{4/3} (H' - z)}{(2A_{melt})^{1/3} L \rho_w} = - \frac{k}{\mu_w} \left( \frac{dp}{dz} + \rho_w g \right)$$

$$= - \frac{k}{\mu_w} (\rho_w - \rho_{ice}) g \quad \text{if } p = \text{ice overburden pressure} = \rho_{ice} g (H - z)$$

$$\Rightarrow \text{porosity } n \leq 5 \times 10^{-4} \text{ mm} / d_g \leq 5 \times 10^{-4}$$

**Dragon Margin,  
along Whillans  
upstream  
branch B2,  
profile S1**



Perol and Rice,  
(AGU Abstr, 2011)

**2D, antiplane strain analysis :** velocity =  $u(y,z)\vec{e}_x$  ,  $\dot{\gamma} = \sqrt{\vec{\nabla}u \cdot \vec{\nabla}u}$

**Coupled non - linear Poisson equation system**

(for velocity  $u$  and temperature  $T$ ) :

$$\frac{\partial}{\partial y} \left( \frac{\tau(\dot{\gamma}, T)}{\dot{\gamma}} \frac{\partial u}{\partial y} \right) + \frac{\partial}{\partial z} \left( \frac{\tau(\dot{\gamma}, T)}{\dot{\gamma}} \frac{\partial u}{\partial z} \right) = -\rho g S \quad \left( \tau(\dot{\gamma}, T) = \left( \frac{\dot{\gamma}}{2A(T)} \right)^{1/3} \right)$$

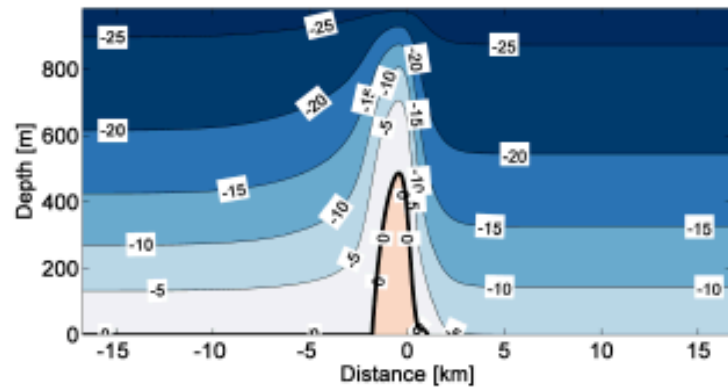
$$\begin{aligned} & \frac{\partial}{\partial y} \left( K(T) \frac{\partial T}{\partial y} \right) + \frac{\partial}{\partial z} \left( K(T) \frac{\partial T}{\partial z} \right) \\ & = -[1 - \hat{H}(T - T_{melt})] \tau(\dot{\gamma}, T) \dot{\gamma} + \rho C(T) \left( v \frac{\partial T}{\partial y} + w \frac{\partial T}{\partial z} \right) \end{aligned}$$

(here,  $v$  &  $w$  are regarded as given, e.g., Zotikov's  $w = -az / H$ ,  $v = \text{const.}$ ,  $v_o$ )

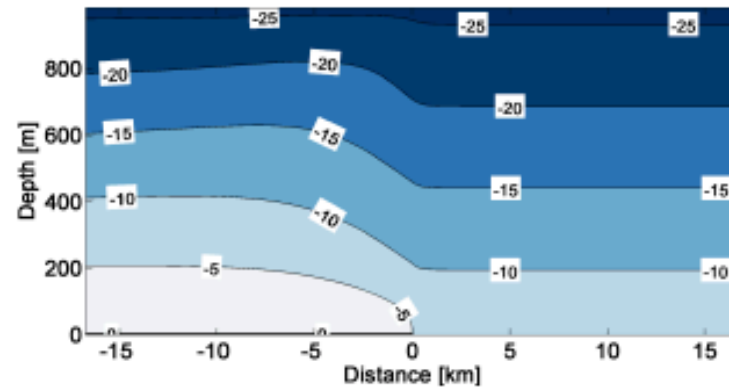
**Computational Approach (Suckale, Platt, Perol, Rice, to JGR, 2013) :**

- **Multigrid methodology** for iterative solution of coupled nonlinear Poisson systems, embedding constraint  $T \leq T_{melt}$ .

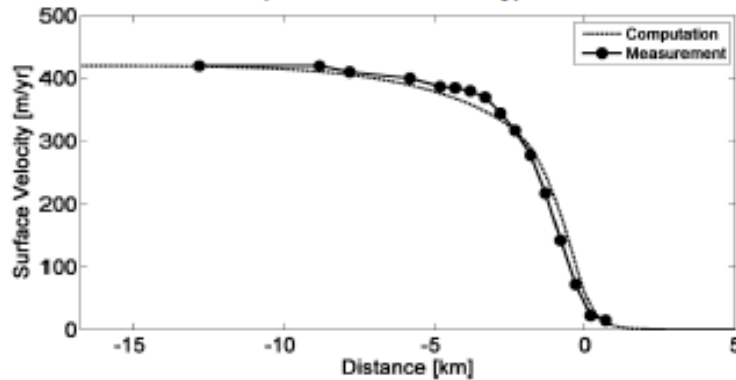
A1. Temperature field (vertical advection only)



A2. Temperature field (horizontal advection only)



B1. Surface velocities (vertical advection only)



B2. Surface velocities (horizontal advection only)

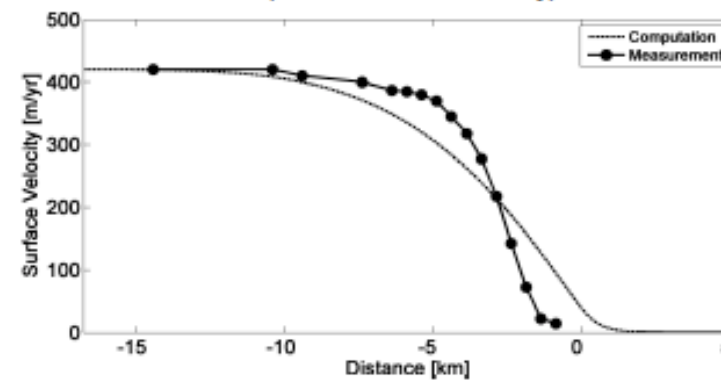
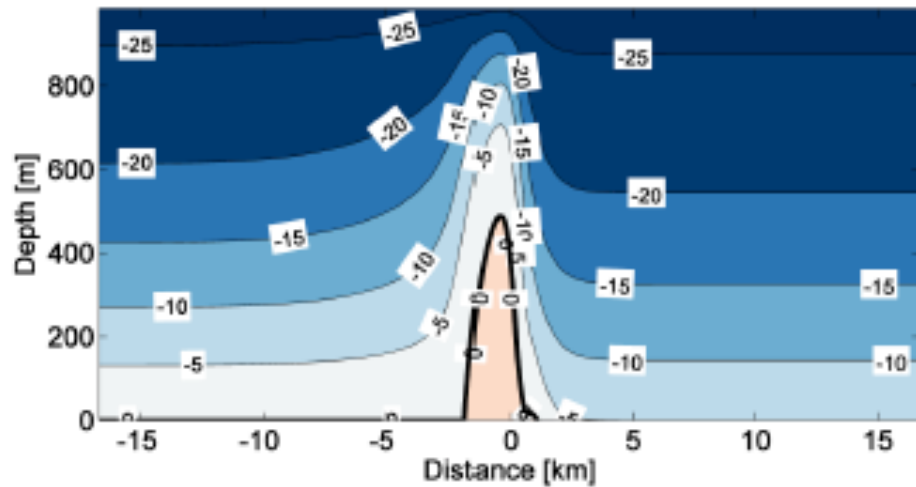


**Figure 8.** Temperature fields and surface velocities for Dragon margin when including only vertical advection (A1 and B1) with  $a = 0.1$  m/yr and only horizontal advection (A2 and B2) with  $v = -7.3$  km/yr, respectively. The best fitting basal stresses are  $\tau_{base} = 5.31$  kPa (A1 and B1) and  $\tau_{base} = 0.94$  kPa (A2 and B2), respectively. Both computations neglect surface crevassing.



A1. Temperature field (vertical advection only)



B1. Surface velocities (vertical advection only)

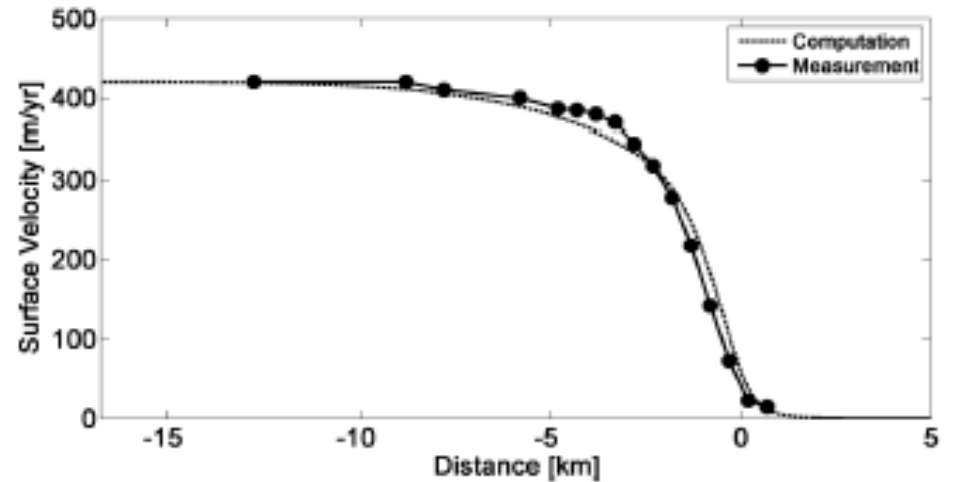


Figure 8. Temperature fields and surface velocities for Dragon margin when including only vertical advection (A1 and B1) with  $a = 0.1$  m/yr and only horizontal advection (A2 and B2)

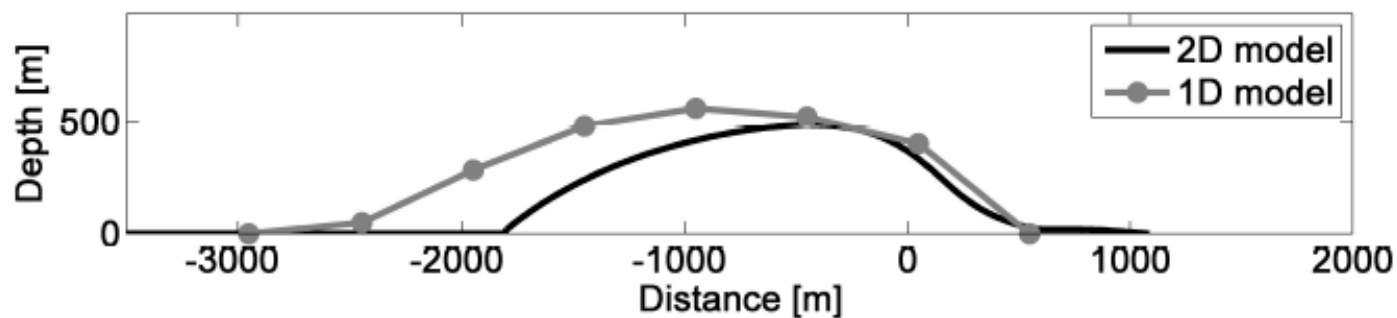
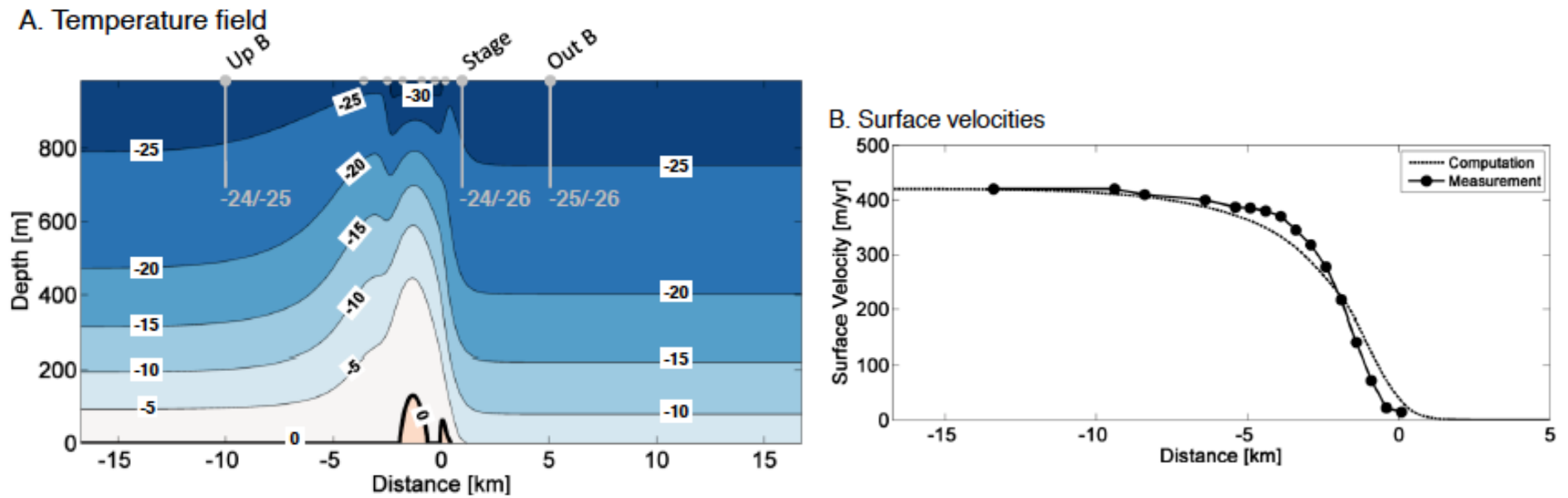
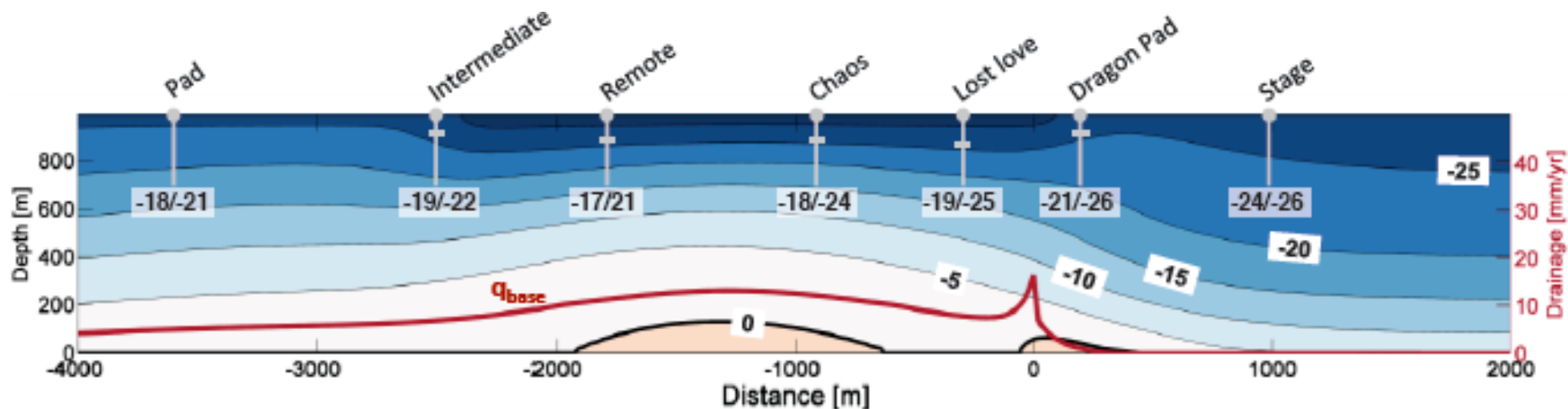


Figure 9. Comparison of the temperate zone from Fig. 8A1 and B1, replotted on a 1:1 scale, with the simplified 1D model by *Perol and Rice* [2011] using measured surface velocities

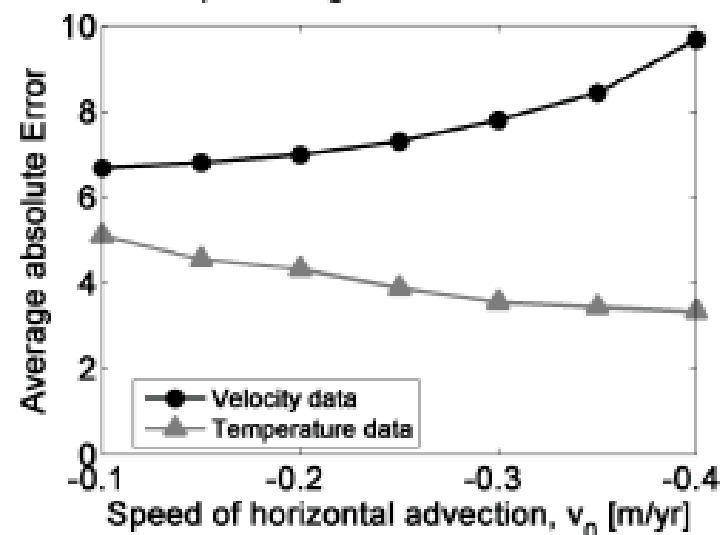


**Figure 10.** Temperature field (A) and surface velocities (B) for Dragon when attempting to match the observed borehole temperatures [Harrison *et al.*, 1998], see Figs. 1 and 2 for borehole locations, and surface velocities [Echelmeyer and Harrison, 1999] simultaneously. The computation is based on the model parameters  $\tau_{base} = 1.22$  kPa, accumulation  $a = 0.23$  m/yr, geothermal heat flux  $G = 85$  mW/m<sup>2</sup>, and horizontal advection at  $v = -0.35$  m/yr. The approximate locations of the nine boreholes considered in Harrison *et al.* [1998] are indicated as grey dots. We highlight the boreholes located far from margin as grey lines in accordance to their depth. The left numbers represent the computed value and the right number the measured value at maximum depth.

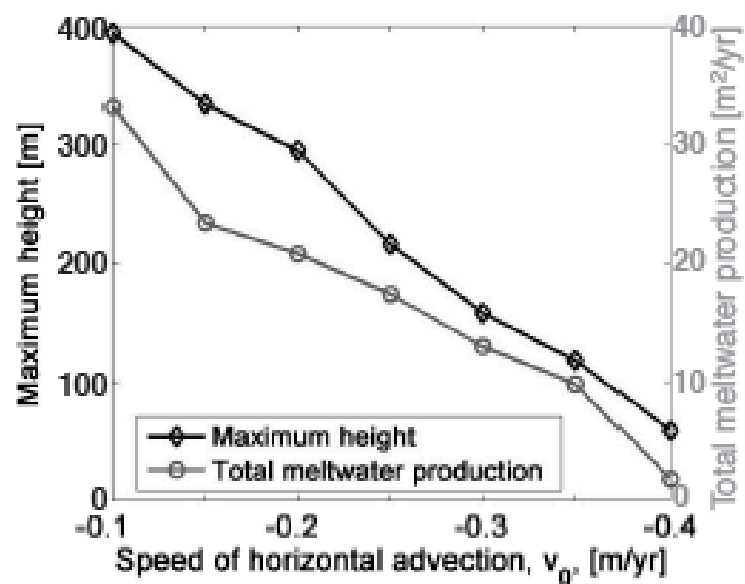


**Figure 11.** Extent of a potential temperate zone at Dragon margin plotted on a 1:1 scale and meltwater flux at the base of the ice,  $q_{base}$ , in mm/yr (grey line) for the computation also shown in Fig. 10. The total meltwater produced in the temperate zone is  $25 \text{ m}^2/\text{yr}$ . The approximate locations of the boreholes from *Harrison et al.* [1998] are highlighted in grey with the left number representing the computed temperature and the right value the measured temperature at a depth of approximately 700 m. Small horizontal dashes along the boreholes in the vicinity of the shear margin indicate the approximate position of the  $-26^\circ\text{C}$  contour.

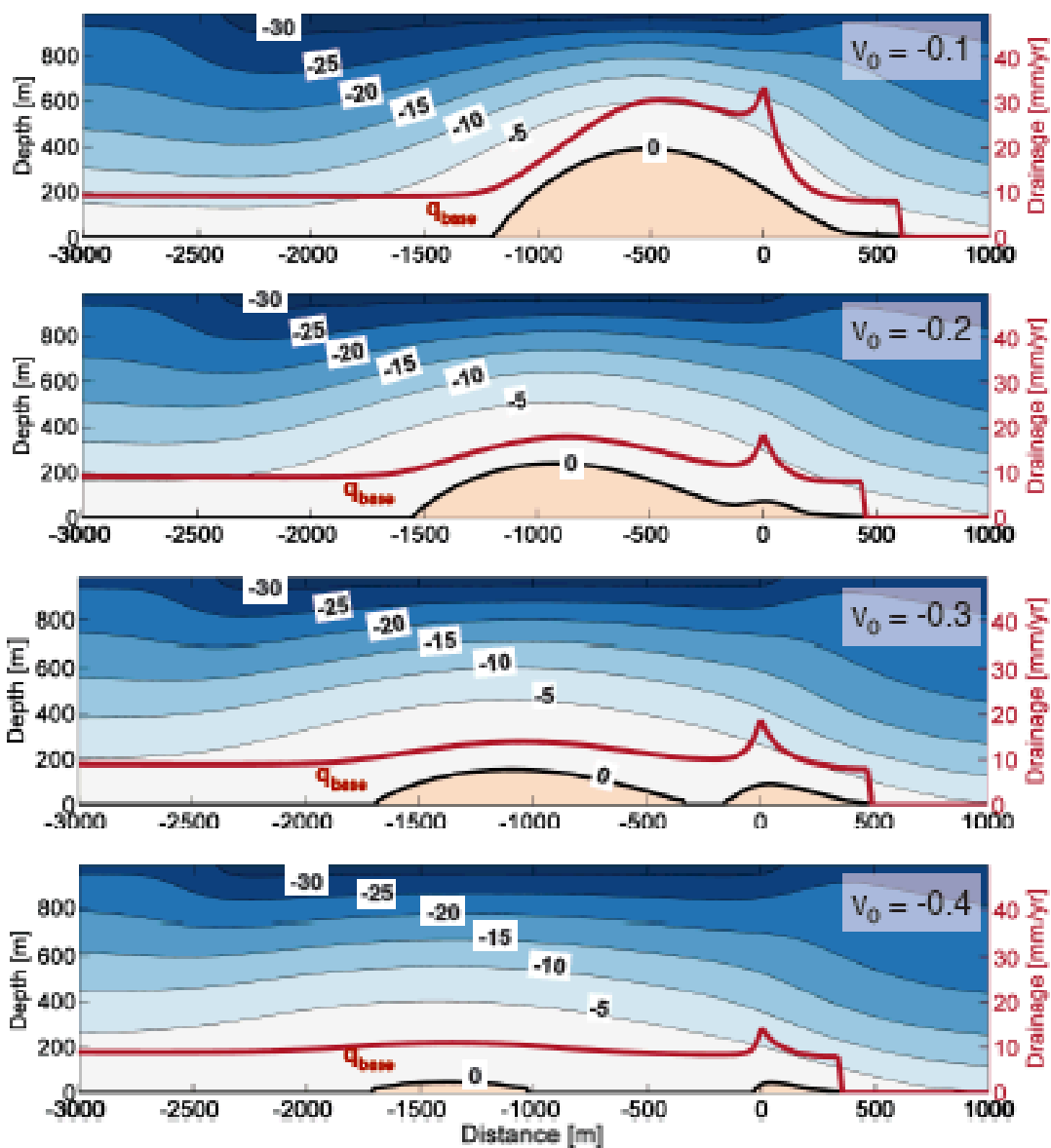
A. Error in reproducing observational data



B. Properties of the temperate zones



C. Temperature and drainage for specific speeds of horizontal advection





For  $Q_w = 100 \text{ km} \times 41 \text{ m}^3 / \text{m} \cdot \text{yr}$ , and  $S = 0.0012$ :

**Rothlisberger-Shreve channel analysis**

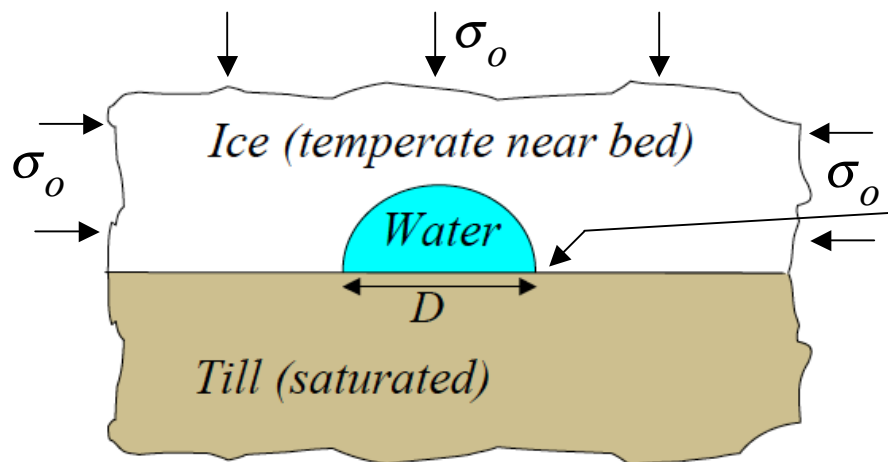
Manning Coefficient, $n_M$ (s / m <sup>1/3</sup> )	0.01	0.02	0.03	0.04
Equivalent Nikuradse Roughness, $k$ (cm)	0.03	1.6	18.0	101.1
Channel Diameter, $D$ (m)	0.9	1.1	1.3	1.5
Effective Normal Stress at Channel Margin, $\sigma_{hoop} - p_{ch}$ (kPa)	369	310	280	261

Clarke sub-glacial flooding range

Assumed plausible here

$$\sigma_{hoop} - p_{ch} = \frac{2}{3}(\sigma_o - p_{ch})$$

**Sensitivity:**  $Q_w \rightarrow 0.25Q_w \Rightarrow D \rightarrow 0.59D$ ,  $(\sigma_{hoop} - p_{ch}) \rightarrow 0.89(\sigma_{hoop} - p_{ch})$



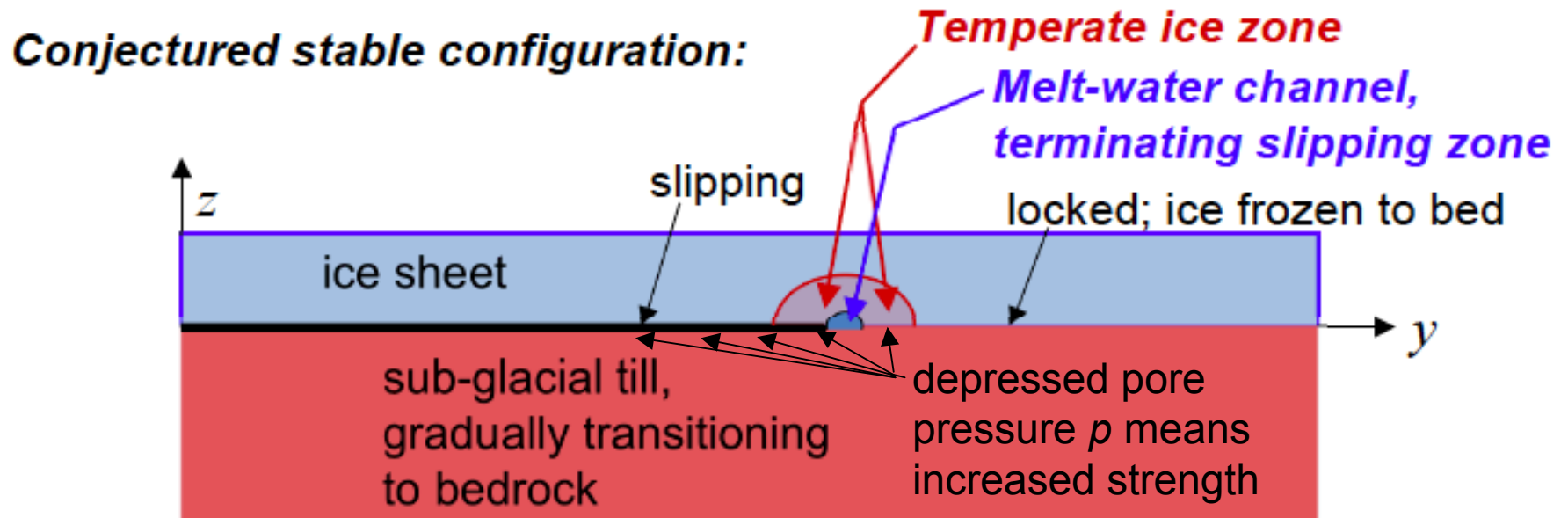
Strength  $\tau_{ch} = f(\sigma_{hoop} - p_{ch})$   
 $\approx 0.5(\sigma_{hoop} - p_{ch}) \approx 150 \text{ kPa}$   
 $\therefore \tau_{ch} / \tau_{base} \approx 20 \text{ to } 45$

For the 6 major streams,  $\tau_{ch} / \tau_{base}$  average = 32, and range = 12 to 56.

- Meltwater channel formation is likely near a region of intense melt generation.
- A crack ending in a channel has greatly diminished stress and strain rate concentration, and the high Terzaghi effective stress just outside the channel will contribute to resisting continued expansion of the slipping zone.

$$\text{Strength ratio } \frac{\tau_{ch}}{\tau_{base}} = \frac{(\sigma_{hoop} - p_{ch})}{(\sigma_{base} - p_{base})} \approx 20 \text{ to } 45 \text{ (avg. 32)}$$

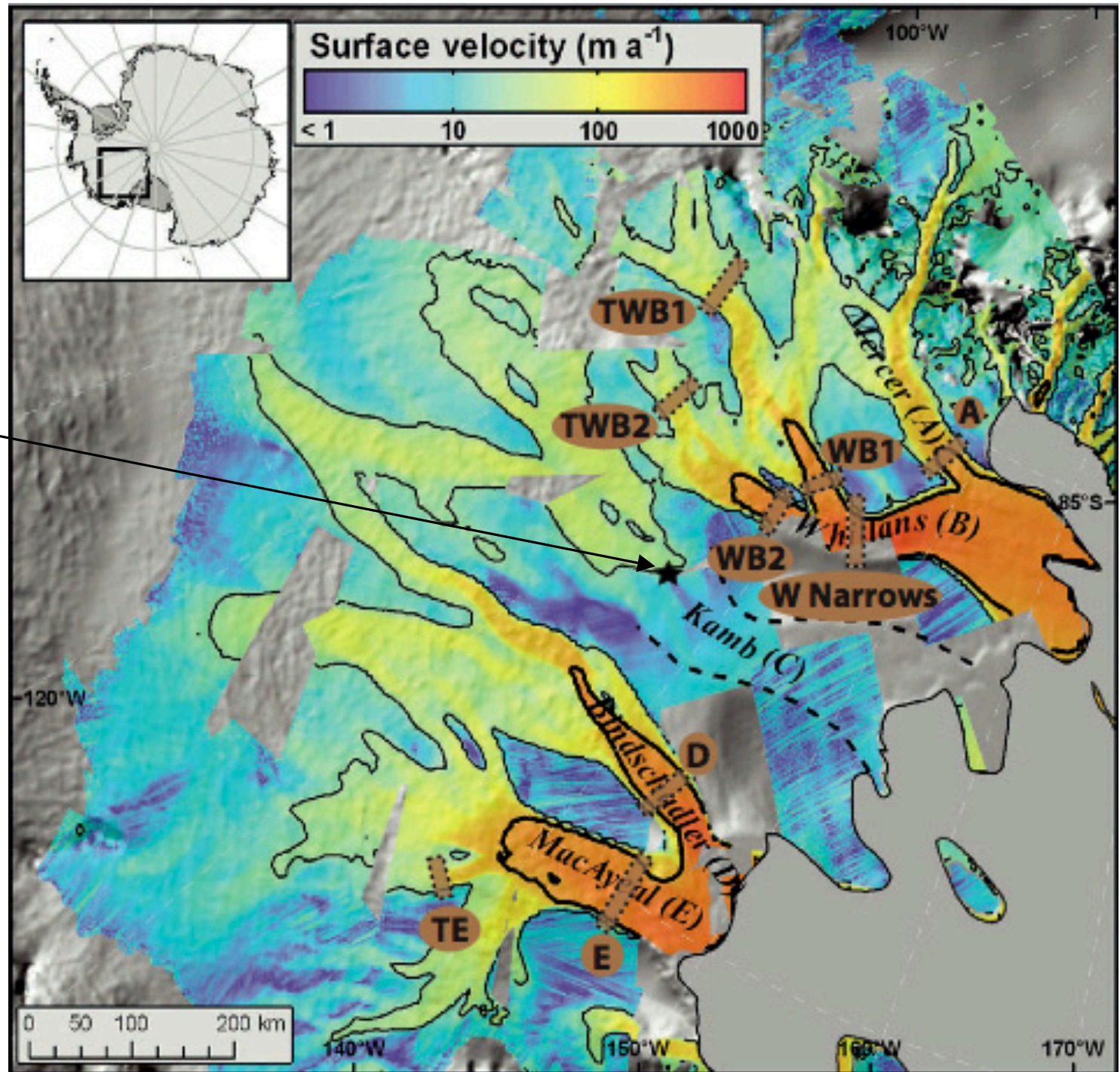
- **Very important: Advective effect** (not well yet modeled -- complicated!!) of slow lateral expansion of slipping zone towards the cold ice ridge could **chill ice near the stress concentrator** and **reduce or eliminate a partial-melt zone**.



**Field evidence, possible temperate ice and melt channels at margins**

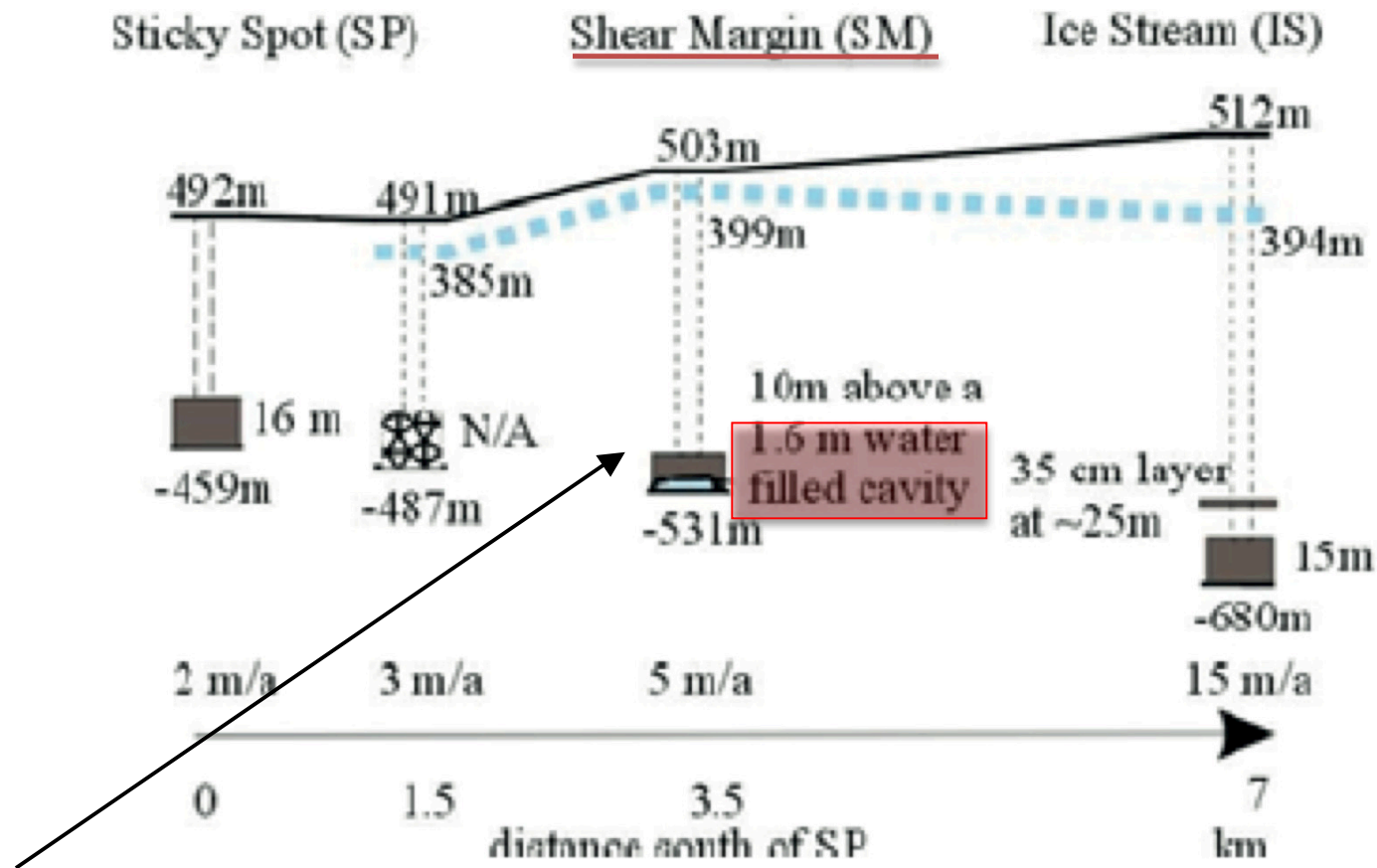
Borehole drilled into a dying shear margin of *Kamb* (C) ice stream

[Vogel (*PhD Thesis*, Caltech, 2004) and Vogel et al. (*Geophys Res Lett*, 2005)]





## Evidence of channel at margins



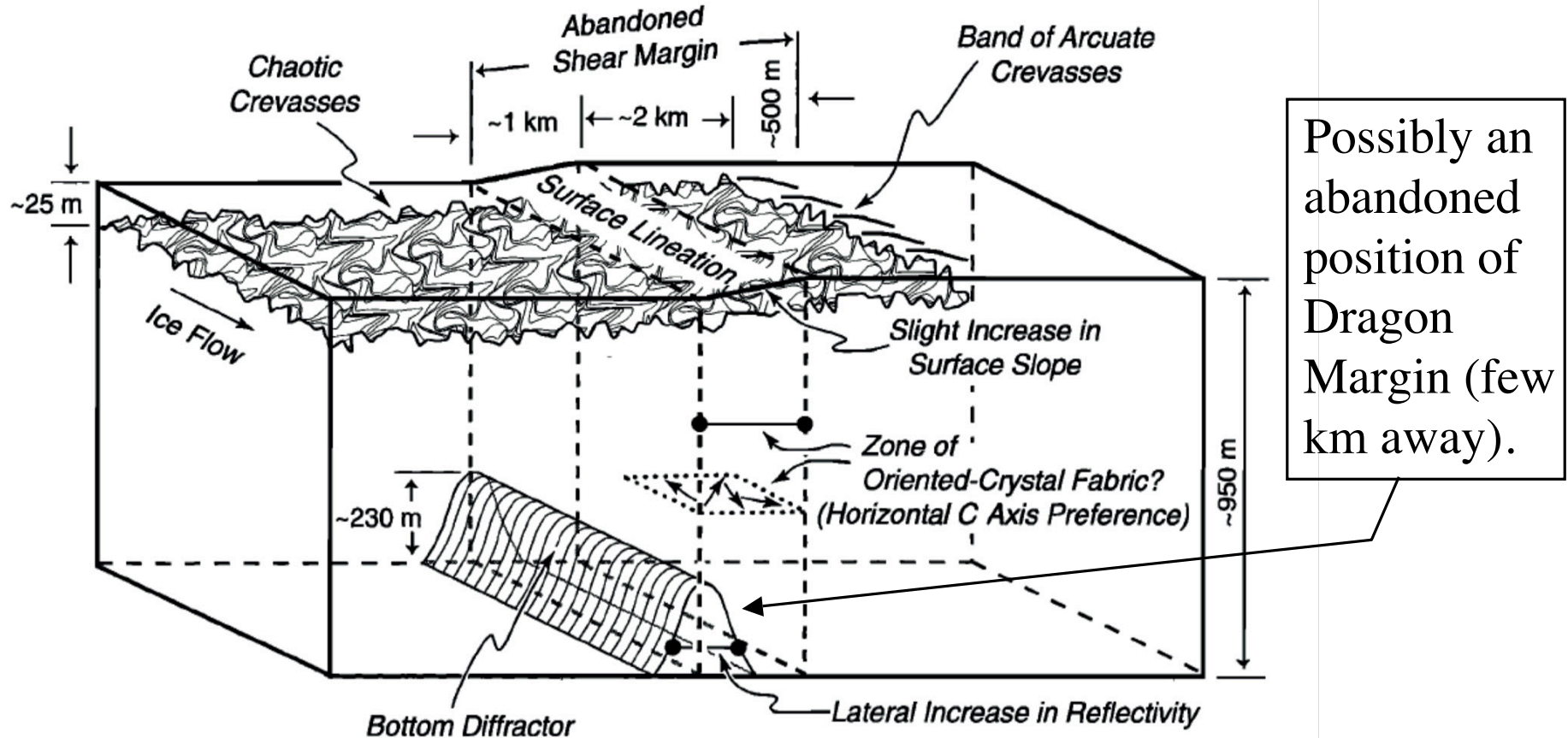
Borehole observation at the presently inactive shear margin of *Kamb* (C) ice stream:

- Found a 1.6 m tall water-filled cavity between ice sheet and bed.
- Video of the borehole shows horizontal acceleration of particles sinking into the cavity, indicating flow of water within the cavity -- part of a channel?

[Modified from Vogel PhD (Thesis, 2004) and Vogel et al. (GRL, 2005).]



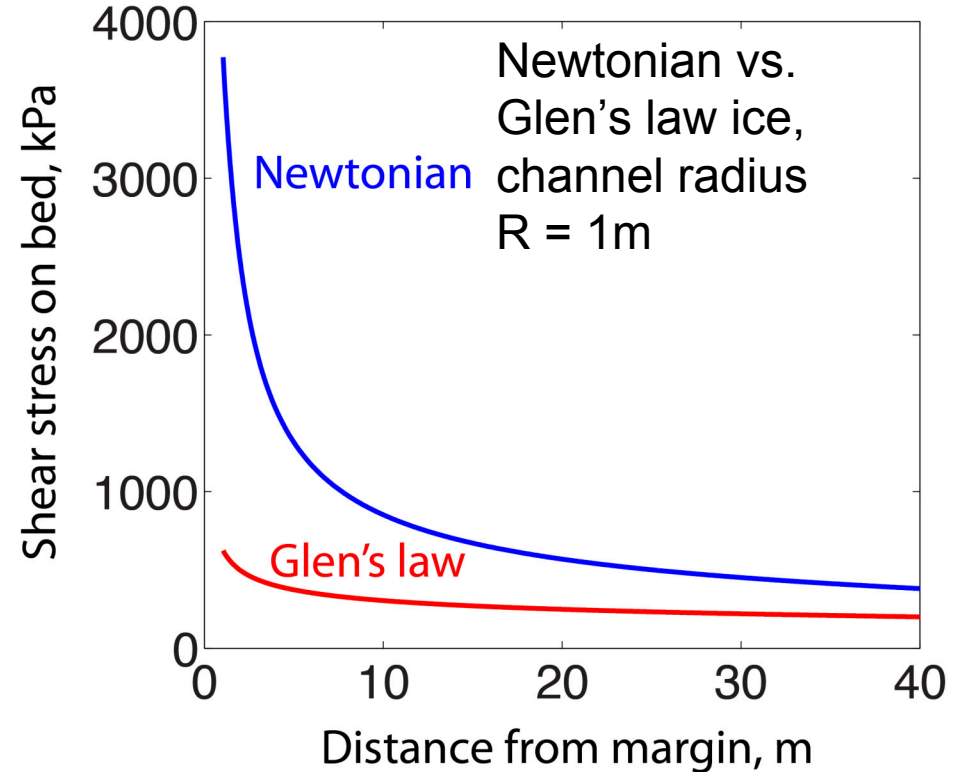
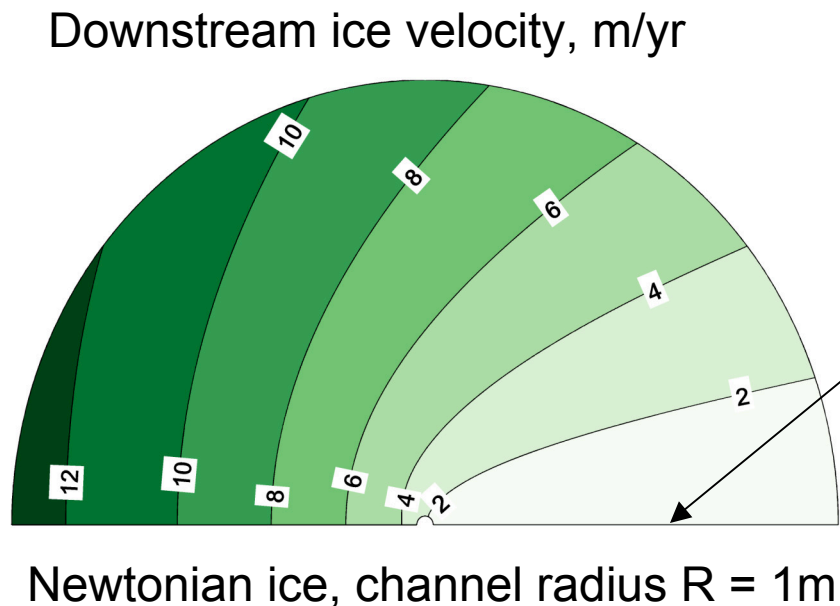
# Possible field evidence of internal melting at margins



- Clarke et al. [2000], in order to explain the bottom diffractors, have invoked **partial melting in temperate ice to a height of 230 m**, due to strain heating, among other possibilities (**entrained sediments, bottom crevasses**).
- Also, Clarke et al. noted a personal communication from H. Engelhardt (Caltech): Abnormal drill resistance encountered from  $\approx 56$  m above bed. Fresh scratches found on drill tip (assumed to due to **entrained sediments**).

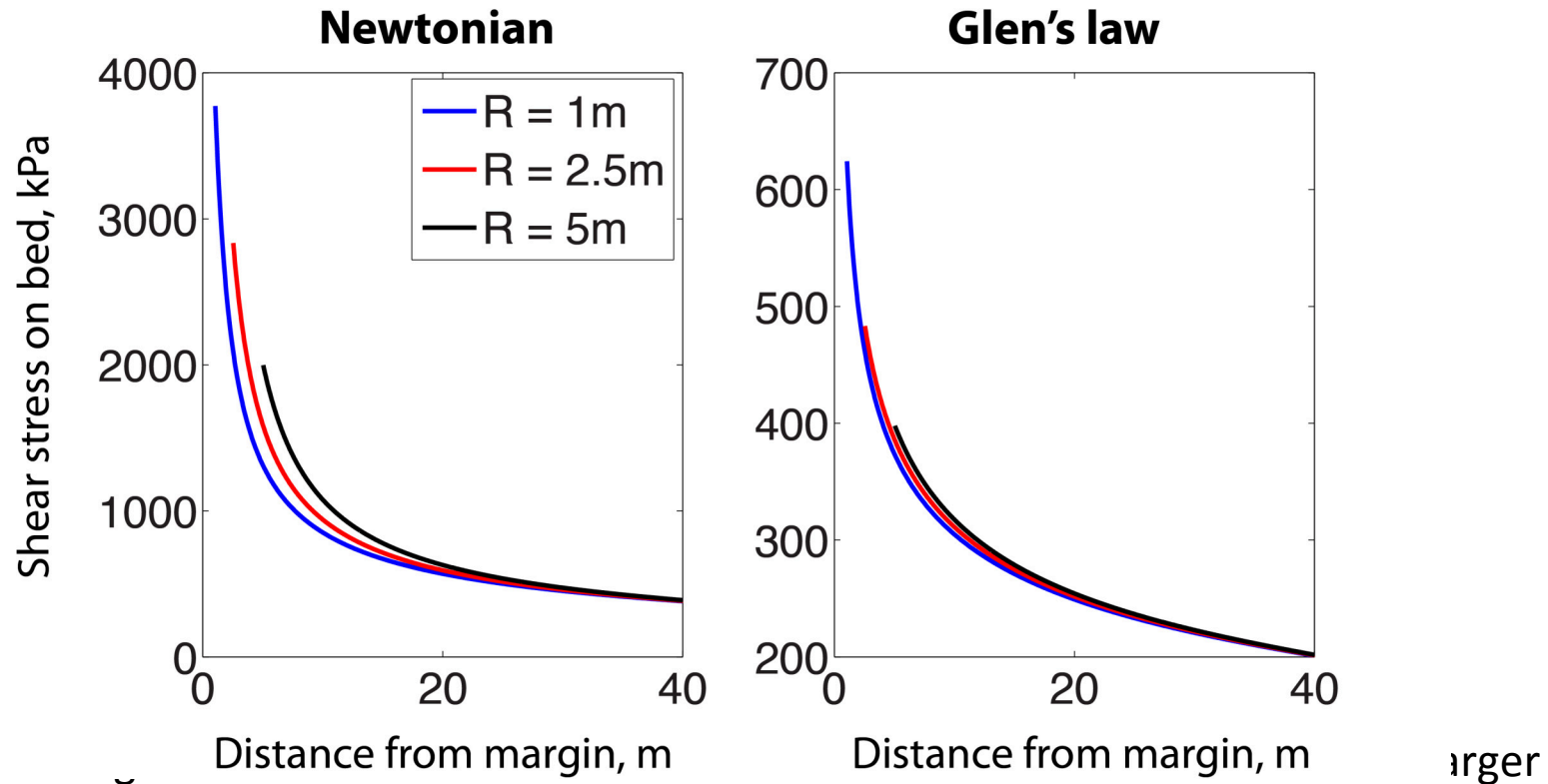
# Flow of ice around a channel

- A finite radius of curvature at a crack tip blunts the stress concentration.
- Motivated by this we consider a slipping to locked transition that occurs across a channel.



# Influence of channel size

- The channel size also influences the maximum stress on the bed.



- Distance from margin, m
  - larger strength of the ice-bed interface.
- Even if the the stress is larger than the strength the channel may still facilitate locking through a cohesive zone (Dugdale [1960]; Barenblatt [1962]; Schoof [2012]).

# Conclusions, West Antarctic Ice Stream Margins

- The transition from a slipping to a locked bed concentrates stress beneath the ridge.
- Our model (**without lateral advection**) predicts that shear heating at the margin leads to temperate ice and melting for almost all ice streams. This melt may lead to channel formation beneath ice stream margins.
- Such a channel limits the maximum stress on the locked bed and increases the strength of the ice-bed interface, providing a mechanism that may facilitate locking.
- The maximum stress on the locked portion of the bed decreases with increasing channel radius.
- Glen's law leads to a substantially lower maximum stress than a Newtonian rheology.
- We have **not proven** that the mechanisms outlined could stabilize a shear margin, and we **have no simple way at present of more fully evaluating the important effects of lateral thermal advection**. So this is an **interim report!**



Subsequent pages were not included in the lecture presentation

***Shear localization due to thermal  
pressurization of pore fluids in  
rapidly sheared granular media  
(rapidly sheared fault zones)***

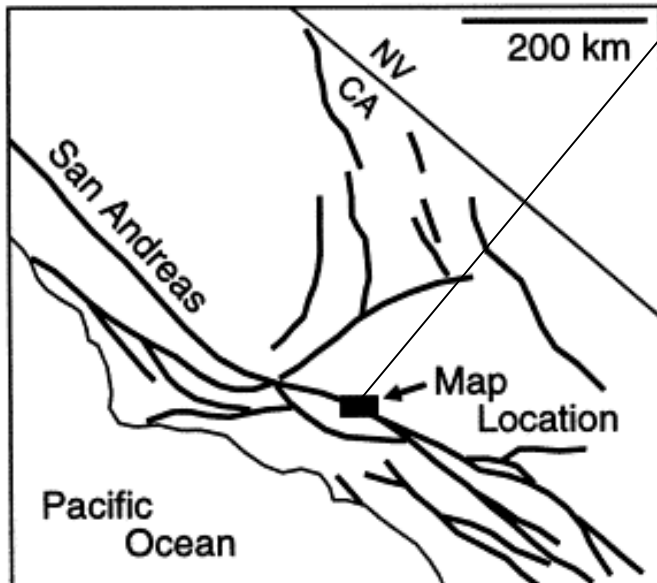
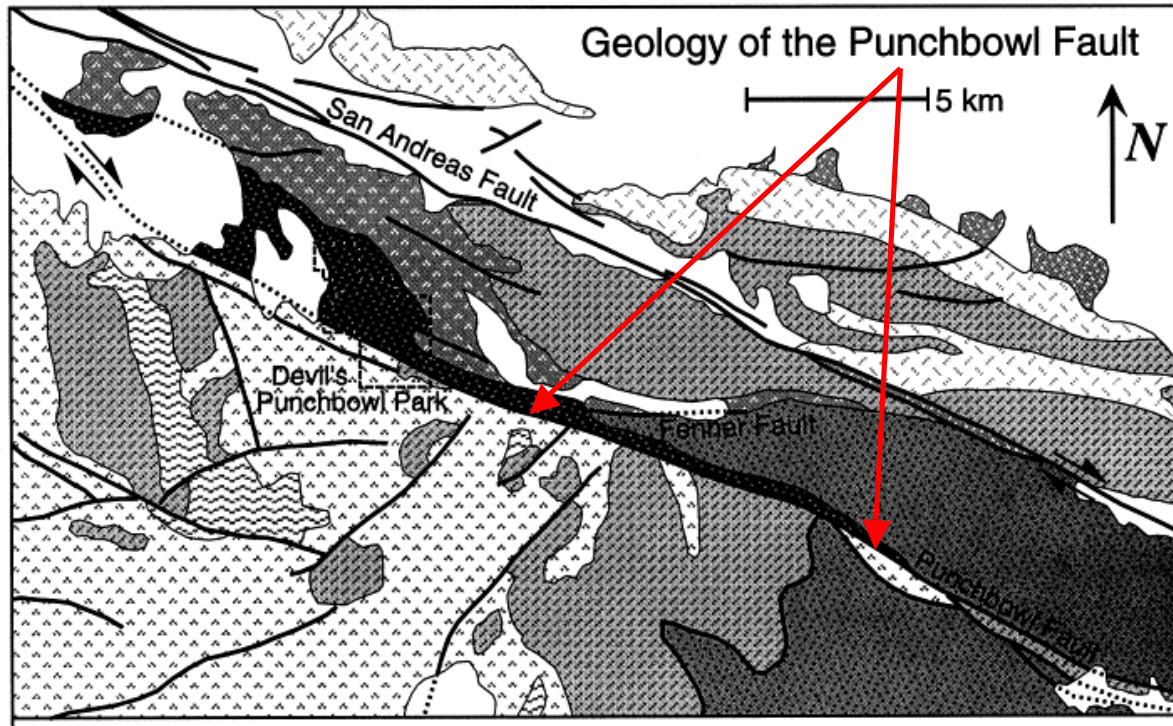
**Nicolas Brantut (Univ. Col. London)**

**John D. Platt (Harvard)**

**James R. Rice (Harvard)**

**John W. Rudnicki (Northwestern)**

Chester & Chester  
[*Tectonophys.*, 1998]





# Earthquake shear is highly localized

Punchbowl PSS, composite based on Chester & Chester [*Tectonophysics* '98] & Chester & Goldsby [*SCEC* '03]

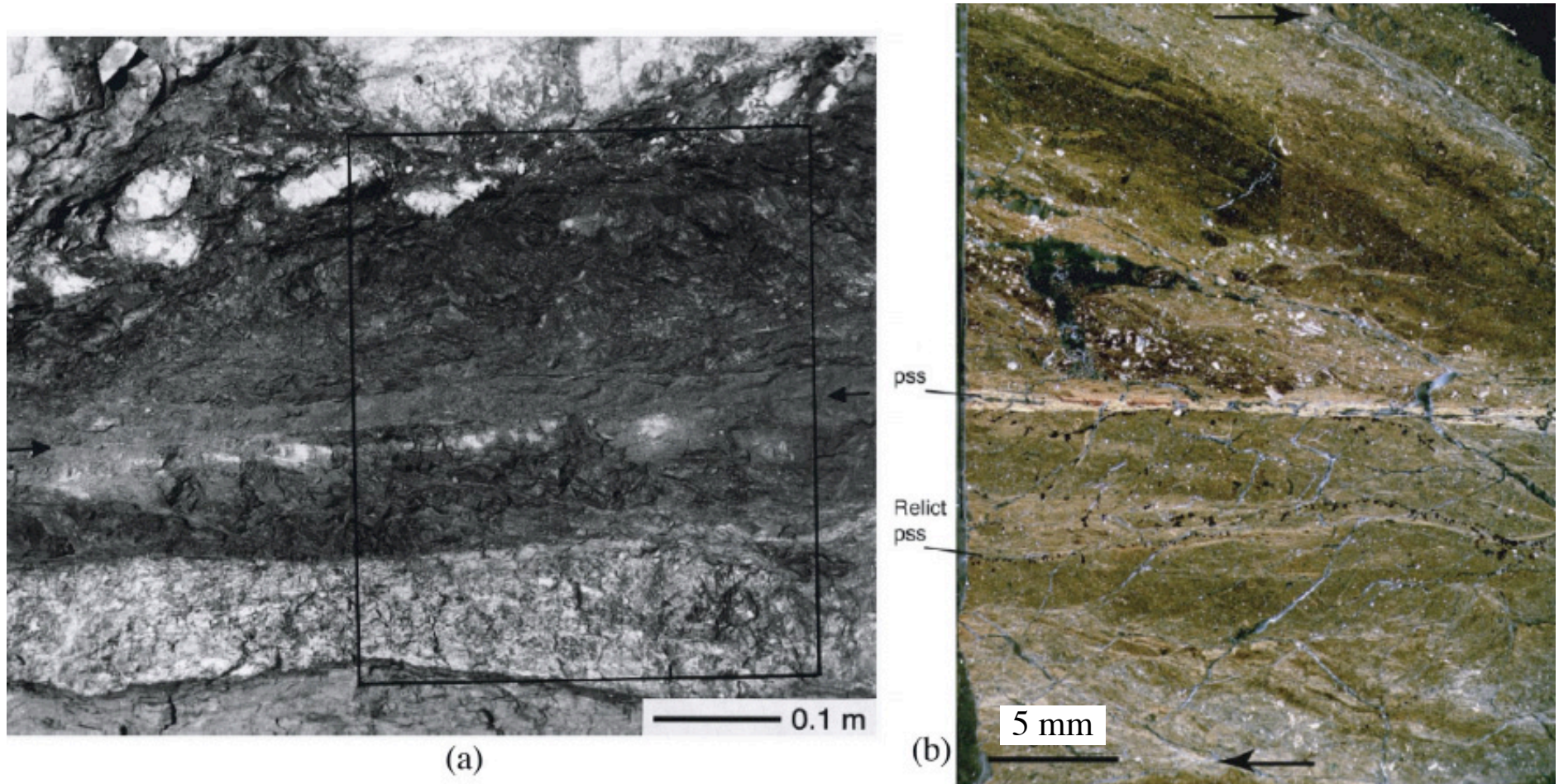


**Figure 1.** Principal slip surface (PSS) along the Punchbowl fault. (a) From *Chester and Chester* [1998]: Ultracataclasite zone with PSS marked by black arrows; note 100 mm scale bar. (b) From *Chester et al.* (manuscript in preparation, 2005) [also *Chester et al.*, 2003; *Chester and Goldsby*, 2003]: Thin section; note 5 mm scale bar and  $\sim 1$  mm localization zone (bright strip when viewed in crossed polarizers due to preferred orientation), with microshear localization of most intense straining to  $\sim 100\text{--}300$   $\mu\text{m}$  thickness.



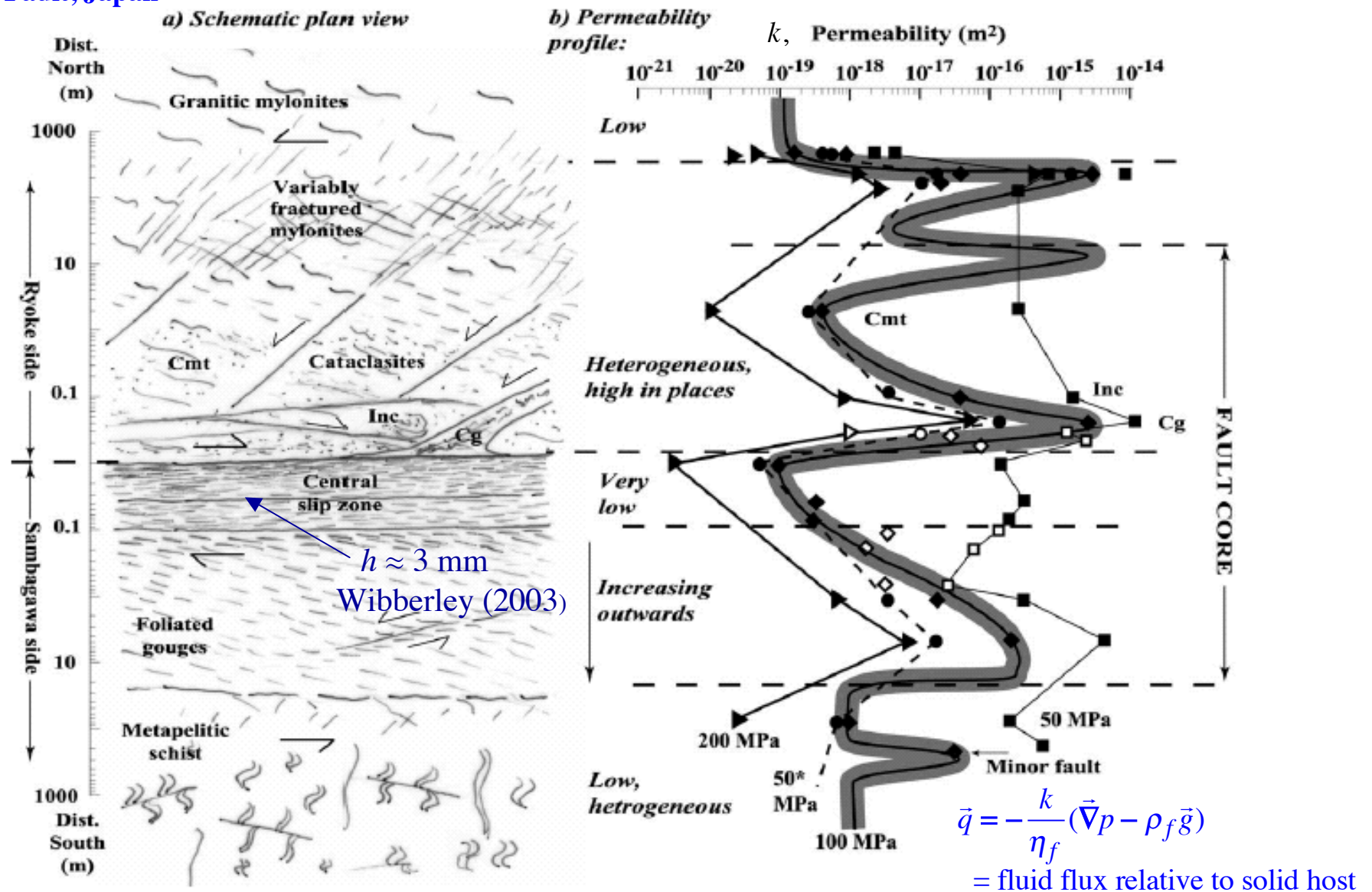


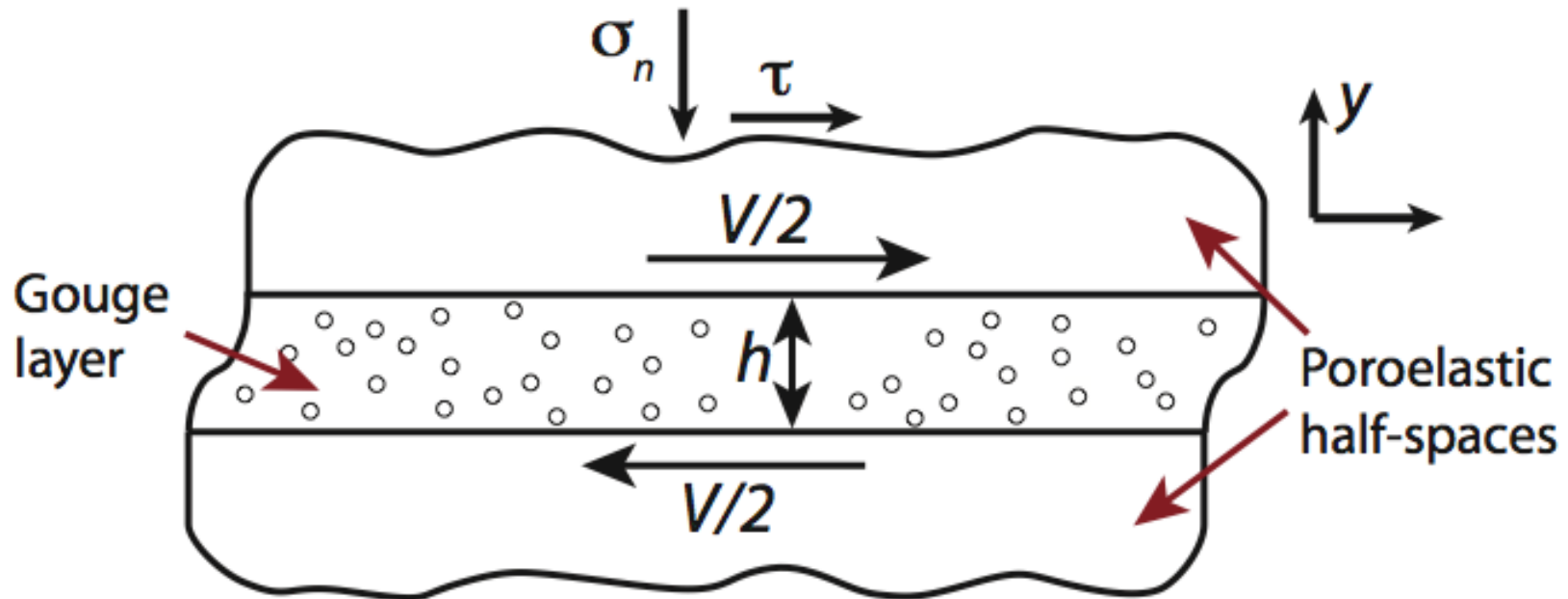
Fig. 11. Sketch summary of the main elements of permeability structure across the Median Tectonic Line. (a) Summary of the structural zones; (b) summary permeability data distribution for different confining pressures (stated at the base, with \* denoting data from the deconfining path), for 20 MPa pore pressure, given the mapped distribution of fault rocks shown in Figs. 1–3. Note that the distance axis is logarithmic in both directions away from the Ryoke/Sambagawa contact. 'Cmt' and 'Inc' denote cemented and incohesive foliated cataclasites, respectively, and 'Cg' denotes crenulated gouge.

$$\tau = f \times (\sigma_n - p)$$

*Statically strong but dynamically weak faults, e.g., due to thermal weakening in rapid, large slip:*

- *Process expected to be important from start of seismic slip:*
  - Thermal pressurization of in-situ pore fluid, reduces effective stress.
- *Process that may set in at large enough rise in T:*
  - Thermal decomposition, fluid product phase at high pressure (e.g., CO<sub>2</sub> from carbonates; H<sub>2</sub>O from clays or serpentines).
- *Ultimately:*
  - Melting at large slip, if above have not limited increase of T.

## Shear of a fluid-saturated gouge layer



- Two non-yielding half-spaces are moved relative to each other at a speed  $V$ .
- All inelastic deformation accommodated in gouge layer, leading to a nominal strain rate  $\dot{\gamma}_0 = V / h$ .

## Thermo-mechanical model in gouge layer

- To model the deforming gouge layer we use,

Mechanical equilibrium  $\frac{\partial \tau}{\partial y} = 0, \quad \frac{\partial \sigma_n}{\partial y} = 0$

Conservation of energy  $\frac{\partial T}{\partial t} - \alpha_{th} \frac{\partial^2 T}{\partial y^2} = \frac{\tau \dot{\gamma}}{\rho c}$

Conservation of fluid mass  $\frac{\partial p}{\partial t} - \alpha_{hy} \frac{\partial^2 p}{\partial y^2} = \Lambda \frac{\partial T}{\partial t}$

- Shear stress modeled using the effective stress and **rate-strengthening** friction,

$$\tau = f(\dot{\gamma})(\sigma_n - p) \quad f(\dot{\gamma}) = f_0 + (a - b) \log\left(\frac{\dot{\gamma}}{\dot{\gamma}_0}\right)$$

$$\left( \text{We assume } a - b \equiv \left( \dot{\gamma} \frac{df(\dot{\gamma})}{d\dot{\gamma}} \right)_{\dot{\gamma}=\dot{\gamma}_0} > 0 \right)$$



**Shear between moving rigid blocks of perfectly insulating, impermeable material :**

**Exact homogeneous shear solution (Lachenbruch, JGR, 1980, version ignoring dilatancy) :**

$$\tau(t) = f_o (\sigma_n - p(t)) = f_o (\sigma_n - p_a) \exp\left(-f_o \frac{\Lambda}{\rho c} \dot{\gamma}_o t\right),$$

$$(\dot{\gamma}_o = V / h)$$

**Linearized perturbation analysis :**

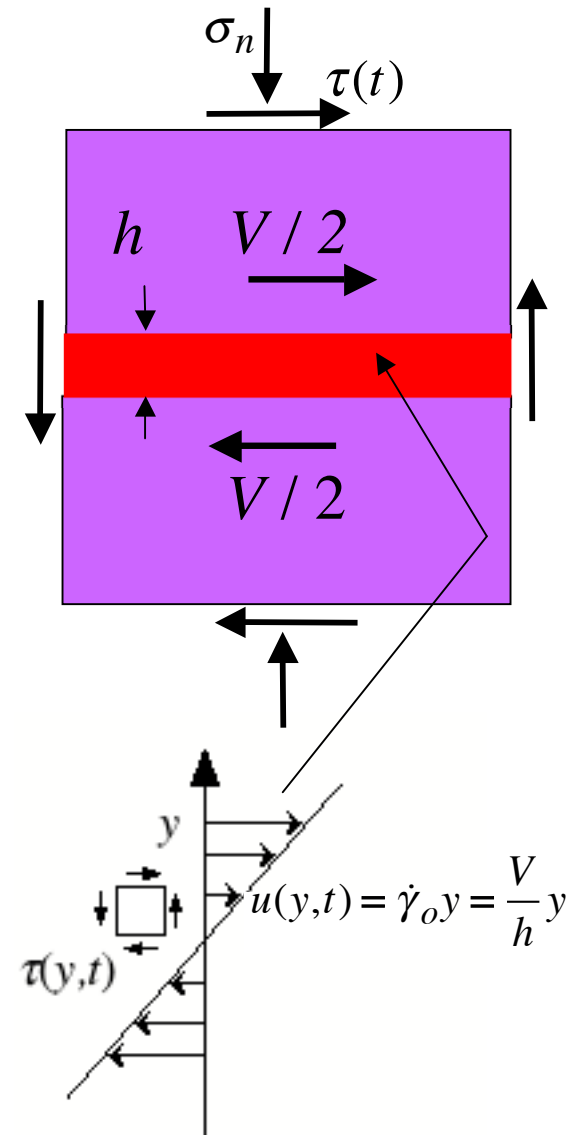
**Is that solution stable to small perturbations?**

*Not unless h is very small !*

$$\text{Stable only if } h \leq W_{crit} \equiv \frac{\pi^2}{\left(2 + \frac{f_o}{a-b}\right)} \frac{\rho c}{f_o \Lambda} \frac{(\alpha_{th} + \alpha_{hy})}{V}.$$

$$\left( \text{Typically, } \frac{f_o}{a-b} \gg 2 \Rightarrow W_{crit} \approx \pi^2 \frac{a-b}{f_o^2} \frac{\rho c}{\Lambda} \frac{\alpha_{th} + \alpha_{hy}}{V} \right)$$

[ $W_{crit} = \lambda_{shr} / 2$ , where  $\lambda_{shr}$  = longest wavelength  $\lambda$  for stable linearized response to infinitesimal  $\exp(2\pi i y / \lambda)$  perturbation]



Rice, Rudnicki & Platt (to JGR 2013)

*Estimates of maximum stable shear layer thickness (i.e., localized zone width)  $W_{crit}$*

Results, using  $f_o = 0.4$ ,  $\frac{f_o}{a-b} = 20$ ,  $V = 1 \frac{\text{m}}{\text{s}}$ ,  $\alpha_{th} = 0.7 \frac{\text{mm}^2}{\text{s}}$ ,  $\rho c = 2.7 \frac{\text{MPa}}{^\circ\text{C}}$  :

**Corresponding to ~ 7 km depth :**

*Low estimate* (Based on lab properties of *intact* Median Tectonic Line gouge [Wibberley and Shimamoto, 2003] at effective confining stress = 125 MPa and  $T = 200^\circ\text{C}$ ):

$$\Lambda = 0.70 \frac{\text{MPa}}{^\circ\text{C}}, \text{ and } \alpha_{hy} = 1.5 \frac{\text{mm}^2}{\text{s}} \Rightarrow \boxed{W_{crit} = 3-5 \mu\text{m}}$$

*High estimate* (Accounts very roughly for *fresh damage* of the initially intact fault gouge, introduced at the rupture front just before and during shear, by increasing permeability  $k$  to  $k^{dmg} = 5-10 k$ , and increasing drained compressibility  $\beta_d$  to  $\beta_d^{dmg} = 1.5-2 \beta_d$ ):

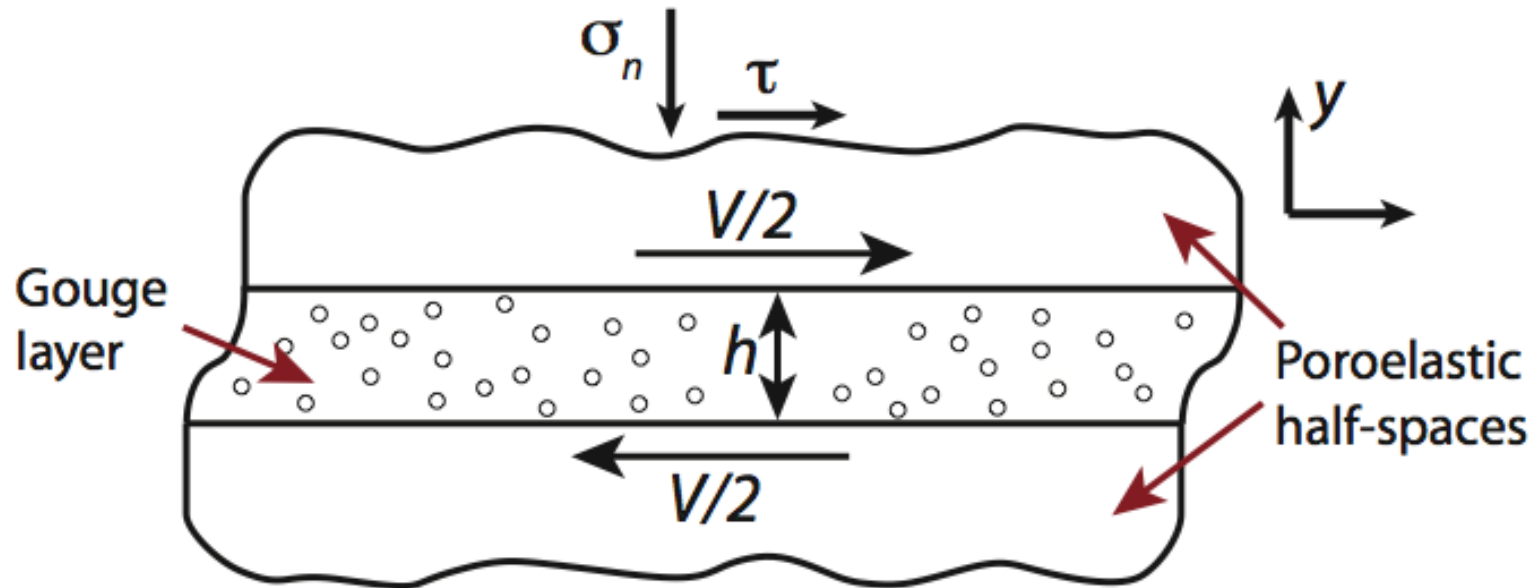
$$\Lambda \approx 0.34 \frac{\text{MPa}}{^\circ\text{C}}, \text{ and } \alpha_{hy} \approx 3.5 \frac{\text{mm}^2}{\text{s}} \Rightarrow \boxed{W_{crit} \approx 25-40 \mu\text{m}}$$

**Corresponding to ~ 1 km depth :**

*Low estimate* :  $\boxed{W_{crit} \sim 25 \mu\text{m}}$

*High estimate* :  $\boxed{W_{crit} \sim 200 \mu\text{m}}$

Shear of a fluid-saturated gouge layer:  
**Full nonlinear numerical solutions**  
(vs. linearized perturbations)

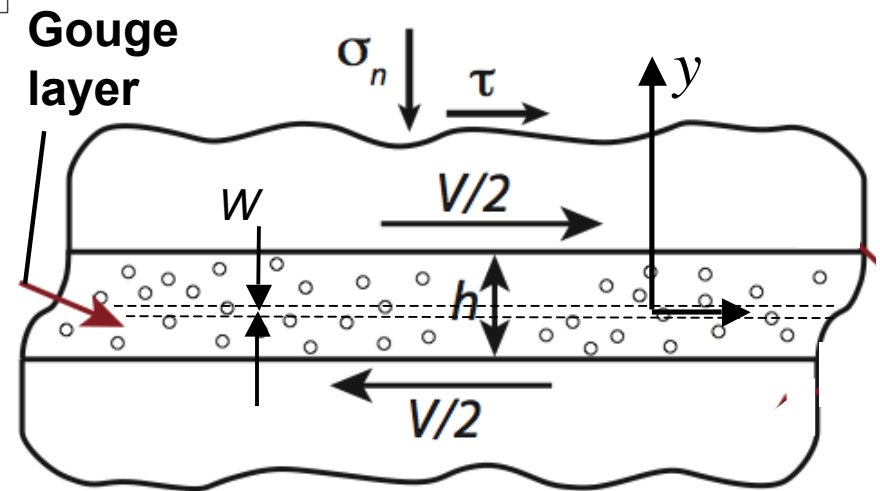
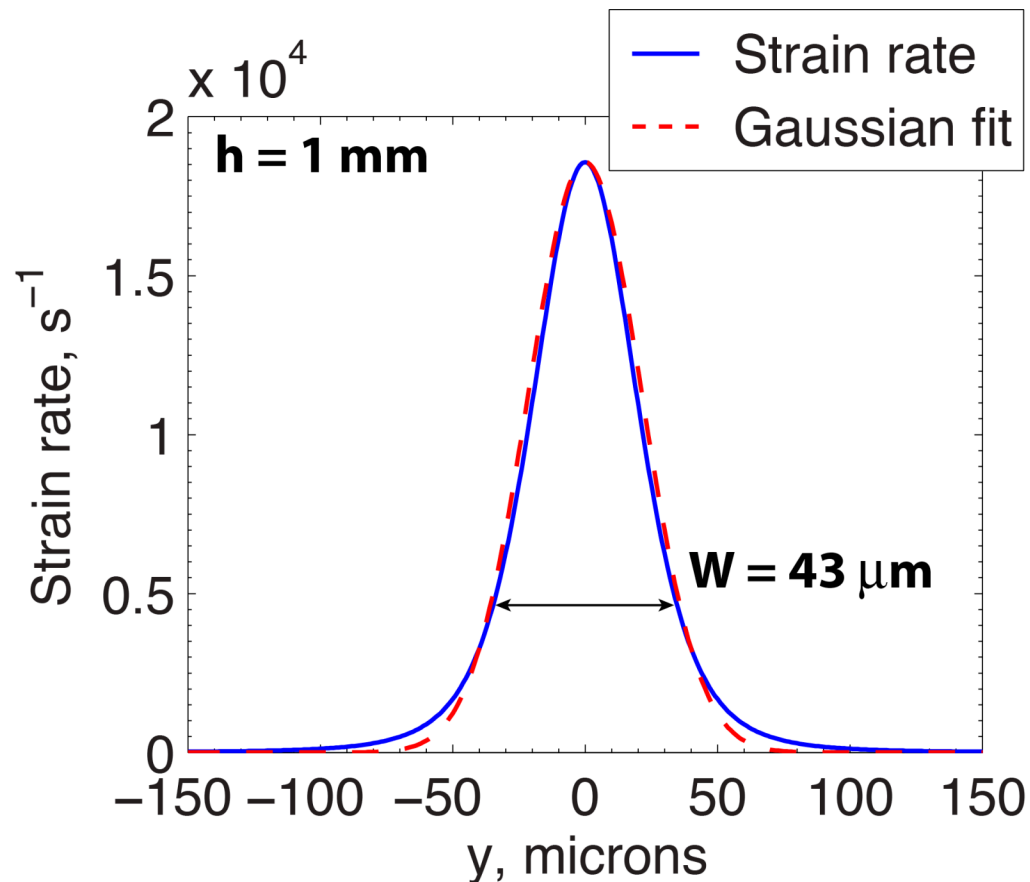


- Two non-yielding half-spaces are moved relative to each other at a speed  $V$  (taken as 1 m/s).
- All deformation accommodated in gouge layer leading to a nominal strain rate,

$$\dot{\gamma}_o = \frac{V}{h}$$

# Strain localization

- Simulations using representative physical values show that strain localization does occur.



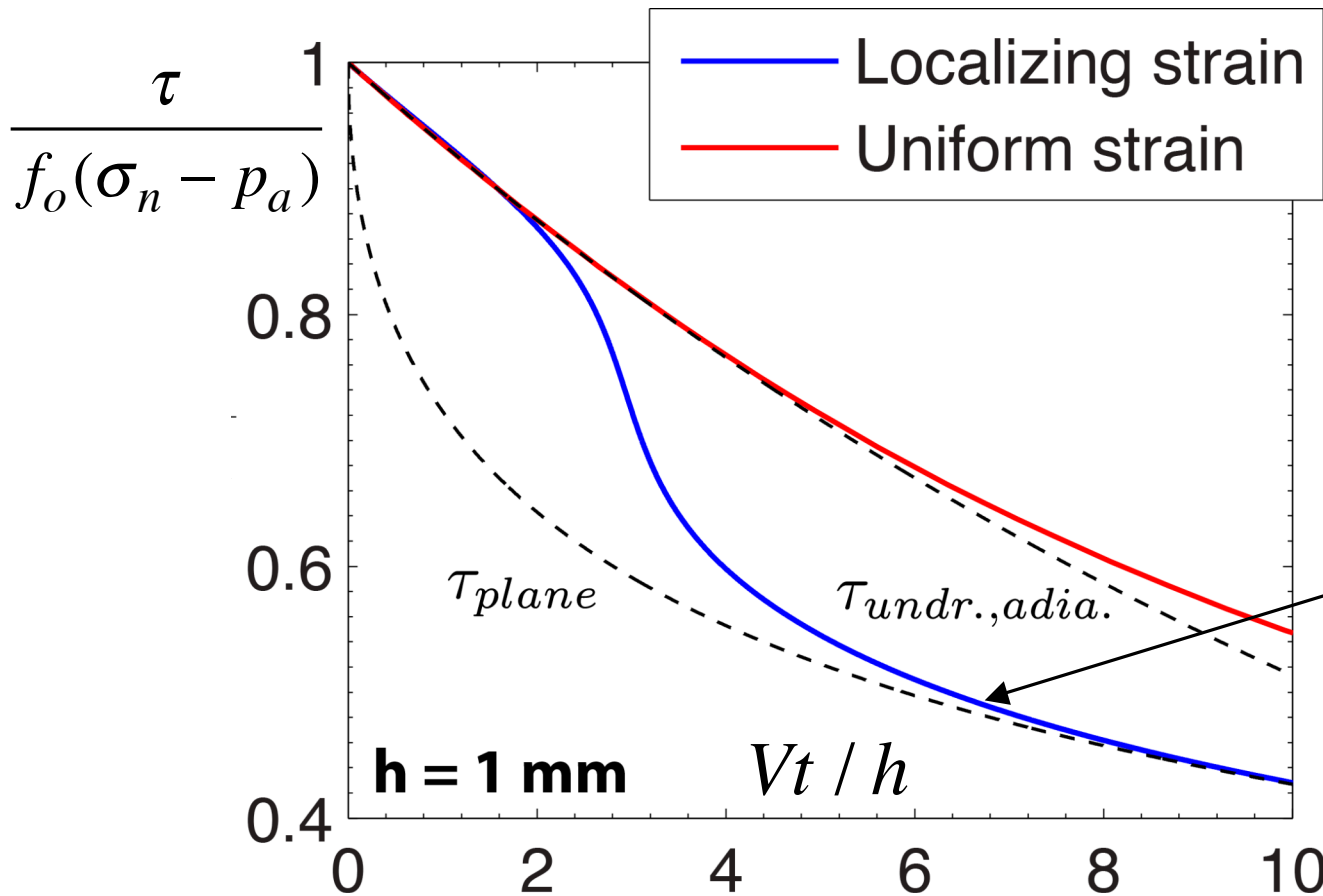
- Deformation has localized to a zone much thinner than the layer,  $W \ll h$  ( $43 \text{ } \mu\text{m} \ll 1,000 \text{ } \mu\text{m}$ ).

$W_{\text{nonlin. calc.}}$  is comparable to  $W_{\text{lin. pert.}}$  .



# Implications, dynamic weakening

- Weakening of the gouge layers during localization



Closely follows  
“slip on a plane”  
analysis of Rice  
[JGR, 2006], see  
also Mase &  
Smith [JGR, 1987]

- Localization leads to additional weakening.

$$\tau = f_o(\sigma_n - p_a) \exp\left(\frac{Vt}{L^*}\right) \operatorname{erfc}\left(\sqrt{\frac{Vt}{L^*}}\right) \quad \text{where} \quad L^* = \left(\frac{2\rho c}{f_o\Omega}\right)^2 \frac{\left(\sqrt{\alpha_{hy}} + \sqrt{\alpha_{th}}\right)^2}{V}$$

$$\tau = f \times (\sigma_n - p)$$

*Statically strong but dynamically weak faults, e.g., due to thermal weakening in rapid, large slip:*

- *Process expected to be important from start of seismic slip:*
  - Thermal pressurization of in-situ pore fluid, reduces effective stress.
- *Process that may set in at large enough rise in T:*
  - Thermal decomposition, fluid product phase at high pressure (e.g., CO<sub>2</sub> from carbonates; H<sub>2</sub>O from clays or serpentines).
- *Ultimately:*
  - Melting at large slip, if above have not limited increase of T.

***Examples, thermal decomposition:***

***Dolomite, CaMg(CO<sub>3</sub>)<sub>2</sub>*** (De Paola et al., *Tectonics*, 2008, *Geology*, 2011; Goren et al., *J. Geophys. Res.*, 2010):

- At  $T \sim 550^\circ\text{C}$ , dolomite decomposes to calcite, periclase, and carbon dioxide:  
$$\text{CaMg}(\text{CO}_3)_2 \rightarrow \text{CaCO}_3 + \text{MgO} + \text{CO}_2$$
- At  $T \sim 700\text{-}900^\circ\text{C}$ , the calcite further decomposes to lime and carbon dioxide:  
$$\text{CaCO}_3 \rightarrow \text{CaO} + \text{CO}_2$$

***Many clays and hydrous silicates*** (Brantut et al., *J. Geophys. Res.*, 2010):

- At  $T \sim 500^\circ\text{C}$  ( $\sim 300^\circ\text{C}$  for smectite,  $\sim 800^\circ\text{C}$  for chlorite), decomposition releasing  $\text{H}_2\text{O}$  starts.

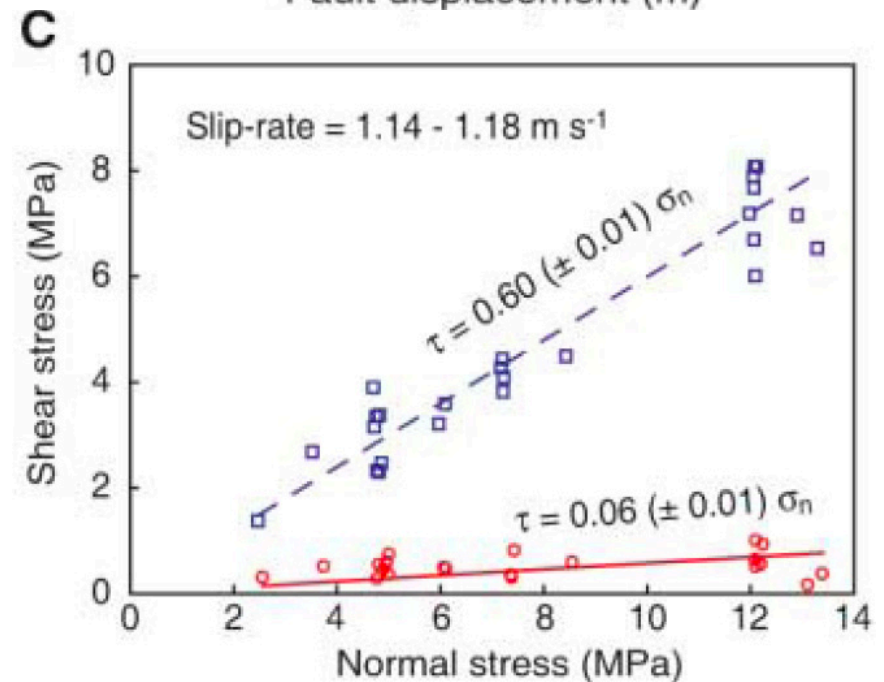
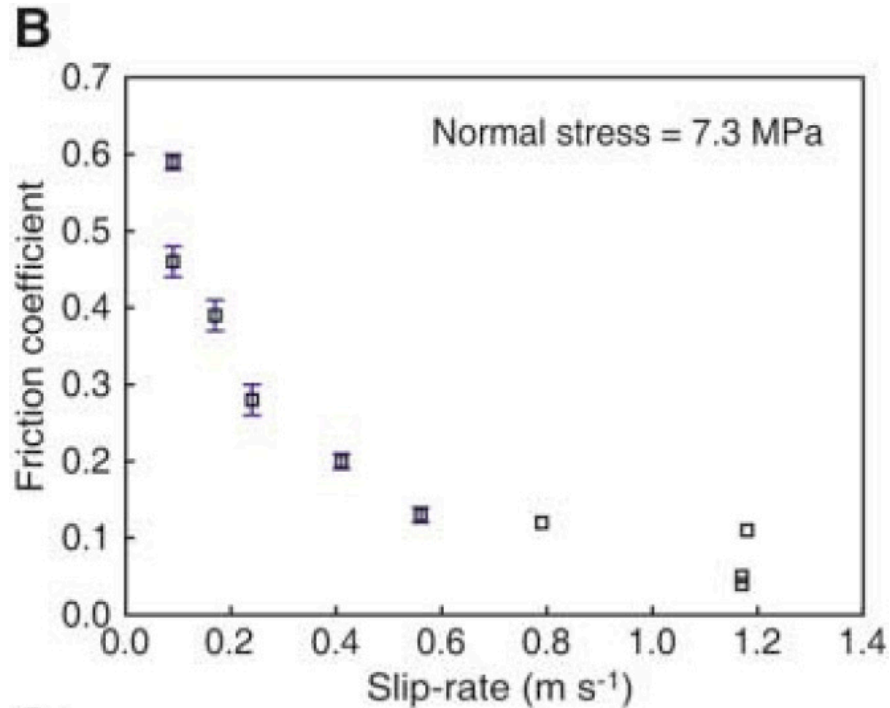
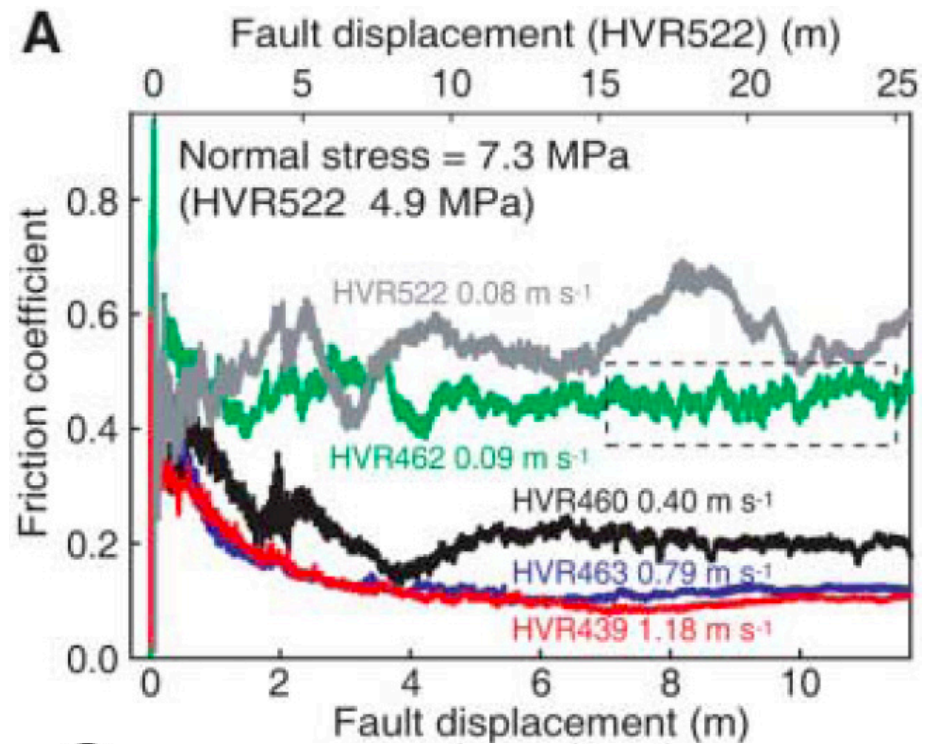
***Gypsum, CaSO<sub>4</sub>(H<sub>2</sub>O)<sub>2</sub>*** (Brantut et al., *Geology*, 2010):

- At  $T \sim 100^\circ\text{C}$ , gypsum dehydrates to form bassanite:  
$$\text{CaSO}_4(\text{H}_2\text{O})_2 \rightarrow \text{CaSO}_4(\text{H}_2\text{O})_{0.5} + 1.5 \text{H}_2\text{O}$$
- At  $T \sim 140^\circ\text{C}$ , bassanite turns into anhydrite  
$$\text{CaSO}_4(\text{H}_2\text{O})_{0.5} \rightarrow \text{CaSO}_4 + 0.5 \text{H}_2\text{O}$$

[Han, Shimamoto, Hirose, Ree & Ando, *Sci.*, 2007]:

### Carbonate Faults

Simulated faults in Carrara Marble at subseismic to seismic slip rates)

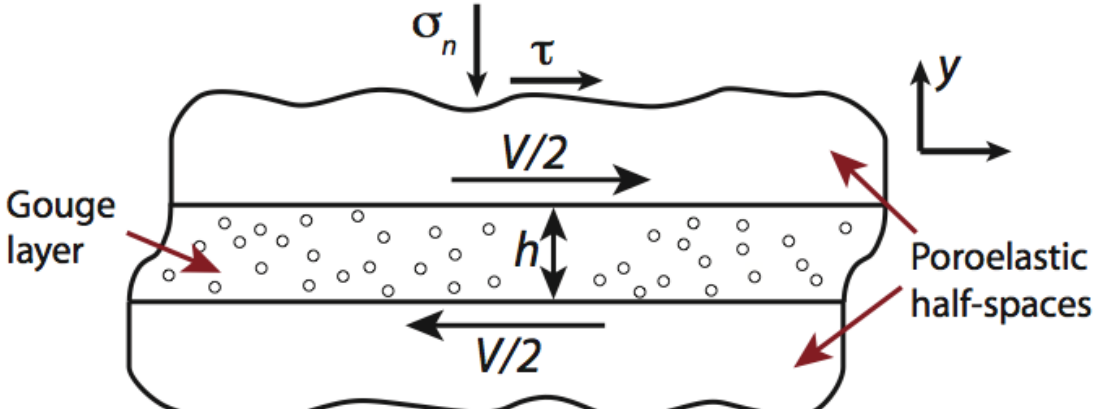




# Model for decomposing gouge material

- To model the deforming gouge layer we use, based on J. Sulem and co-workers (Vardoulakis, Brantut, Ghabezloo, Famin, Lazar, Noda, Schubnel, Stefanou, Veveakis, ...),

$$\frac{\partial T}{\partial t} = \frac{\tau \dot{\gamma}}{\rho c} + \alpha_{th} \frac{\partial^2 T}{\partial y^2} - E_r \frac{\partial \xi}{\partial t}$$

$$\frac{\partial p}{\partial t} = \Lambda \frac{\partial T}{\partial t} + \alpha_{hy} \frac{\partial^2 p}{\partial y^2} + P_r \frac{\partial \xi}{\partial t}$$


The diagram illustrates a cross-section of a gouge layer between two poroelastic half-spaces. The gouge layer is shown as a central region with a thickness  $h$ , containing small circles representing particles. The top half-space is subjected to a normal stress  $\sigma_n$  (downward arrow) and a shear stress  $\tau$  (rightward arrow). The gouge layer moves with a velocity  $V/2$  to the right, while the half-spaces move with a velocity  $V/2$  to the left. A coordinate system with a vertical  $y$ -axis is shown on the right.

- We assume that the reaction follows an Arrhenius kinetic law,

$$\frac{\partial \xi}{\partial t} = A(1 - \xi) \exp\left(-\frac{Q}{RT}\right)$$

# Different materials

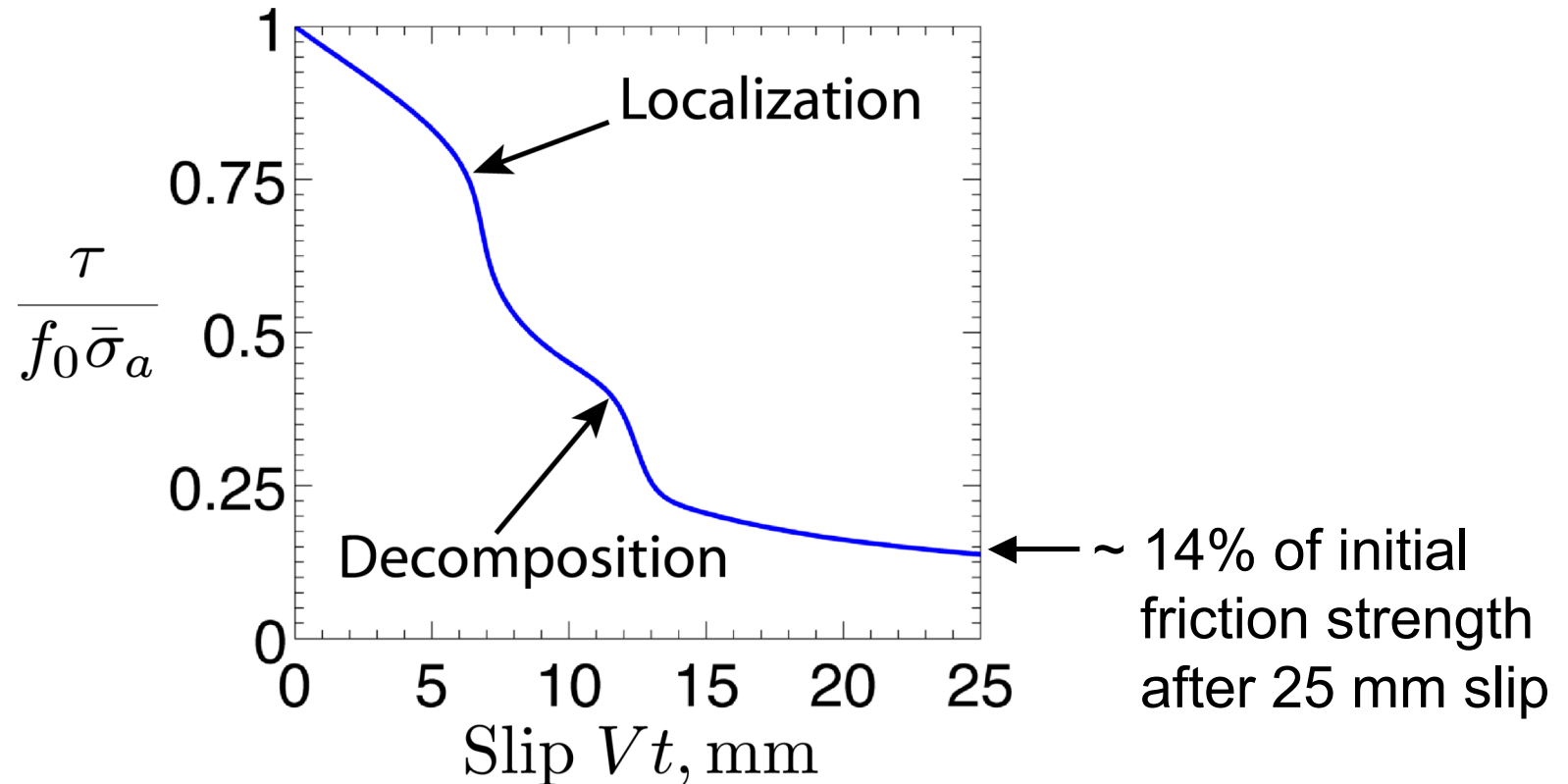
Platt, Brantut & Rice (AGU,  
Fall 2011; in prep 2013 for *JGR*)

Mineral	$E_r$ (K)	$P_r$ (MPa)	$W$ ( $\mu\text{m}$ )	$T_c$ ( $^{\circ}\text{C}$ )
Calcite	3093	6421	18	900
Lizardite	228	1252	6	550
Kaolinite	3627	1599	86	500
Talc	496	586	32	800
Gypsum	89	1635	2	100

Linear perturbation estimate, localization zone width  $W$ ,

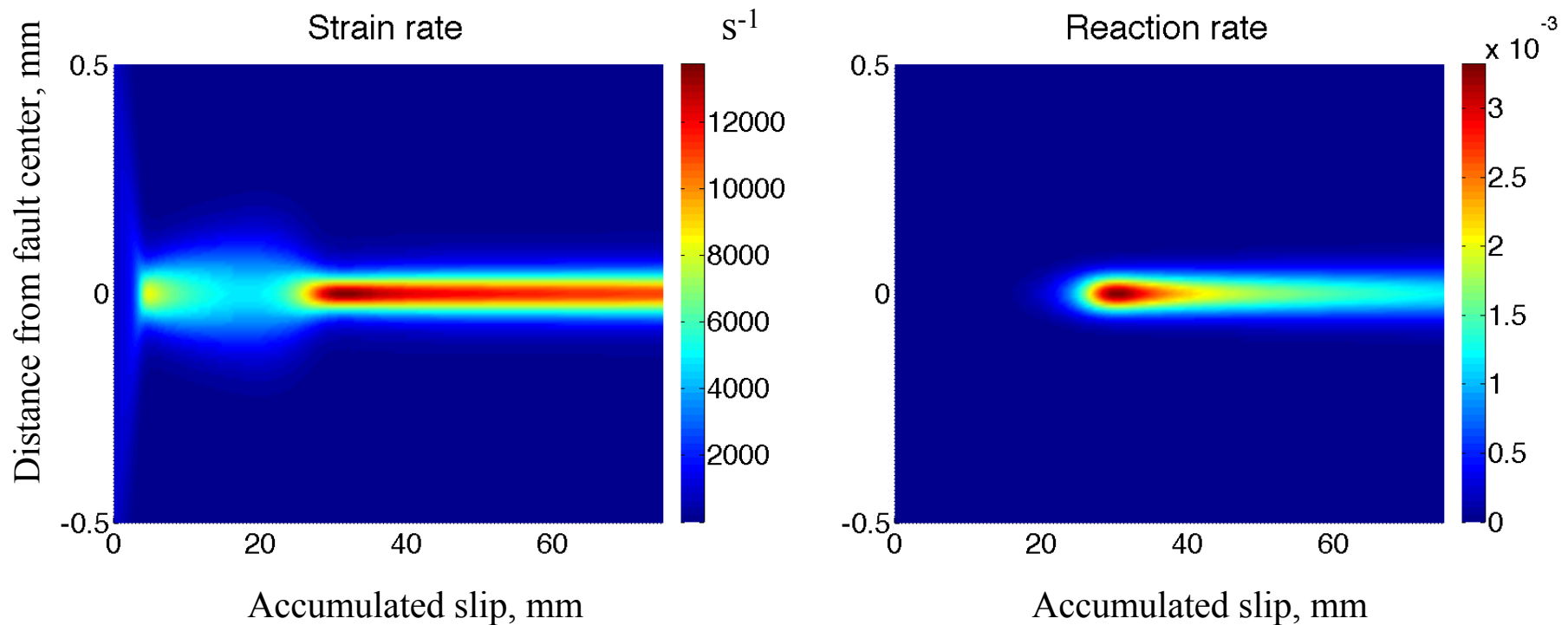
high  $T$ , fast reaction rate limit: 
$$W = \pi^2 \frac{\alpha_{hy}}{V} \frac{(a-b)}{f_o^2} \frac{\rho c E_r}{P_r}$$

# Representative simulations: thermal pressurization of in-situ fluids, followed by thermal decomposition



**Suggests faults may be *strong* but *brittle*  
(quickly lose strength after slip is initiated  
at a place of localized stress concentration)**

- Numerical solutions for a 1 mm wide gouge layer.

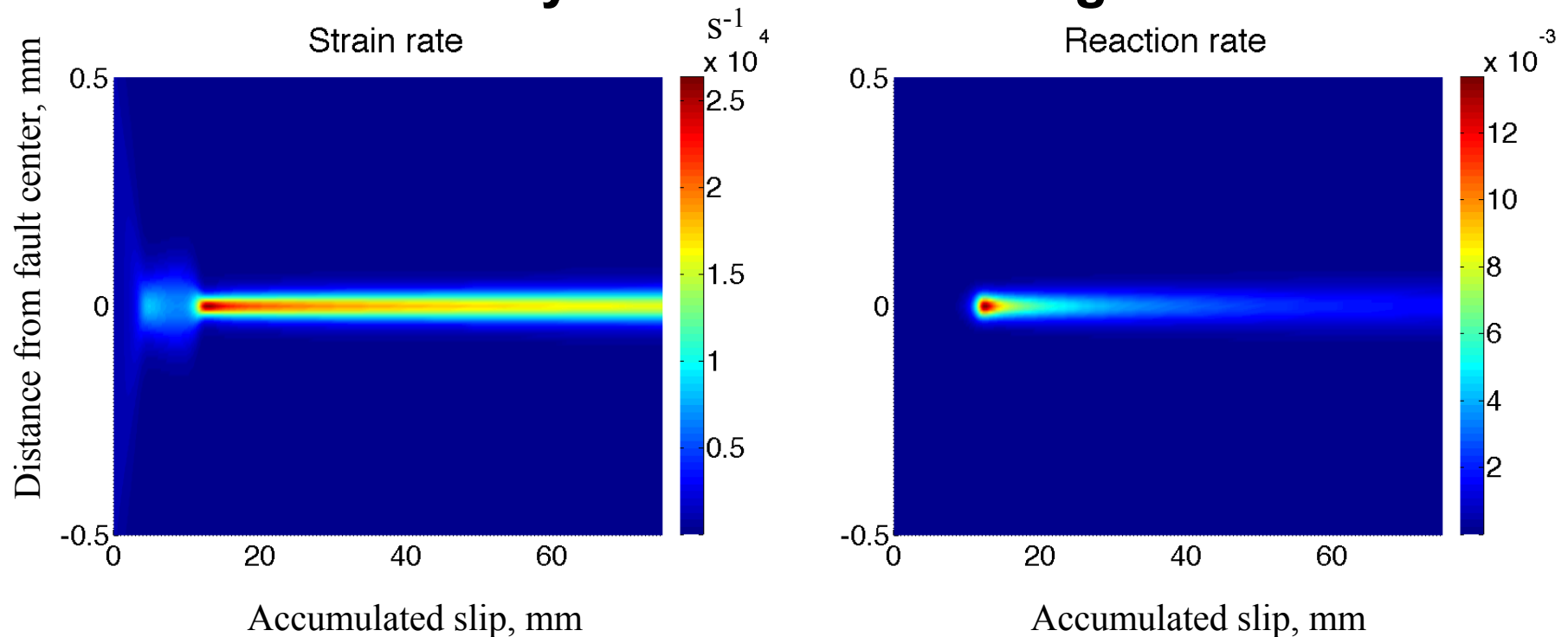


- When the reaction becomes important, we observe significant strain localization ( $W_{\text{nonlin. calc.}}$  of order  $\sim 2 \times W_{\text{lin. pert.}}$ ).



# Independence of reaction rate

- Our linear stability analysis predicts the localized zone width is independent of kinetic parameters. To test this we **increase  $A$  by three orders of magnitude.**

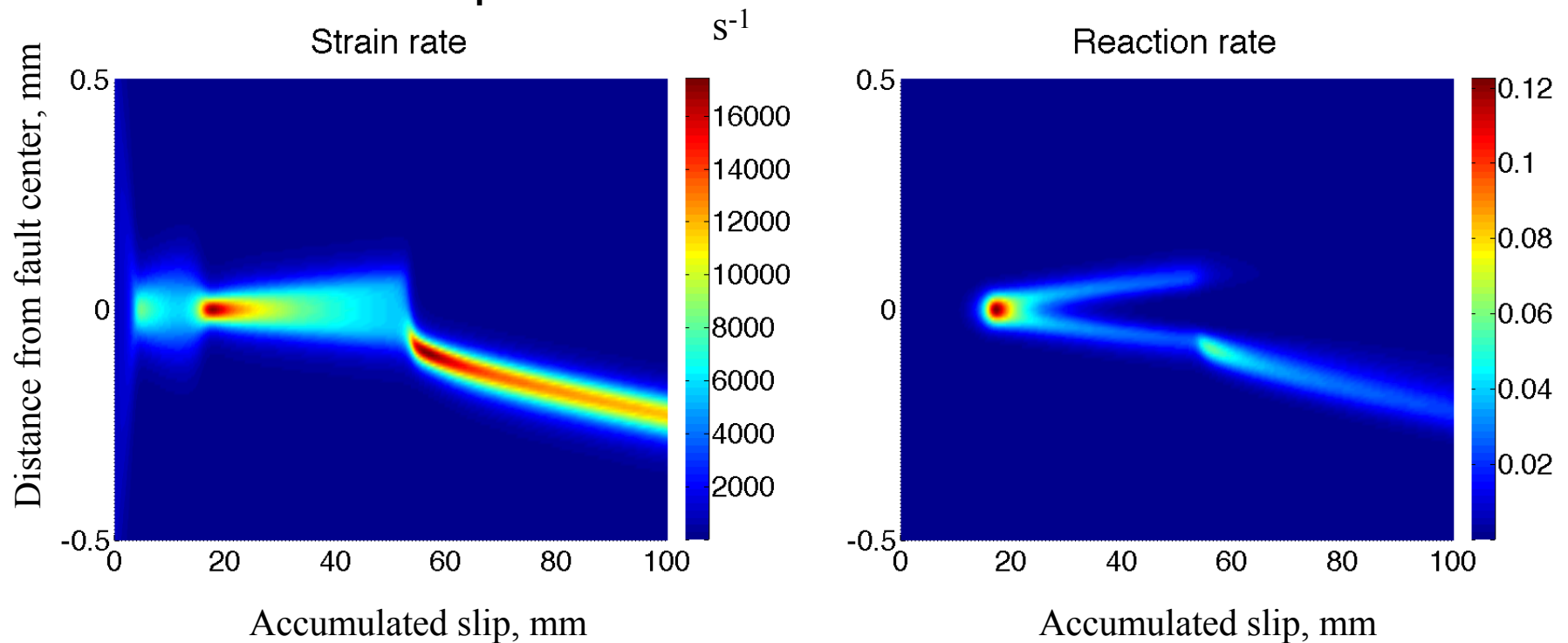


- The localized zone width has only decreased by a factor of two.

Platt, Brantut & Rice (AGU, Fall 2011; in prep 2013 for *JGR*)

# Localized zone migration

- Now we investigate a case for which **depletion of reactant** is important.

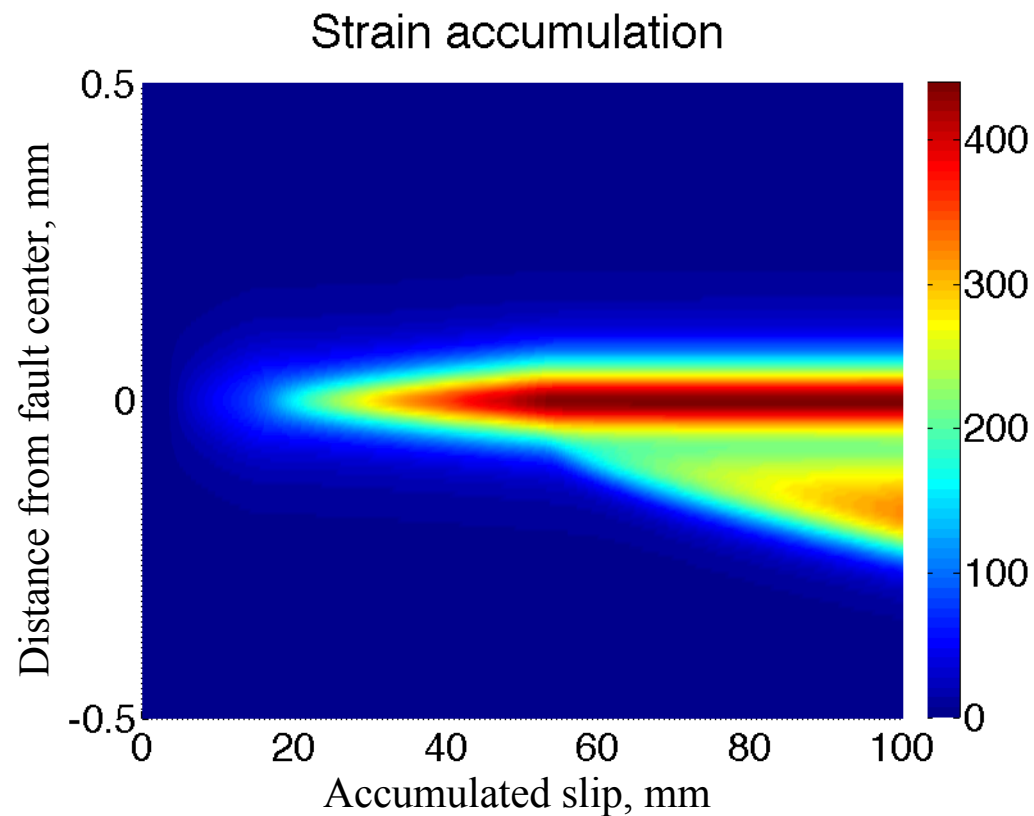


- Depletion causes the zone of localized straining to migrate. The strain rate and reaction rate profiles are strongly coupled.

Platt, Brantut & Rice (AGU, Fall 2011; in prep 2013 for *JGR*)

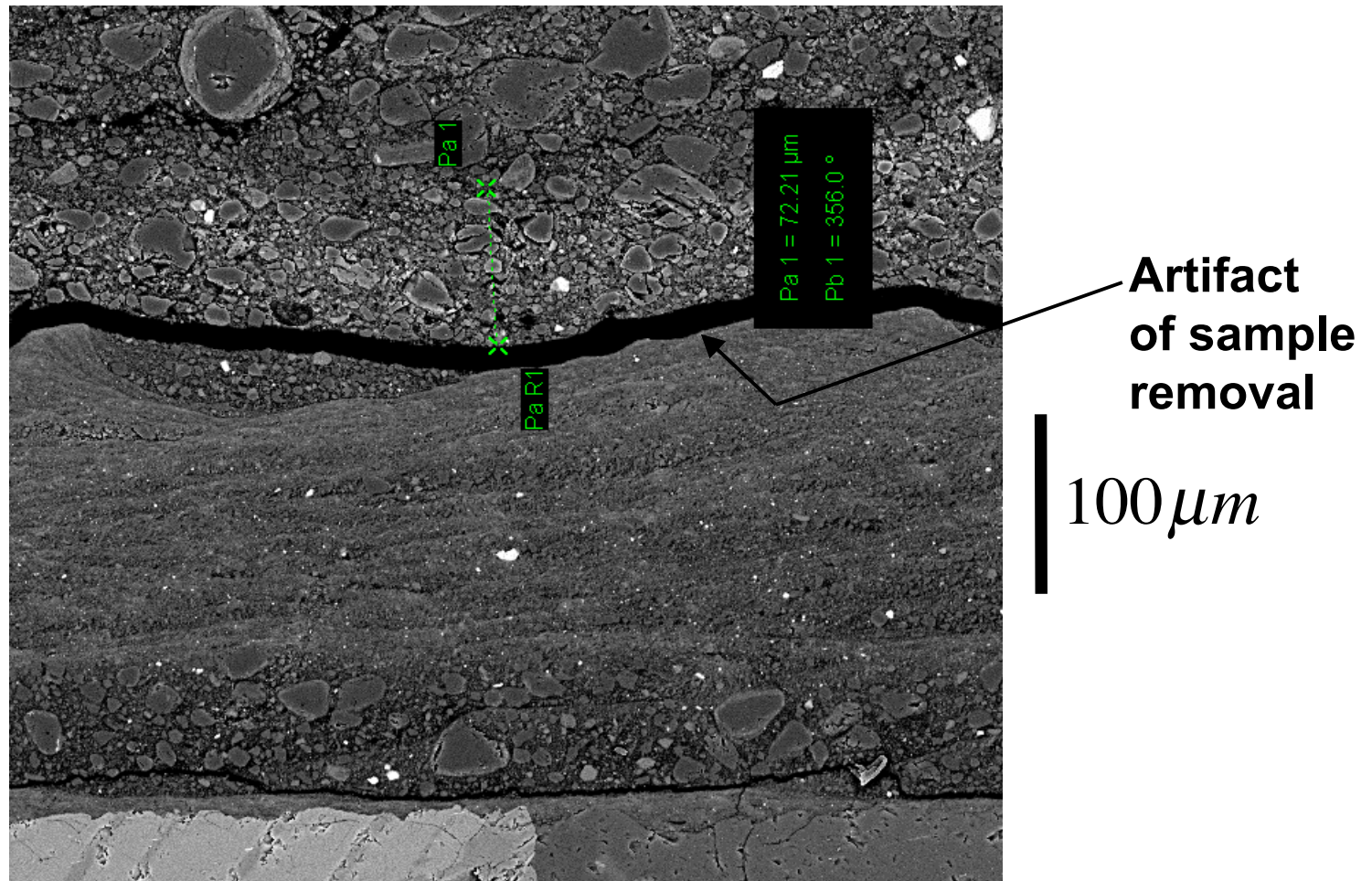
# Localized zone migration

- This localized zone migration leads to a complex, non-monotonic, strain history.



Platt, Brantut & Rice (AGU, Fall 2011; in prep 2013 for *JGR*)

# Observation suggesting migration (in rotary shear of carbonate sample)

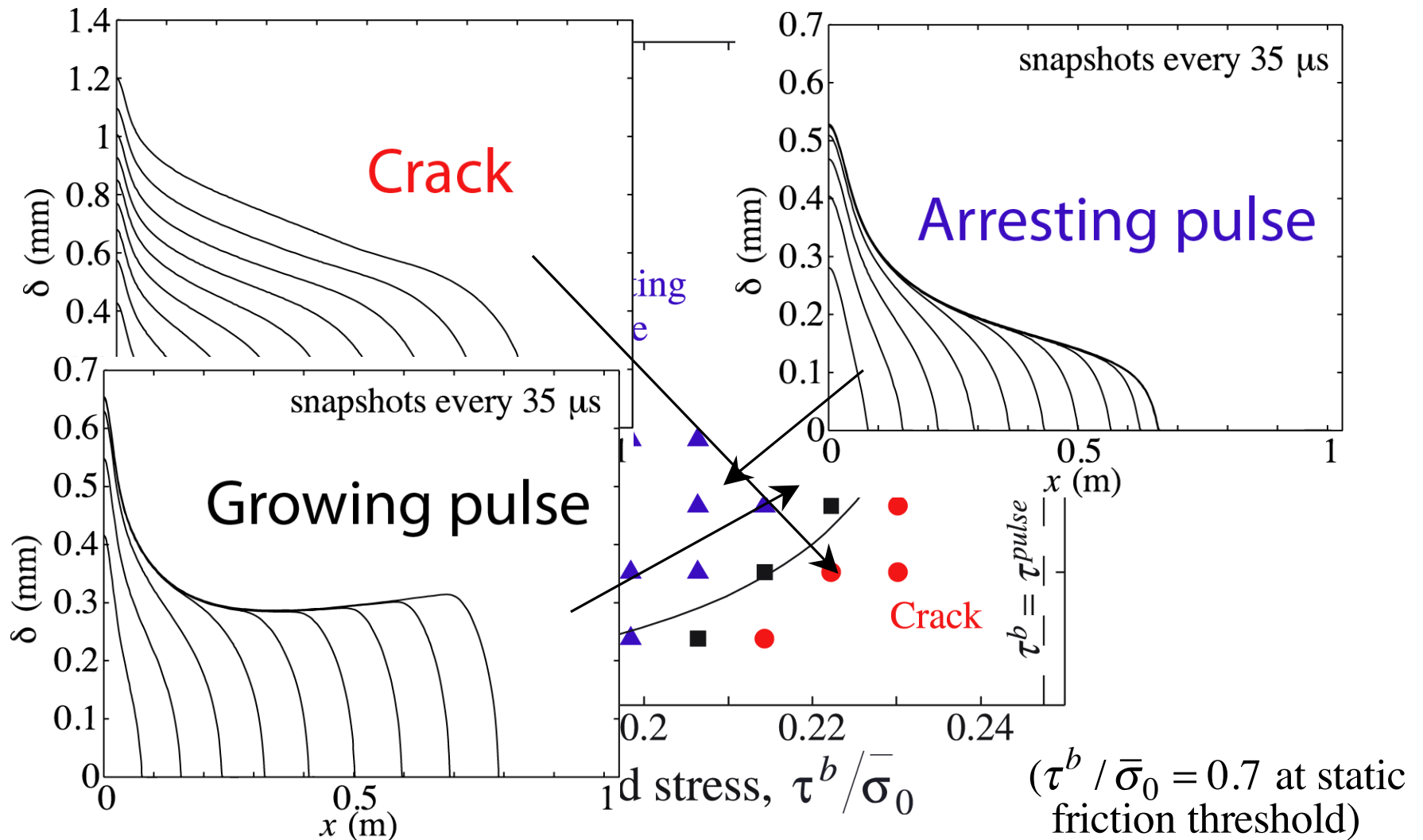


from T. Mitchell, Univ. Col. London (*private comm.*)



Noda, Dunham & Rice (JGR, 2009)

*Effect of strong dynamic weakening (thermal pressurization + flash heating/weakening of frictional contacts) on when a rupture, once nucleated, can propagate to a large spatial extent.*



# Conclusions

- **Thermal Pressurization of Fluid (Water) Present In-Situ**
  - Linear stability analysis predicts very thin slip zones, width  $W \approx 5 - 200 \mu\text{m}$ , within observed range.
  - Full nonlinear analysis also predicts very thin slip zones independent of initial layer thickness.
  - Localization causes additional weakening consistent with “slip on a plane” analysis
- **Thermal Pressurization by Decomposition Fluid**
  - Localization to comparable zones ,  $W \approx 2 - 180 \mu\text{m}$  width
  - Simulations indicated progress of reaction triggers localization
  - Width of localized zone is independent of kinetic parameters.
- **For a wide range of representative parameters, both processes lead to slip on very narrow zones (within the range of observations) causing additional dynamic weakening**

Concepts of fluid and solid mechanics, integrated with materials and thermal sciences, provide a valuable framework for addressing large-scale natural phenomena. We considered their applications to the following:

**(1) Ice sheet flow and subglacial hydrology:**

- Large iceberg calving as the enigmatic source of glacial earthquakes.
- Rapid glacial underflooding events as natural hydraulic fractures, like in a well-characterized spontaneous lake drainage on the Greenland Ice Sheet.
- Partial internal melting from shear heating as a control on flow resistance at the margins of rapidly flowing ice streams as on the Western Antarctic Ice Sheet.

**(2) Fault zones undergoing seismic slip:**

- Frictional heating leads to dynamic pressurization of pore fluids (native ground fluids, or decomposition products from clays and carbonates) within fault gouge.
- Result is dramatic shear-weakening results, with consequences for the dynamics of rupture propagation and earthquake phenomenology (strong but brittle faults, operating at low overall stress, no pronounced heat outflow, self-healing ruptures).

**Common theme in cases considered:**

Solid media considered are, or may become, fluid-infiltrated. Pressurization of the fluid weakens shear resistance and, in an extreme limit, may hydraulically fracture the host.

